Studies on Excited/States Dynamics for Organic Long/Persistent Luminescence Materials

林, 澤森

https://doi.org/10.15017/4060117

出版情報：九州大学, 2019, 博士（工学）, 課程博士
バージョン：
権利関係：

2020

Doctoral Thesis

Studies on Excited-States Dynamics for Organic Long-Persistent Luminescence Materials

Zesen Lin

Department of Chemistry and Biochemistry

Graduate School of Engineering

Kyushu University

Table of Contents

Chapter 1: Introduction 1

1.1. Terminology 2

1.2. Long Persistent Luminescence (LPL) in Inorganic Materials 4

1.2.1. Brief History 4

1.2.2. Material Composition and Classification 7

1.2.3. Mechanism 9

1.2.4. Features 11

1.2.5. Kinetic Models 13

1.3. Photophysics of Organic Molecules 15

1.3.1. Excited State, Fluorescence, Phosphorescence and Delayed Fluorescence 15

1.3.2. Exciplex and Charge Transfer 18

1.4. Organic Long Persistent Luminescence (OLPL) 19

1.4.1. OLPL at Low Temperature 21

1.4.2. Kinetic Models 24

1.4.3. OLPL at Room Temperature 26

1.4.4. Mechanism of Room-Temperature OLPL 28

1.4.5. Advantages of Room-Temperature OLPL Materials 29

1.4.6. Open Issues of OLPL 31

1.5. Motivation and Outline of This Thesis 32

1.6. References 33

Chapter 2: Orange Organic Long Persistent Luminescence from an Electron Donor/Acceptor Binary System 37

2.1. Introduction 38

2.2. Results and Discussion 40

2.3. Summary 44

2.4. Experimental 45
2.5. References 47

Chapter 3: Influence of energy gap between charge-transfer and locally excited states on organic long persistence luminescence 48
3.1. Introduction 49
3.2. Results and Discussion 52
3.3. Summary 73
3.4. Experimental 74
3.4.1. Materials and Synthesis 74
3.4.2. General Methods 76
3.4.3. Quantum Chemistry Calculations of the Dipole Moment 78
3.4.4. Film Fabrication 78
3.5. References 79

Chapter 4: Polymer-based Organic Long Persistent Luminescence Materials 80
4.1. Introduction 81
4.2. Results and Discussion 83
4.3. Summary 92
4.4. Experimental 93
4.4.1. Materials and Synthesis 93
4.4.2. General Methods 93
4.4.3. Film Fabrication 95
4.5. References 97

Chapter 5: Conclusions and Perspective 99
5.1. Conclusions 100
5.2. Perspective 102
5.3. References 103

Acknowledgements 104

Appendixes 108

List of Abbreviations 108

List of Publications and Conferences 112

Chapter 1

Introduction

1.1 Terminology

Long-persistent luminescence (LPL), also known as the glow-in-the-dark effect, noctilucent or long afterglow, is a self-sustained light emission phenomenon by which a material emits light for a very long time (longer than several minutes) after removal the excitation sources which are typically visible light, ultraviolet (UV) light, electron beams or high energy radiation such as X-, α-, β- or γ-rays.[1, 2] Since the mid-1990s,[3] highly efficient LPL materials were used in many commercial products for emission indicators without electricity, including luminous paints, watch dials, fire safety signs, and glow-in-the-dark toys (Figure 1-1). Recently, LPL materials are also being investigated for applications in *in vivo* bioimaging because their long-lived emission can be used to take long time-resolved images after excitation.[4]

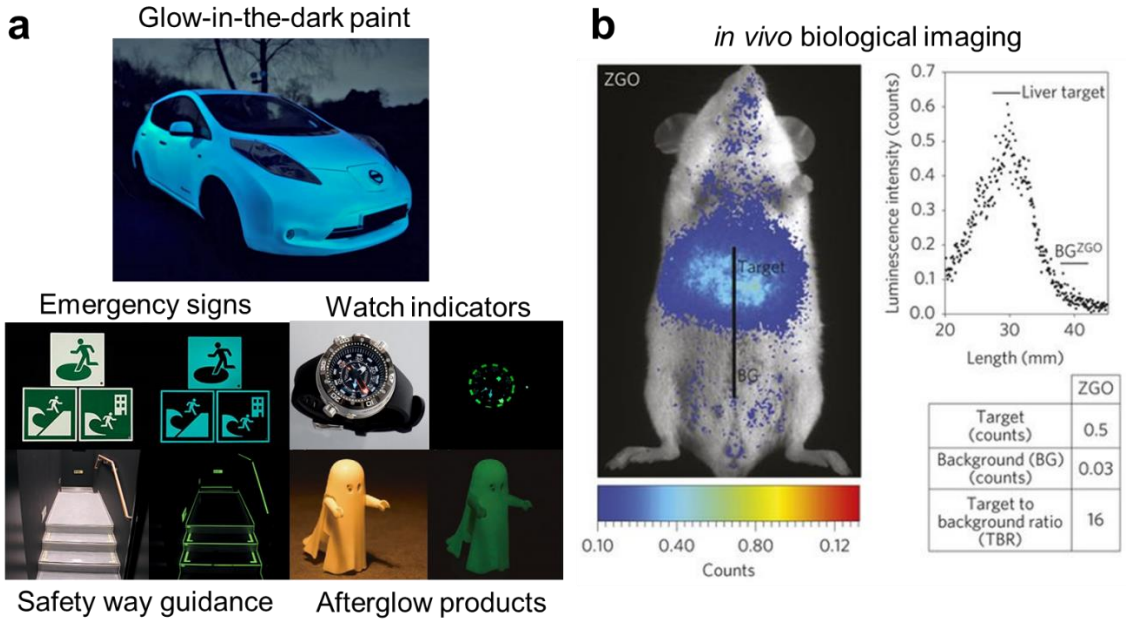

Figure 1-1. Applications of long persistent luminescence materials. (**a**) Glow-in-the-dark products. (**b**) *in vivo* bioimaging. ZGO is the abbreviation of $ZnGa_2O_4:Cr^{3+}$. Adapted from Ref. 4.

All of the LPL materials that can be used at room temperature are made by inorganic materials until the organic LPL emitter was discovered in 2017.[5] Therefore, the origin and meaning of the terminology related to the long-persistent luminescence phenomena and materials must first be explained, because of the different habits in inorganic and organic research fields.[6]

The word "**phosphor**" was invented for the denotation of "Bolognian stone" with the LPL phenomenon (see 1.2.1 for details) in the early 17th century and means "light bearer". This meaning remains unchanged, and now this word is still used for calling the inorganic materials with persisting light emission of a few hours after the exciting radiation has ceased. The word "**phosphorescence**" was derived from the word "**phosphor**" for representing this phenomenon. To distinguish **phosphorescence**, the term "**fluorescence**" was introduced to denote the imperceptible short afterglow of the mineral fluorite (CaF_2) after excitation. The word "**luminescence**", derived from the Latin word *lumen* with the meaning of light, is defined as a phenomenon in which a substance excited by external energy gives off the excitation energy as light. Obviously, luminescence includes both fluorescence and phosphorescence.

In modern usage, for inorganic materials, the luminescence from a substance during excitation is called **fluorescence**, whereas the afterglow that is detectable by the human eyes after stopping excitation is termed **phosphorescence**. However, for organic materials, the luminescence from a singlet excited state is called **fluorescence**, while that from a triplet excited state is referred to as **phosphorescence** (β-phosphorescence, to distinguish it from LPL which was also called α-phosphorescence[7]). The definition of the term "**phosphor**" is still dependent on users, because of the unclear definition. In a broad sense, the word is equivalent

to “a solid luminescent material”. In a narrow sense, the word “**phosphor**” is defined to mean “inorganic phosphors” usually in a powder form and synthesized for practical applications, and rarely used to call single crystals, thin films, and organic molecules that exhibit luminescence.

Because of the vague definition of phosphorescence in the earlier time, LPL was always called long-period phosphorescence or long phosphorescence in the inorganic materials research field in the past. The word “**phosphorescence**” in organic materials research field is now mainly labeled as the long-lived luminescence from the triplet excited states, lasting not longer than a few minutes. In these materials, the luminescence decay curves with time follow the first-order reaction kinetics, which is significantly different from LPL. In recent years, luminescence phenomena similar to organic phosphorescence are also found in inorganic materials[8], and researches in the inorganic LPL field have progressively started to use “**persistent luminescence**” to replace phosphorescence to denote the LPL phenomenon.[9] In this thesis, for distinguishing LPL and phosphorescence in the organic research field, the word “**phosphorescence**” is not used to describe LPL phenomena.

1.2 Long Persistent Luminescence (LPL) in Inorganic Materials

1.2.1 Brief History

In many countries, there are many ancient stories about LPL phenomena, for example, “night shining jewel” or “yeh kuang pi” in Chinese history.[10] The earliest documented evidence of this phenomenon is about an afterglow ink and can be traced back to a thousand years ago, described in a compilation of historical and folk tales, “Xiāng Shān Yě Lù”, published in the Song dynasty (960-1279 A.D.) by Wen Ying (Figure 1-2a). The raw materials might be sulfide

phosphors (CaS) made from seashells and volcanic activity naturally.[11] Possibly, the ink used was the first man-made LPL material. However, because of the dubious accuracy of this compilation, the recognized preliminary scientific reports were "*De Illuminabili Lapide Bononiensi Epistola*" by Montalbani and "*Litheosphorus Sive De Lapide Boboniensi*" by Licetus from the University of Bologna, Italy in 1634 and 1640, respectively.[11, 12] These books discussed the properties of the Bolognian Stone (BaS) discovered by Casciarolo in 1602, which has an orange or reddish afterglow in the dark (Figure 1-2b). Limited to the scientific level at that time, the LPL mechanism of this stone was explained by H ö ls ä and Bettinelli et al. in 2012. The LPL is originated from the emission of monovalent copper (Cu^+) impurities peaking at ~ 610 nm in the reduced product (BaS) of the natural baryte ($BaSO_4$).[13] Because the knowledge and technology level required to explain the LPL mechanism is far beyond people's at that time, only scattered researches were reported since the 17th century.[1]

In 1866, Sidot obtained good LPL emission from a ZnS crystal fabricated by a sublimation method, named Sidot's blende.[14] After approximate half century, P. Lenard and co-workers clarified the composition of the Sidot's blende and explained that LPL is derived from the trace amounts of Cu^+ in ZnS for the first time in history.[1] Based on this result, they also found other alkali-earth sulfides exist LPL in the dark such as Bi^{3+}, Eu^{2+} or Ce^{3+} doped $(Ca_{1-x}Sr_x)S$, which are known as Lenard's phosphors later.[6, 11] Klasens used the elements of the iron group as co-doping electron traps and found ZnS:Cu^+,Co^+ exhibited a longer LPL duration.[15, 16] However, although many physical models were founded to explain the detailed mechanism, all of LPL materials were sulfide-type until the end of the 20th century. Due to their weak brightness and short LPL duration as well as high hydrolyzability under ambient conditions, their applications

were limited. In order to prolong duration, some radioactive elements were introduced into sulfides.[6] But since people have realized the severe health problems and environmental pollution caused by radioactive elements, such self-sustained light materials are difficult to enter the market.[1]

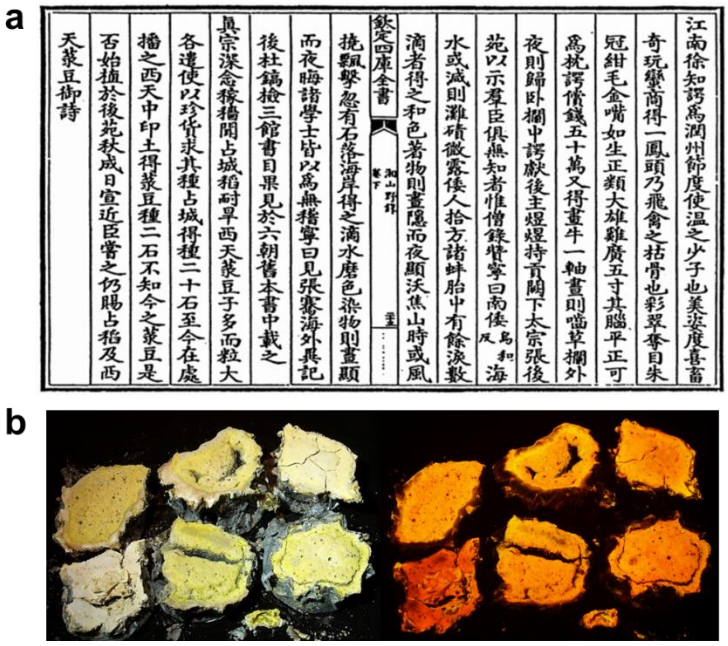

Figure 1-2. (a) Copy of the Chinese text describing the acquisition of a luminescent painting by Xu Zhi-e written for a compilation of historical and folk tales published in the Song dynasty (960–1279 A.D.) by Wen Ying, the English translation of the whole content can be found in page 446 of Ref. 11; **(b)** the Bologna Stone (BaS: Cu^{+}) and its LPL.

The true widespread use of LPL materials began with the modern LPL materials, $SrAl_2O_4:Eu^{2+},Dy^{3+}$, developed by Murayama and his colleagues in the mid-1990s.[3] Comparing with traditional sulfide-type LPL materials, $SrAl_2O_4:Eu^{2+},Dy^{3+}$ is capable of over 30 h of LPL before the emission intensity dropping upon 0.32 mcd/m^2 (Figure 1-3a), which is the lower limit of dark-adapted sensitivity of human eyes.[3] The emission color of this material is green peaking at 520 nm that matches the human's photopic vision (maximum sensitivity at 555 nm) and scotopic vision (maximum sensitivity at 510 nm).[17, 18] The broad absorption band (the edge

over 450 nm, Figure 1-3b) is suitable for the excitation by conventional fluorescent lamps (also white light-emitting diodes). With these nearly perfect properties, $SrAl_2O_4:Eu^{2+},Dy^{3+}$ with the famous brand name, LumiNova®, rapidly prevailed in the market. In 2001, Lin *et al*. reported the first silicates type LPL material, $Sr_2MgSi_2O_7:Eu^{2+},Dy^{3+}$, with the blue emission peaking at 476 nm and longer duration than that of $SrAl_2O_4:Eu^{2+},Dy^{3+}$.[19] Today, these two materials are the most common LPL material in the market, which is why the LPL is always green or blue emission in our perception.

However, although many new LPL materials have invented for more than two decades after the discovery of $SrAl_2O_4:Eu^{2+},Dy^{3+}$, surprisingly, the number of known materials with a decent LPL brightness and duration is still rather limited (see 1.2.2, Table 1.1).

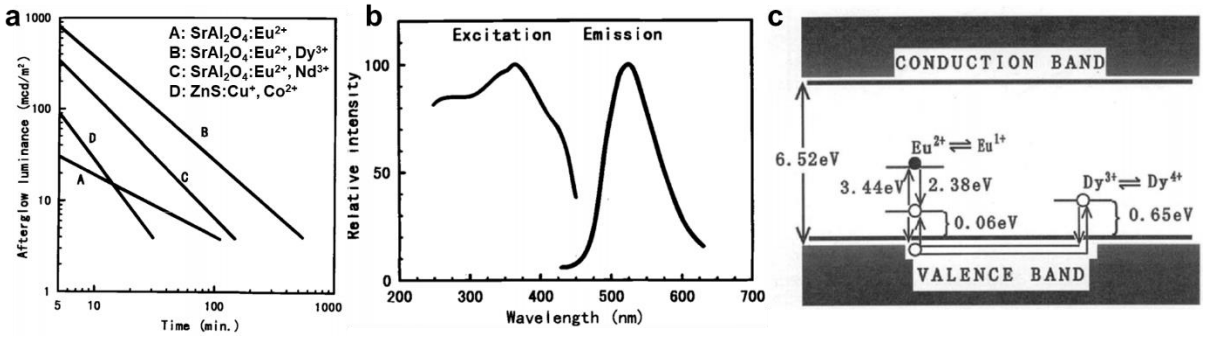

Figure 1-3. (**a**) The long-persistent luminescence characteristics of several inorganic LPL materials; (**b**) Emission and excitation spectra of the $SrAl_2O_4:Eu^{2+},Dy^{3+}$; (**c**) Proposed emission mechanism of $SrAl_2O_4:Eu^{2+},Dy^{3+}$. Adapted from Ref. 3.

1.2.2 Material Composition and Classification

In general, the existing inorganic LPL materials are made by a **host material** with two kinds of dopants: **activators** and **traps**.[1, 2] Although a wide variety of inorganic host materials are used as luminescent compounds, relatively few hosts are used to persistent luminescence, such as aluminates, silicates, sulfides and phosphates, *etc*.[2, 20-22] Among them, aluminates and

silicates are currently the most mainstream host materials. **Activators**, namely emission centers, include lanthanide ions (*e.g.*, Ce^{3+}, Eu^{2+}, Nd^{3+}, Er^{3+}, in which Eu^{2+} is the most popularly used), transition metal ions (*e.g.*, Cr^{3+}, Mn^{2+}, Mn^{4+}, Ni^{2+}) and main group metal ions (*e.g.*, Pb^{2+}, Bi^{3+}), *etc*.[20, 23-25] **Traps** contain crystallographic defects (*e.g.*, oxygen vacancies, Farbe center, anti-site defects) and metal ion co-dopants as impurities (*e.g.*, Cu^{+}, Co^{2+}, Ti^{3+}) or induced intentionally (*e.g.*, Dy^{3+} in $SrAl_2O_4:Eu^{2+}$; Nd^{3+} in $CaAl_2O_4:Eu^{2+}$; Cr^{3+} in $Y_3Al_2Ga_3O_{12}:Ce^{3+}$), *etc*.[1, 3, 26-31] The emitting centers can also play the role of trap centers, *e.g.*, Cr^{3+}.[32, 33] The best LPL materials currently contain intentionally introduced aliovalent or isovalent co-dopants as traps. Generally, the concentration of dopants as activators and co-dopants as traps in inorganic LPL materials is lower than 2% and mainly 1%, which is obviously lower than corresponding inorganic fluorescence materials.[20]

Table 1-1. The reported best different color-emitting inorganic LPL material

Color	Host material	Activator	Trap	Maximum emission (nm)	Afterglow duration (h)	Reference
Blue	$Sr_2MgSi_2O_7$	Eu^{2+}	Dy^{3+}	476	20	19
	$Sr_4Al_{14}O_{25}$	Eu^{2+}	Dy^{3+}	490	20	34
Green	$SrAl_2O_4$	Eu^{2+}	Dy^{3+}	520	30	3
Yellow	$Ca_2Al_2SiO_7$	Mn^{2+}	Ce^{3+}	550	10	35
Red	Y_2O_2S	Eu^{3+},Mg^{2+}	Ti^{4+}	615/626	3	26, 36
	$MgSiO_3$	Mn^{2+},Eu^{2+}	Dy^{3+}	660	4	35
White	$(Li,Na)_8Al_6Si_6O_{24}(Cl,S)_2$	Ti^{3+}	Defect	500	100[a], ~ 7[b]	28
	$CaAl_2O_4 + Y_3Al_5O_{12}$	Eu^{2+}, Ce^{3+}	Nd^{3+}	424,560	48	37
NIR	$LiGa_5O_8$	Cr^{3+}	Defect	716	1000	38
	$Zn_3Ga_2Ge_2O_{10}$	Cr^{3+}	Defect	650–1000	360	39
	$MgGeO_3$	Pr^{3+}	Defect	1085	120	40
	$CdSiO_3$	Pr^{3+}	Defect	1100	120	40

[a] Duration by detector. [b] Duration upon 0.32 mcd/m^2.

According to the emission color, the inorganic LPL materials are generally divided into five groups: blue, green, red, white, and near-infrared (NIR).[2] Here, only the best inorganic long afterglow material types of different colors were summarized (Table 1-1). Some related reviews and books have been published to summarize the existing inorganic LPL materials in detail.[1, 2, 20, 23] The host materials mainly contains six families: aluminates, silicates, aluminosilicates, oxides, oxysulfides, and sulfides.[41] The durations of LPL materials with yellow and red emission are limited comparing to other color LPL materials.

1.2.3 Mechanism

For understanding the mechanism of the LPL in inorganic materials, many physical models have been proposed,[1, 3, 20, 42] ranging from very basic conceptual models to complex systems with multiple charge traps of various types and depths. But all of these models are based on the trapping–detrapping mechanism framework: 1) Excitation process: the excitons are generated by external excitation; 2) Trapping process: the generated electrons or holes (charge carriers) are separated and captured by the electron or hole traps instead of the direct radiation. Because of the long lifetime of trapped charge carriers, this material can store the excitation energy for a long time. Therefore, this phenomenon can also be called an “optical battery”; 3) Detrapping process: after cutoff of the excitation, the captured charge carriers are only gradually released from these traps mainly by thermal activation or back tunneling assisted by thermal fluctuations; 4) Recombination luminescence process: the detrapped charge carriers recombined with their counter charge carriers and regenerated excitons that emit the luminescence.

The difference between these models lies in the details of the framework, such as whether the host is excited or the activators are excited, whether the electrons or holes are trapped, and

whether the trapping and detrapping processes of charge carriers between traps and activators are through the conduction band (CB) or the valence band (VB) of the host materials or direct tunneling, as well as details of redox species in these inorganic LPL materials. Both energy levels of activators and traps are located inside the forbidden band of host materials. Normally, the trap energy levels are less than 1 eV below the bottom of the CB (electron trap) or above the top of the VB (hole trap).

However, these models are more or less inadequate to explain some experimental phenomena, and there is no universal model until now. Researchers of inorganic LPL materials always chose the relatively appropriate model to explain the phenomena of their materials. For example, in the Matsuzawa model (Figure 1-3c),[3] Eu^{2+} ions are as the activators (Eu^{2+}/Eu^{+}) and holes are assumed to be the main charge carriers and captured by the traps, Dy^{3+} (Dy^{3+}/Dy^{4+}). This model can explain the influence of the rare earth codoping effect well. However, this model ignored the observed weak LPL in non-codoped $SrAl_2O_4:Eu^{2+}$.[43] Moreover, Eu^{+} and Dy^{4+} ions are chemically unstable ions.[42]

Based on the previous studies, the long-lived separated charges from photo-generated excitons are critical to LPL, which are stabilized by traps with suitable depth in inorganic LPL materials. The recombination of these trap-stabilized long-lived separated charges resulted in the key feature, i.e., the LPL obeying a power law (see 1.2.4) in the long time scale as shown in Figure 1-3a and 1-4. If the energy level of traps is too shallow, the captured electrons can easily escape from traps at room temperature, resulting in too short LPL duration or even no observable LPL. On the other hand, too deep trap energy level will lead to a few or no escaped electrons at room temperature, which is also not appropriate to the LPL performance.

1.2.4 Features

Two apparent features are always used to distinguish LPL and phosphorescence: (i) the almost identical spectra between photoluminescence and LPL (Figure 1-4c&d); (ii) long emission duration from minutes to even days after cutoff excitation sources. The first feature can be found in most inorganic LPL materials with two dopants because the fluorescence and LPL come from the identical energy state of emission center ions.[1] This is an evident discrepancy between LPL and phosphorescence since the phosphorescence always shows a conspicuous redshift comparing with the corresponding fluorescence (the reason see 1.3.1).

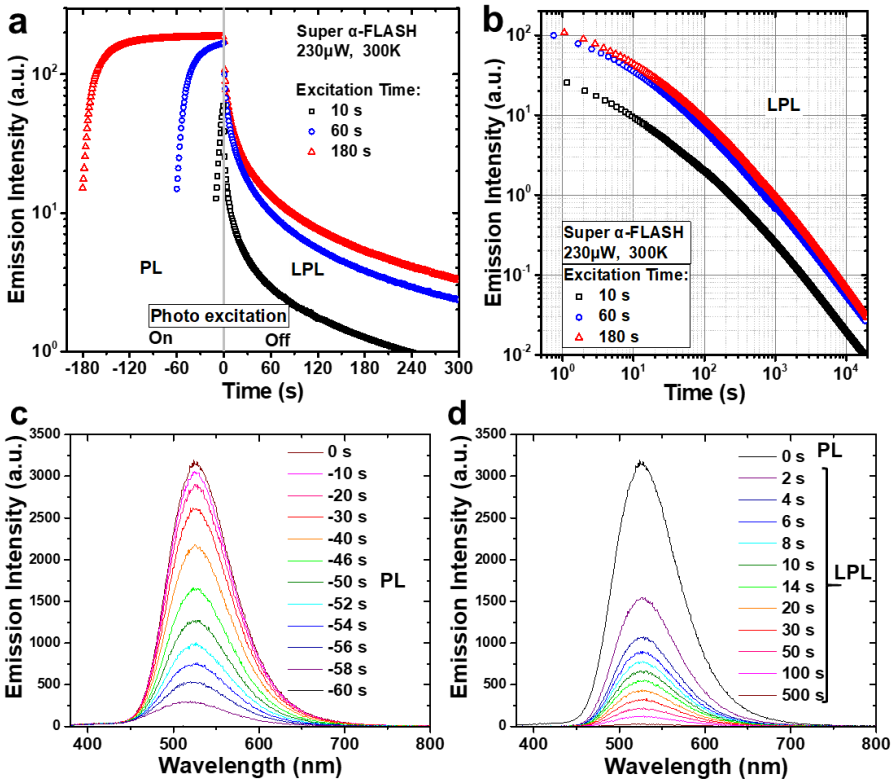

Figure 1-4. The LPL performance of a commercial inorganic LPL tape (Super alpha-FLASH, 1 cm^2 area): semi-logarithmic plots (**a**) and logarithmic plots (**b**) of the emission decay profiles with different excitation duration; Emission spectra during photoexcitation (**c**) and after the excitation (**d**) of inorganic LPL material. All samples were 1 cm^2 and were excited for 60 s by a 340-nm LED source with the same power of 230 μW at 300 K.

The second feature is crucial and entirely different with room-temperature phosphorescence (generally up to seconds) because their decay follows the different law: the LPL (refer in particular to the isothermal luminescence) obeys a power law ($I(t) \sim t^{-m}$, with m = 0.5~2, mostly 1, hyperbola[44, 45]) in the long time scale as shown in Figures 1-3a and 1-4a&b (the straight-line on the log–log plot is often called the signature of a power law.[46]), while the phosphorescence follows an exponential law (the straight line on the semi-log plot,[47] specifically log-linear plot in this case as shown in Figure 1-5).

The long emission decay properties of LPL originate from the mathematic properties of the power law. The one important mathematic property of the power law is that the power-law graph has a longer tail than that of the exponential law (Figure 1-5).[46, 48] This is the reason why the duration of LPL is appreciably longer than that of phosphorescence. The scale invariance (scale free) of power law leads to the straight-line on the log-log plot.[48] However, the phosphorescence decay obeying the exponential law is slow in a short time-scale but fast in a long time-scale (Figure 1-5).

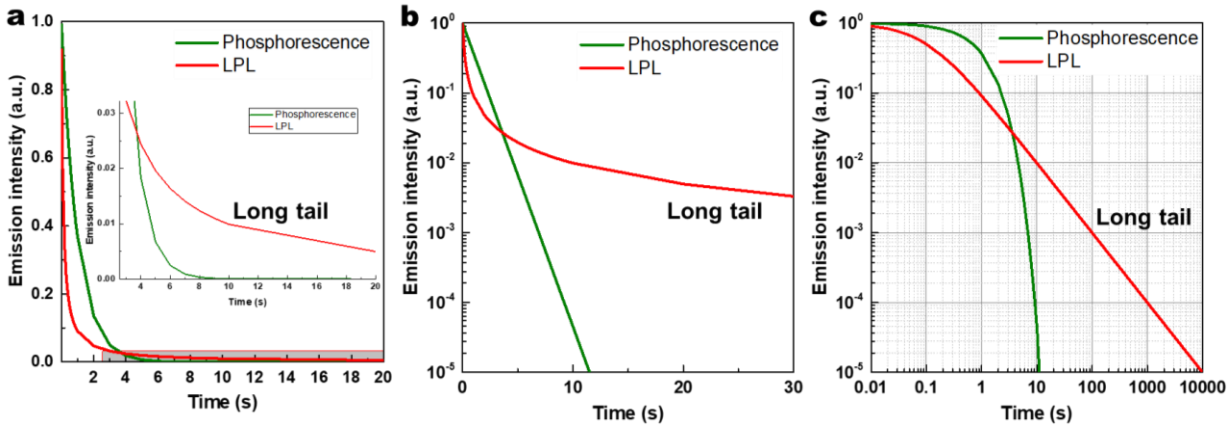

Figure 1-5. The ideal emission decay profiles of phosphorescence and LPL on (**a**) linear, (**b**) log-linear, (**c**) log–log plots. Phosphorescence follows an exponential decay $I(t) = \exp(-t)$, and LPL a power-law decay $I(t) = (1+10t)^{-1}$.

Another mathematics property of the power law is the lack of well-defined average value (mean): a power-law x^{-k} has a well-defined mean over $x \in [1, \infty)$ only if $k > 2$.[48] Therefore, we cannot obtain the lifetime of LPL ($I(t) \sim t^{-m}$, with m = 0.5~2). On the other hand, the mean of experiential law $e^{-\lambda x}$ is 1/λ, in which λ is a constant. So the lifetime of phosphorescence is a constant. The excitation conditions containing the excitation duration must be identical to evaluate commercial LPL materials,[1, 49, 50] while the identical excitation power and duration are not required to evaluate phosphorescence.

In addition to these two apparent features between LPL and phosphorescence, LPL materials often show **thermoluminescence (TL)** or **thermally stimulated luminescence (TSL)**, although that is not found in phosphorescent materials.[51] The phenomenological definition of TL is as follows "The type of light emission that occurs when the heat is applied to an insulator or to a semiconductor which has been previously irradiated by ionizing radiations".[52] The LPL can exhibit TL even excited by non-ionizing radiations, e.g., ultraviolet-visible (UV-vis) light. Since the TL profile provides information on "trap depth" that is the energy required for carriers to escape from the traps, the TL profile is used to analyze the emission mechanism. However, phosphorescent materials do not exhibit TL and often quenched by non-radiative transitions with increasing temperature.

1.2.5 Kinetic Models

Based on empirical kinetics, when a luminescence process controlled by a rate-determining step with the reaction order $n > 1$, the relationship between luminescence intensity $I(t)$ and time t obeys a power law

$$I(t) = \frac{k_L a_0^n}{[1+(n-1)k_L a_0^{n-1} t]^{\frac{n}{n-1}}} = \frac{I(0)}{[1+(n-1)k_L^{\frac{1}{n}} I(0)^{\frac{n-1}{n}} t]^{\frac{n}{n-1}}} = \frac{I(0)}{(1+\frac{t}{\tau})^{\frac{n}{n-1}}} \quad (1\text{-}1)$$

in which k_L is the rate constant of the whole luminescence process, a_0 is the initial concentration of reactants of the rate-determining step. Here, the concentrations of all reactants are equal to a_t at the arbitrary time t and τ is the lifetime. $\tau = (n\text{-}1)^{-1} k_L^{-1} a_0^{1-n}$ means that the lifetime is depends on a_0. However, t^{-1} power law cannot be obtained from empirical kinetics.

According to the trapping-detrapping mechanism (the detrapping process is the rate-determining step, see 1.2.3), if the retrapping possibility of electrons or holes is assumed to be negligible, the afterglow decay profile will obey first order kinetics, which is described by Randall and Wilkins in 1940s.[53] If the retrapping probability is equal to the electron-hole recombination probability, the afterglow decay profile can be described by $(1 + t)^{-2}$ behavior when the limit $t \rightarrow \infty$, i.e., second order kinetics, as derived by Garlick and Gibson in 1948.[54] May and Partridge described general order kinetics.[55] Therefore, the above assumptions are ideal and do not correspond to the actual situation.

In order to explain the t^{-1} power law, many kinetic models based upon different assumptions have been proposed in history.[51, 52, 56] They can be divided into two categories based on different assumptions: **trap depth distribution model** and **electron tunneling model**. Several reviews[51, 52, 56] have clearly summarized the merits and demerits of these models.

The combination of multi-exponential processes can mimic a power law.[57] Thus, a common approach is to assume the presence of multiple discrete energy levels obeying first order kinetics. Many researchers fitted the delay profile by a multi-exponential (three or more) function and called these exponential components “fast,” “slow,” or “intermediate”.[56] However,

these exponential components are always difficult to interpret physically. Moreover, the large number of parameters involved make the fitting procedure unreliable.[56]

1.3 Photophysics of Organic Molecules[58-60]

1.3.1 Excited State, Fluorescence, Phosphorescence and Delayed Fluorescence

For the photophysics of organic molecules, the scope of discussion is mainly the **electronic state** change of molecules, of which energy range is in the UV-vis band. Therefore, in terms of organic molecular photophysics, the electronic state of the molecule is also denoted by the molecular **state**. The **ground state** of a molecule is its lowest-energy state, that is, electrons preferentially occupy all molecular orbitals from the lower energy levels. When the molecule absorbs electromagnetic waves in the UV-vis band, an electron in the ground state molecule will transit to the higher energy orbitals. At this time, this molecule is on an **excited state**. Although there are a huge number of possible excited states for a molecule, in theory, only two or three excited states normally need to be considered for photophysical and photochemical discussions of organic molecules, because of the energy range of UV-vis light.

The ground state of conventional organic molecules is closed-shell (all electrons paired and two electrons per orbital). In a closed-shell molecule, the occupied orbital with the highest energy level is called the **Highest Occupied Molecular Orbital (HOMO)**, and the unoccupied orbital with the lowest energy level is called the **Lowest Unoccupied Molecular Orbital (LUMO)**. For many organic molecules, the orbital that is losing an electron mainly is the HOMO, while the orbital receiving the electron is the LUMO or an orbital near it in energy (e.g., LUMO+1).

One molecular orbital can be occupied by a pair of electrons with two spin states: spin-up and spin-down (the spin quantum number *s* is -1/2 and 1/2, respectively). When the total electron spin quantum number (*S*) of this molecule is zero, there is only one spectral line from this molecule state, which is a **single state** ($N = 2S+1$, N is the number of spectral lines. In this case, $N = 1$). When $S = 1/2$, $N = 2$, the molecule is at a **doublet state**. When $S = 1$, $N = 3$, the molecule is at the **triplet state**. Because the ground state of the organic molecule is a closed shell, its ground state is a singlet state (S_0), and the excited state is a singlet state (S_n) or a triplet state (T_n). In the same electronic configuration, the triplet excited state is more stable than the singlet excited state because of the exchange interaction of two unpaired electrons located in two different orbitals. Thus, the molecular excited state can automatically convert from S_n to T_n through the **intersystem crossing (ISC)** process.

Since the molecules in their excited states are unstable, they tend to release energy through radiative transitions and non-radiative transitions. The **radiative transition** of an electron from a high energy level orbital to a low energy level orbital is the **luminescence** process. According to the Kasha rule, the luminescence process of most organic molecules involves only the lowest excited states (S_1 or T_1), because relaxations (**internal conversion**) from the higher excited states (S_n or T_n) to the lowest excited states (S_1 or T_1) are much faster than that of luminescence. The radiative transition from S_1 to S_0 is called **fluorescence**. The fluorescence emission is spin-allowed radiative transitions with the large radiative rate constant (10^5~10^9 s^{-1}, normally larger than 10^6 s^{-1}), that is why it is named fluorescence (see 1.1). If the luminescence is from T_1 to S_0, it is called **phosphorescence**. Because the transition is spin-forbidden, the rate constant of phosphorescence is small (10^{-2}~10^6 s^{-1}, normally smaller than 10^4 s^{-1}). Since the small exchange

interaction of two electrons on the HOMO and the LUMO, the T_1 state is lower than the S_1 state, leading to the red-shift of phosphorescence from fluorescence.

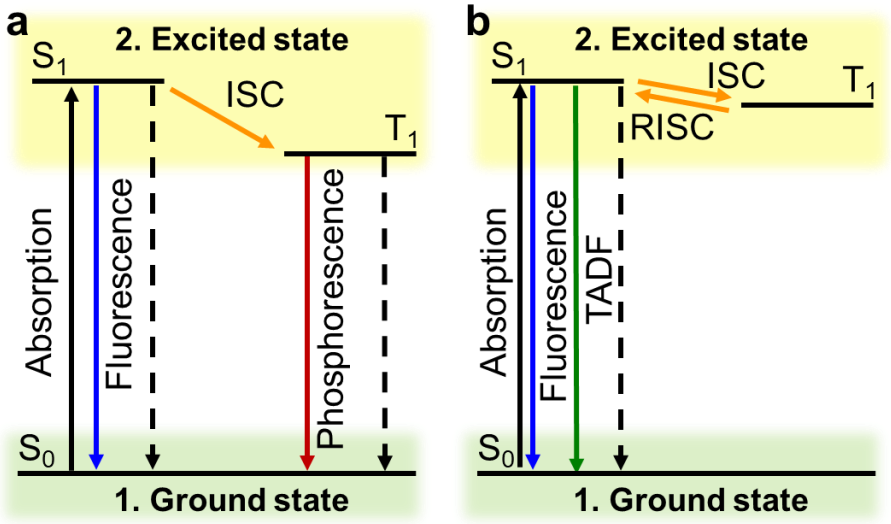

Figure 1-6. The simplified Perrin–Jablonski diagram without higher energy level excited states and rotation and vibration levels. Solid lines with an arrow indicate radiation transition, while dash lines with arrow donate non-radiative transition.

However, in some cases, the emission has the same spectral distribution with the normal fluorescence but a much longer lifetime (10^2~10^6 s^{-1}). This so-called **delayed fluorescence** originates from an up-conversion process from T_1 to S_1 and can be separated into two types based on different up-conversion mechanisms: **"P-type" delayed fluorescence** and **"E-type" delayed fluorescence**. The P-type delayed fluorescence derives from triplet–triplet annihilation (TTA), which can produce fluorescence emission from the reaction of two triplet states. The E-type delayed fluorescence is also called **thermally activated delayed fluorescence (TADF**) because the key up-conversion is a thermally activated process through **reverse intersystem crossing (RISC)**. The efficient RISC can occur when the energy gap between S_1 and T_1 (ΔE_{ST}) is very small (< 0.2 eV), because of a small overlap between the wave functions of the HOMO

and LUMO levels.[61-63] Fluorescence, phosphorescence, TADF and corresponding non-radiative transitions obey the first-order kinetic, because of only one reactant in the rate-determining step. Therefore, the decay profiles of these processes usually follow the exponential law.

1.3.2 Exciplex and Charge Transfer

In the condensed state, an excited molecule can spontaneously be stabilized by some intermolecular interactions. The excited molecule can transfer a fraction of charge to another different molecule on the ground state and forms a stable complex, i.e., **exciplex**. In exciplex, the electron-donating (hole-accepting) molecule is called the **electron donor**, or simply **donor** (D), while the electron-accepting (hole-donating) molecule is called the **electron acceptor**, or simply **acceptor** (A). This stabilization for generating the exciplex can be explained as the partial mixing of frontier orbitals of donor and acceptor molecules (Figure 1-7). Because the interaction between the donor and acceptor is small, this interaction does not form chemical bonds. But this orbital mixing causes an electron/hole delocalization on these two molecules. As a result, the donor transferred a portion of the negative charge to the acceptor during the process forming the exciplex. The process is called **charge transfer**, to distinguish the concept **electron transfer** which normally is denoted as the process that an electron is completely transferred to another molecule. As shown in Figure 1-7, the gap between HOMO and LUMO of exciplex is smaller than that of the corresponding donor and acceptor, so the exciplex always shows a redshift emission.

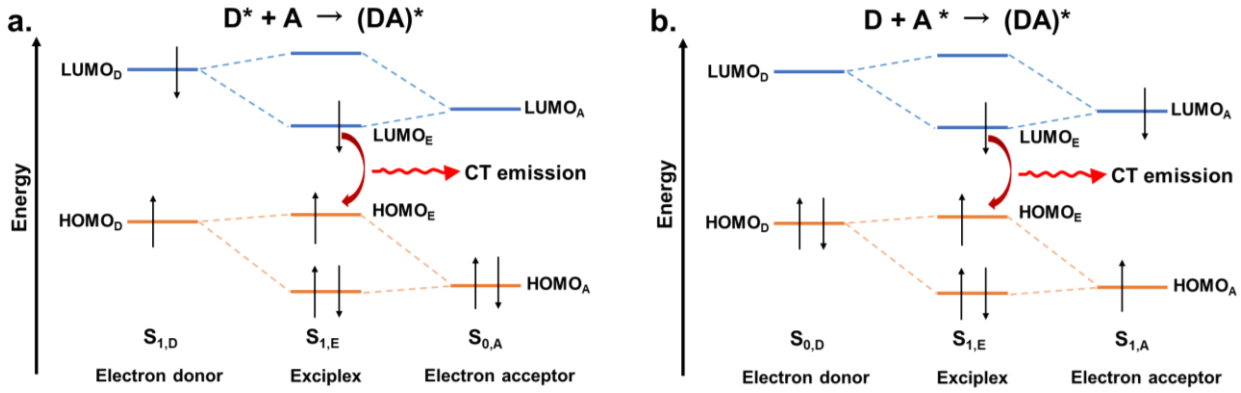

Figure 1-7. The donor-acceptor orbital mixing to generate an exciplex: (**a**) an excited donor and an acceptor on the ground state; (**b**) a donor on the ground state and an excited acceptor.

1.4 Organic Long Persistent Luminescence (OLPL)

Phosphorescence is known to have long emission duration as the organic molecule because of the slow spin-inversion process (see 1.3.1). Since the competition of non-radiative transition from T_1 to S_0 is greatly accelerated by increasing the temperature, a large phosphorescence rate constant is preferred to obtain the room-temperature phosphorescence (RTP). In contrast, a small phosphorescence rate constant is required to get a long phosphorescence lifetime. Therefore, the long-lived RTP of organic molecules is limited in principle. Since the main cause of non-radiative decay owes to the molecular motion, long-lived RTP has been reported by suppressing molecular motion in the solid-state matrix in the middle of the 20 century.[64-66] Now, many RTP from organic molecules have been adopted: molecular design based on n-π transition; usage of rigid matrix[66, 67], e.g., polymer[68], micelles[69, 70], cyclodextrins[71], crown ethers[72] and metal-organic framework (MOF)[73]; generation of new long-lived triplet states by co-crystallization[74], H-aggregation[75, 76], intermolecular ionic[77], hydrogen or halogen bonding[78-80], etc.[64, 65] However, all of these efforts did not change the first order kinetic feature of phosphorescence, i.e., the exponential law. Owing to the mathematic "short tail" feature of the

exponential law, it is impossible to obtain LPL just through extending RTP.

To obtain LPL emission from organic materials, it is the key to obtain the power law emission decay. However, obeying the power law is a necessary condition but not a sufficient condition to judge whether a luminescence process is LPL or not.

For example, the P-type delayed fluorescence derived from TTA can obey a power law (t^{-2} law) in the short time scale:

$$I_{\mathrm{DF}}(t) = \frac{0.5 f k_{\mathrm{TTA}}[\mathrm{T}_0]^2}{(1 + k_{\mathrm{TTA}}[\mathrm{T}_0]t)^2}, \quad k_{\mathrm{TTA}}[\mathrm{T}_t] \gg k_{\mathrm{phos}} + k_{\mathrm{nr}} \tag{1-2}$$

But it will obey an exponential law in the long time scale because the delayed fluorescence changes into the phosphorescence:

$$I_{\mathrm{DF}}(t) = 0.5 f k_{\mathrm{TTA}}[\mathrm{T}_0]^2 \exp[-(k_{\mathrm{phos}} + k_{\mathrm{nr}})t], \quad k_{\mathrm{TTA}}[\mathrm{T}_t] \ll k_{\mathrm{phos}} + k_{\mathrm{nr}} \tag{1-3}$$

in which f is the probability that the reaction complex has spin 0 from Smoluchowski's theory; k_{TTA}, k_{phos}, and k_{nr} are the rate constant of TTA, phosphorescence, and non-radiative transition of T_1 state; $[T_0]$ and $[T_t]$ are the concentration of T_1 excitons at time 0 and t, respectively.[59] This is because the TTA, phosphorescence, and non-radiative decay are all parallel reactions from T_1 excited state. Moreover, if a reverse process of TTA (singlet fission) generates the geminate triplet excitons, the emission decay profile of the diffusion-mediated delayed fluorescence will be $t^{-1.5}$ law (one and three dimensions) or t^{-1} law (two dimensions) in the short time scale (< 1 μs).[81]

This example revealed an important condition to obtain LPL. **The metastable species generating LPL can hardly be quenched by other quick processes**. Therefore, the metastable species must have a long lifetime for the LPL emission over seconds. One possible option is to use the separated geminate charges as the metastable species because the separated

geminate charges can only disappear by recombination but cannot disappear at the isolated states (Figure 1-8). Actually, inorganic LPL materials store the excitation energy into the separated charges by using trap sites. The separated charges should not convert to other stable ionic states by redox reaction or recombine without radiation.

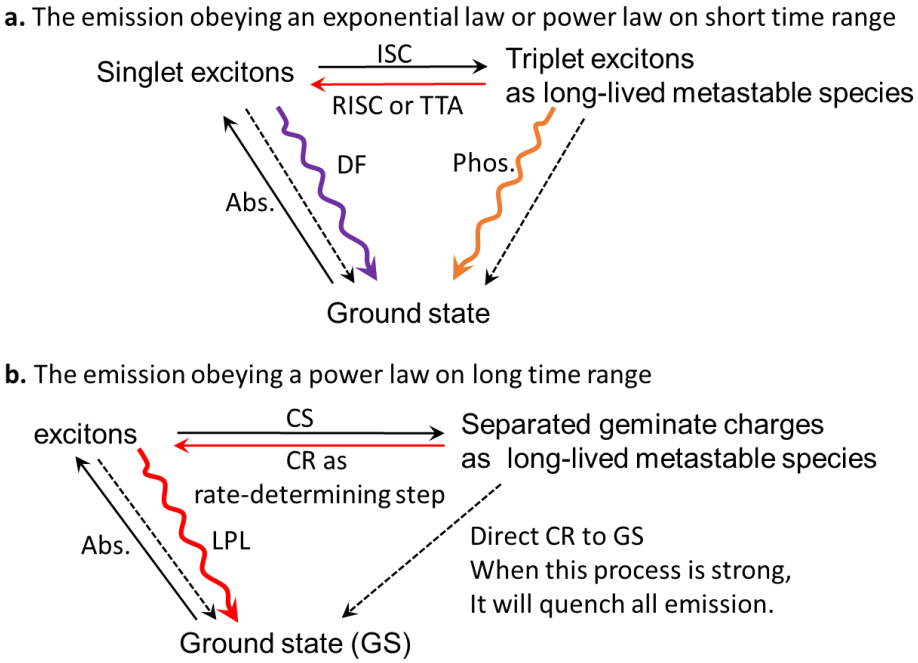

Figure 1-8. The comparison between the afterglow emission process obeying the exponential law and obeying the power law. The uncommented dash arrow represents non-radiative transitions.

1.4.1 OLPL at Low Temperature

OLPL from the recombination of geminate ion pairs in condensed media at a fixed low temperature is known as **isothermal luminescence (ITL)**.[82-84]

Lewis and co-workers investigated the photoionization (or photo-oxidation) of many easily oxidized organic molecules (amines, phenols, dyes, etc.) in frozen organic solution in the 1940s.[85-87] They found some of these compounds can exhibit LPL (even till 1 hour) in the rigid solution after excited by a high-intensity mercury-light source.[82] Linschitz and Berry extended these studies (Figure 1-9) and found that the compounds containing a lone pair (on the nitrogen

atom, oxygen atom, or carbanion), which can be easily oxidized and have a well-marked phosphorescence, show LPL.[82] Thus, the amines give much brighter light emission than the corresponding ethers or phenols. They also described the importance of solvent since the amine solvent may afford better electron traps and thus enhance the luminescence. They also identified the presence of the solvated electrons generated by the photo-oxidization as follows. In addition, the neutral radical resulting from photo-oxidation of a negative ion exerts no long-range coulomb attraction on the electron, and thus even shallow solvent traps suffice to prevent immediate recombination.[82] Lewis and Kasha had already suggested the separated geminate radical ions in this LPL process originate from a stepwise two-photon ionization.[7]

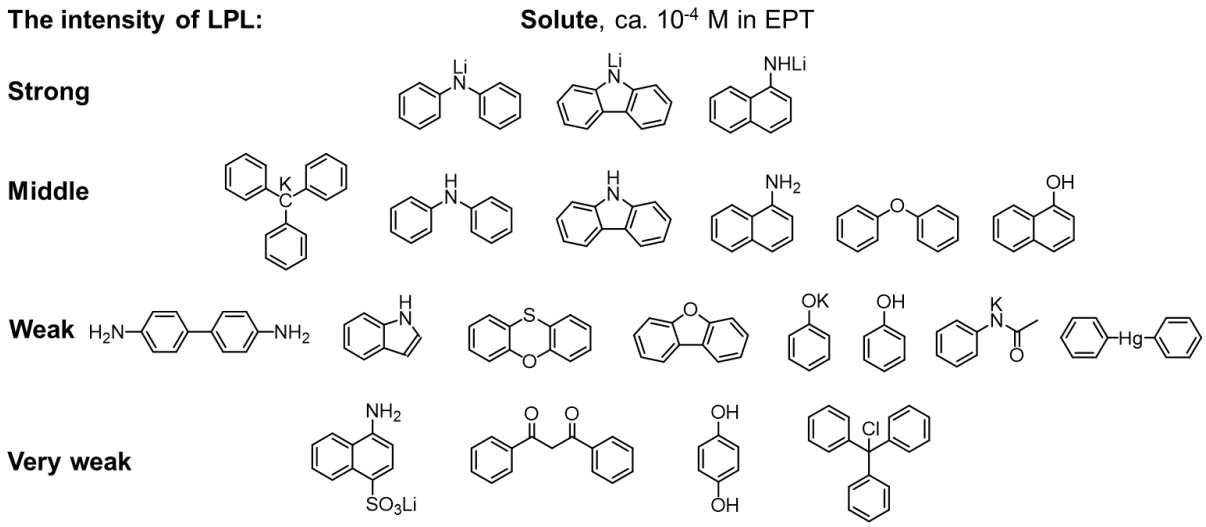

Figure 1-9. Structures of organic molecules as solute investigated by Linschitz and Berry as well as rough results of LPL performance. The solvent EPT is a mixture of ether, isopentane, triethylamine, 2:3:3 or 5:5:2.[82]

After their pioneering works, many examples of low-temperature OLPL were reported, while the high energy ionizing radiations like γ-ray and electron beam are used as the excitation source.[83, 88-91] The adopted condensed media are always organic solvent glass at liquid nitrogen temperature in these reports.

In 1960, Nikolski and Buben firstly reported TL (see 1.2.4) of polymer solids like polyethylene, paraffin, polyisobutylene, Teflon, natural and synthetic rubber, which were irradiated by electron beam at 100 K.[92, 93] The TL glow curve of the irradiated polymer was developed to obtain the information on the motional relaxation of polymer solids. However, there are still some unknown problems on the mechanism of luminescence owing to lack of information on the nature of electron traps.[84]

In the 1990s, Yamamoto *et. al.*[84, 94] observed the low-temperature OLPL (t^{-m} law, $m \approx 1$, at 20 K, Figure 1-10) from a polymer solid doped with small organic molecules after excited by a laser. The dopant, *N*,*N*,*N*′,*N*′-tetramethylbenzidine (TMB), can easily form long-lived radical cations by photo-ionization as Lewis reported.[85-87] The LPL performance was changed by the polarity and the glass-transition temperature (T_g) of polymers. The LPL spectrum contains both the fluorescence and phosphorescence of TMB at the low temperature (< 210 K) (Figure 1-10c). Moreover, both LPL decay profiles at fluorescence and phosphorescence regions show power-law decay (Figure 1-10d), which indicates both fluorescence and phosphorescence are controlled by the charge recombination process. The intensity ratio of phosphorescence (I_F) to fluorescence (I_P), I_F/I_P in the TL spectra indicates that the photo-generated electrons in the poly(alkyl methacrylate)s are more stable than that of in the polystyrene. However, the LPL was quenched at room temperature. A 351-nm pulse laser does not cause direct ionization of TMB, while it can cause two-photon ionization because of the high optical density of the laser.

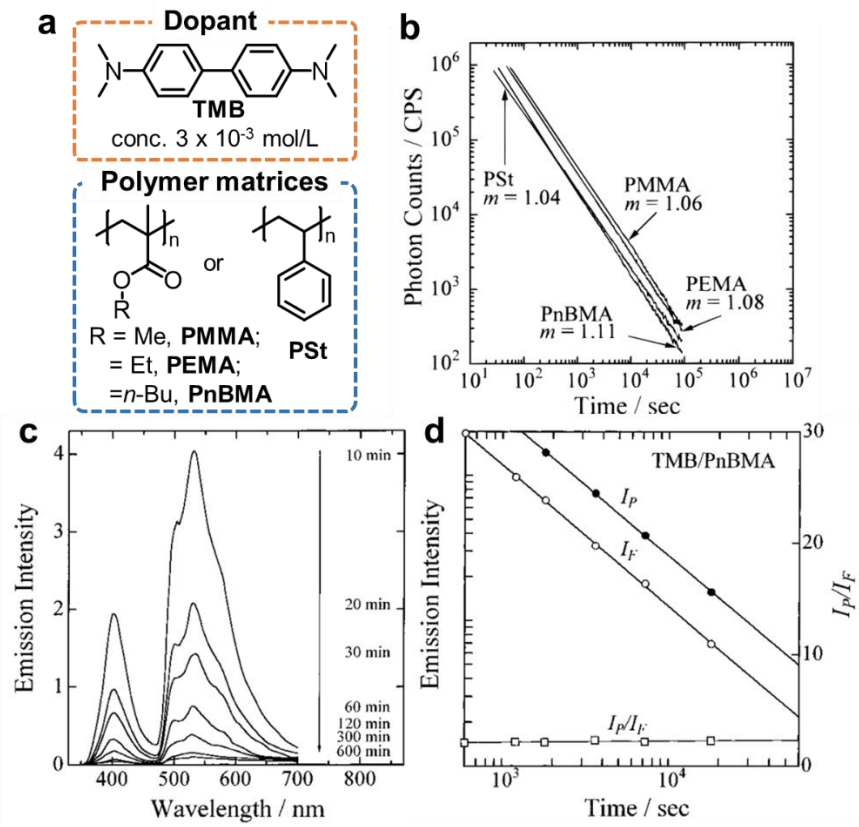

Figure 1-10. (a) The structures of low-temperature OLPL materials; **(b)** LPL duration profile of TMB doped in polymer solids photoirradiated at 20 K. **(c)** Emission spectral change in the LPL for the TMB chromophore doped in a PnBMA film over the time range from 10 to 600 min after the photoirradiation at 20 K. **(d)** Dependence of the fluorescence intensity I_F (open circles), the phosphorescence intensity I_P (closed circles), and the intensity ratio I_P/I_F (open squares) on time change for the ITL at 20 K of the TMB doped in a PnBMA film. The values of *m* represent the slope of the LPL duration profile. Modified from Ref. 84, 94.

1.4.2 Kinetic Models

Similar to LPL in inorganic materials, the function of the low-temperature OLPL intensity and duration normally follows

$$I(t) = \frac{I(0)}{(1+\alpha t)^m}, \; m \approx 1 \tag{1-4}$$

in which the parameters, $I(0)$ and α, depend on irradiation time and dose rate.[95, 96] As previously described in 1.2.5, it cannot be explained by an empirical kinetic. Historically, there were many proposed models to explain this power law. Normally, these models can be separated into two

types according to the recombination of geminate ions by diffusion or electron tunneling.

1. **Diffusion model**. The condensed state of organic molecules does not have VB and CB like inorganic materials while they have separated molecular frontier orbitals. In the diffusion model, we consider the distribution of electrons (radical anions) after the charge separation process. The model based on the diffusion-controlled recombination is the earliest and most popular model. Debye and Edwards proposed $I(t) \propto t^{-m}$, $m = 1$ in terms of a diffusion process and a spatial distribution function of trapped electrons. However, this model cannot explain $m>1$ because it neglects the normalization of the distribution function, which leads to an infinite of the total amount of ionic species when m = 1.[97] By using a normalized distribution function, Abell and Mozumder gave a revised model showing that, when $t\rightarrow\infty$, m is 1.5, which can explain the change of m value over time.[98] Hong and Noolandi also derived the recombination rate $R(t) \propto t^{-m}$, m = 1.5 by solving the time-dependent Smoluchowski equation with Coulomb potential.[99] Stolzenburg, Ries and Bässler proposed $I(t) \propto t^{-m}$, m = 1 based on the Hong-Noolandi model by considering the energetic relaxation of carriers subject to the random walk.[100] Hamill and Funabashi explained the t^{-m} law by using a non-Gaussian diffusion model in which hopping time distribution is an asymptotic type derived from the continuous-time random walk mode by Scher and Montral.[101]
2. **Electron tunneling model**. In the 1970s, Kieffer, Meyer, and Rigaut reported the LPL emission derived from the electron recombination without thermal activation because LPL decay kinetics do not change from 4 to 77 K.[102, 103] Therefore, the electron tunneling model has been used to explain the LPL at low temperatures. The Tachiya-Mozumder model

shows $I(t) \propto t^{-m}$, m is very close to unity over a wide time range.[104] Hama et al. found the distance distribution of cation-electron pairs could be obtained by Laplace inverse transformation of the ITL decay based on an electron tunneling model. The exponent *m* (equation 1-4) depends on irradiation time and dose rate.[96] Ohkita et al. explained their results by this tunneling model.[94]

1.4.3 OLPL at Room Temperature

Although the OLPL is discovered at low temperature by using two-photon ionization of polymer systems, OLPL at room temperature is realized after almost 20 years. The problem was how to obtain stable separated geminate charges by a weak excitation light source at room temperature.

In 2017, Kabe and Adachi realized OLPL at room temperature by using a mixed film of the electron donor TMB and an electron acceptor 2,8-bis(diphenylphosphoryl)dibenzo[b,d]thiophene (PPT), which is a host material commonly used in OLEDs.[5] They found when the TMB concentration is low (1 mol%), the film can show LPL lasting for more than one hour after excited by low-power excitation at room temperature (Figure 1-11). The emission originates from the exciplex formed between TMB and PPT, but not from the phosphorescence of TMB or PPT. Moreover, the afterglow obeys a power-law but not an exponential law. Because both two features are similar to inorganic LPL, this is the first room-temperature OLPL material in the world. Comparing with previous low-temperature OLPL materials, the breakthrough in this research is two points: 1. the use of exciplex (CT exciton) to ease the charge separation (CS) process at room temperature due to the small binding energy of CT excitons compared to the Frenkel excitons in a low-temperature OLPL system.

Thus, CS can happen even by a weak excitation light source. 2. PPT as the electron acceptor and transport material possesses a lower electronic affinity than that of solvent glasses or polymers in low-temperature OLPL systems. This stabilizes PPT radical anions at room temperature with the enough HOMO-LUMO energy gap with TMB for efficient emission.

They also demonstrated the independence of OLPL performance to the fabrication methods: spin coating, thermally evaporating, and melt casting.[105] Moreover, a new OLPL system, *m*-MTDATA/PPT with 1.5-times improved LPL duration over the TMB/PPT system, was demonstrated due to the higher PLQY (32%, but 13% for TMB/PPT).

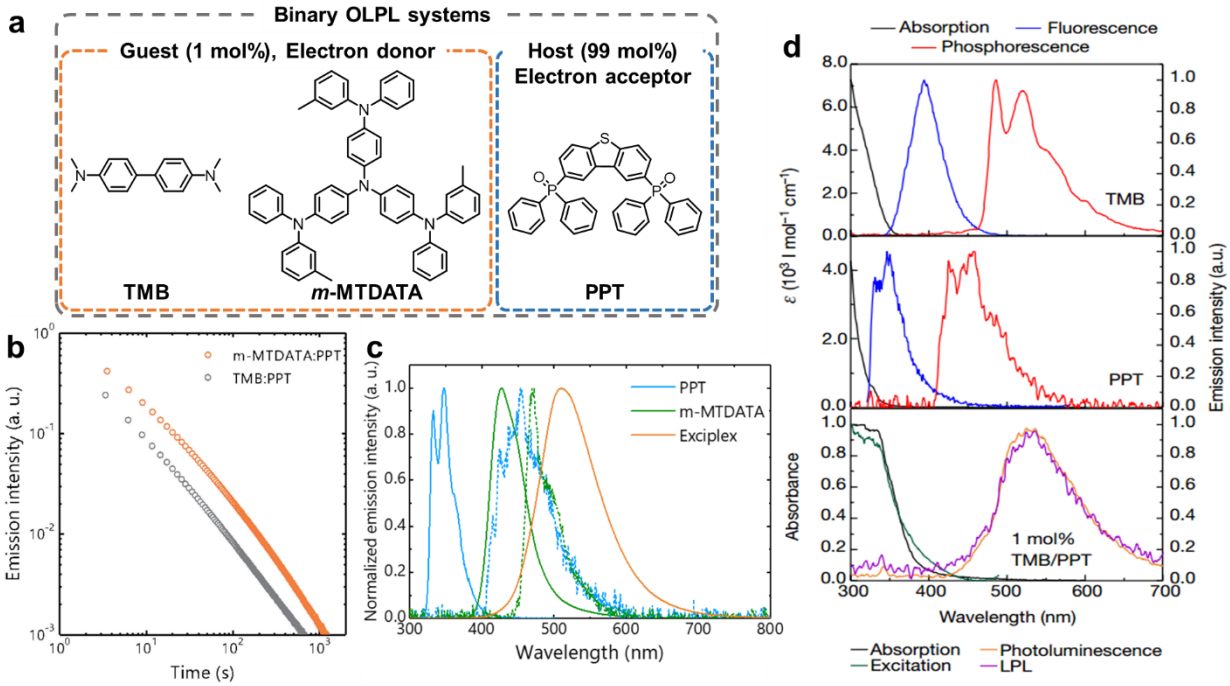

Figure 1-11. Binary room-temperature OLPL systems. (**a**) Material components and their chemical structures; (**b**) Logarithmic plot of the emission decay profile of a 1 mol% TMB/PPT and *m*-MTDATA/PPT melt-casting film (excited by 340 ± 5 nm LED, excitation power, 600μW; excitation time, 60 s; sample temperature, 300 K). The PL and OLPL spectra of *m*-MTDATA/PPT (**c**) and TMB/PPT (**d**). Adapted from Ref. 5, 105.

Multi-component OLPL systems were also reported to realize wide-range emission color tuning from greenish-blue to red and even warm white by Förster energy transfer (FRET)

strategy.[106] The additional emitter dopants also improve emission brightness and extend duration through efficient radiative decay and the trapping of electrons. This result means suitable carrier traps is also important to enhance OLPL systems as that in inorganic LPL systems.

1.4.4 Mechanism of Room-Temperature OLPL

The emission mechanism of OLPL is proposed based on the presence of TMB radical cations after photo-excitation (Figure 1-12 a).[5, 106] The exciplexes generated by a charge transfer between the photo-excited state of acceptor and donor dissociated to form partially charge-separated (CS) states, i.e., geminate radical ion pairs; Because the very low concentration of TMB in PPT, the separated electrons on PPT can hop among PPT molecules and difficultly recombine with the hole on TMB owing to the low probability; Finally, this slow charge recombination (CR) caused by continuous-time random walk of electrons in PPT leads to the LPL with a power-law emission decay at room temperature. Moreover, because of the small ΔE_{ST} of the exciplex, the generated triplet excitons on exciplex can convert to the singlet excitons of exciplex by the RISC process. Therefore, this system does not exhibit the phosphorescence of exciplex at room temperature.[63, 107]

For the ternary OLPL system (Figure 1-12 b), the extra emitter dopants play the role of traps and extend the lifetime of the charge-separated state. On the other hand, the emitter dopants will seize the excitation energy of exciplex by FRET after CR and emit self-fluorescence. Based on the TADF-assisted fluorescence mechanism[108], almost 100% excitons can be transferred to the emitter dopants and the highly efficient emission can be realized because the PLQY of the fluorescence emitter is higher than the exciplex.

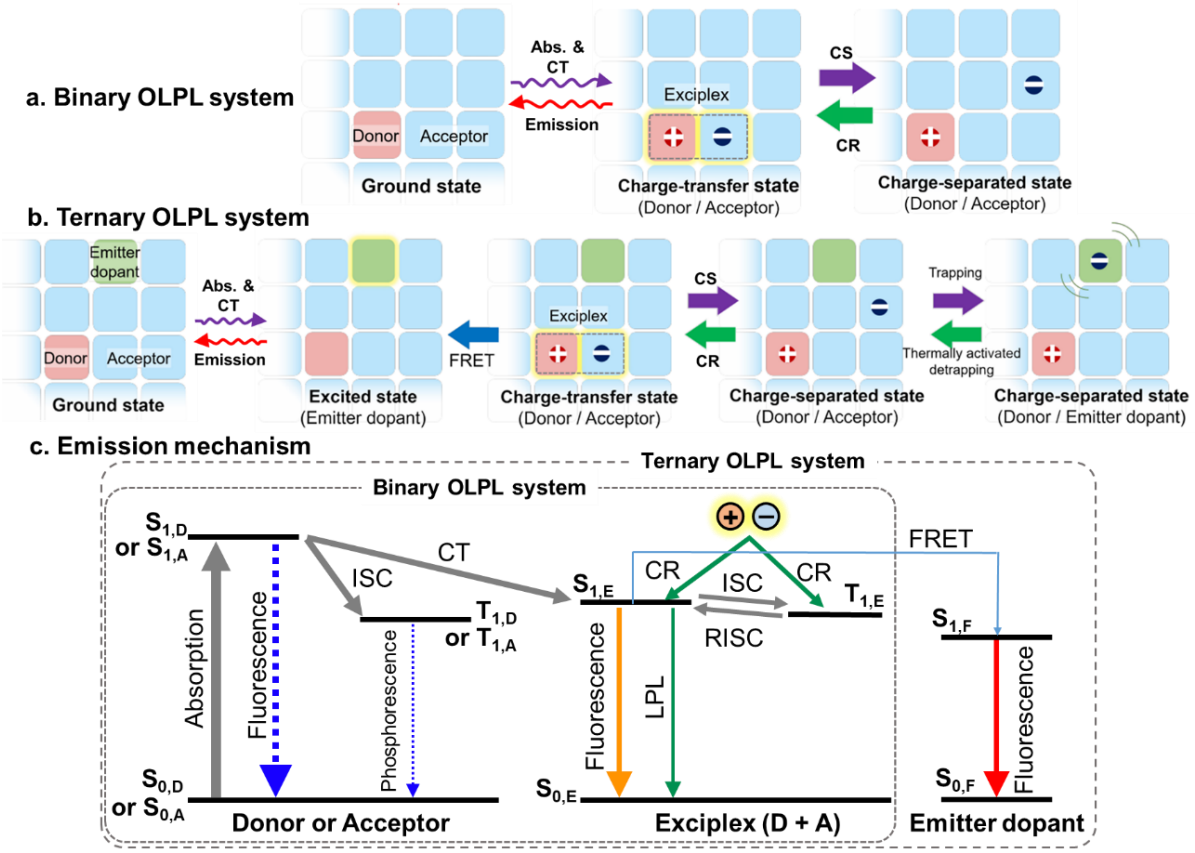

Figure 1-12. Mechanisms of room-temperature OLPL (**a**) in the binary system; (**b**) in the ternary system with emitter dopant; (**c**) Emission mechanisms. Adapted from Ref. 106.

1.4.5 Advantages of Room-Temperature OLPL Materials

Room-temperature OLPL materials have several advantages compared with inorganic LPL materials.

1. **Free of rare earth elements**. The commercial highly efficient inorganic LPL materials contain rare earth elements as activators or traps. Although the doping concentration is low, the mining and refining of rare earth elements always cause serious environmental consequences that are difficult to solve because the rare earth elements are a very low concentration in the environment.[109] If OLPL can replace inorganic LPL materials in the

future, this will save rare earth resources and reduce environmental pollution.

2. **Low fabrication temperature and even solution processing**. Inorganic LPL materials cannot dissolve in any common solvent and normally are prepared in a reducing atmosphere above 1000 ℃, which is a high energy consumption method.[1, 3] OLPL materials can be prepared by melt casting below 300 ℃ and even by the solution processing.[5, 105]

3. **High transparency, good polymer compatibility, and high flexibility potential (can develop into polymer)**. Inorganic LPL materials need to be ground into a powder and blended with a polymer in the majority of applications,[110]. The poor compatibility of the inorganic powders with common polymers results in poor dispersibility.[110, 111] Moreover, the particle size and uniformity of the inorganic powder affect the mechanical properties and transparency of the polymer composites,[110, 111] especially in polymer fibers and films with micrometer-scale diameters or thicknesses.[112] At present, these problems can only be partially solved by the surface treatment of the particles[113] and preparation of nanometer-scale inorganic LPL powders.[111] However, these approaches increase the complexity of the fabrication process and still cannot be used to achieve a transparent LPL system. Now, the OLPL materials show high transparency without scattering in the visual light range because of the mixing at the molecular level. As organic materials, OLPL materials can be also prepared by the blend with a polymer at the molecular level, and even we can design LPL polymers or copolymers.

4. **Mechanism analysis.** The mechanism of the inorganic LPL systems is still unclear because the valence states and redox processes of the dopants are difficult to identify due to the

fabrication-process dependency. For example, the Matsuzawa's model for $SrAl_2O_4:Eu^{2+},Dy^{3+}$ is criticized by Aitasalo[42], because the reduction of Eu^{2+} to Eu^{+} and the oxidation of Dy^{3+} to Dy^{4+} generate chemically unstable ions. In contrast, the organic molecule has an individual molecular structure that does not change by the processing. The detailed optoelectronic processes of organic materials are already discussed in organic semiconducting devices such as organic light-emitting diodes (OLEDs) and organic photovoltaics (OPVs).[59] These features of organic optoelectronic materials provide a clue to understand the LPL mechanism and kinetics.

1.4.6 Open Issues of OLPL

The present room-temperature OLPL systems, e.g., the TMB/PPT system, still faces some outstanding issues.

1. The existing binary OLPL systems exhibit only the green emission color, even though wide-range emission color tuning has been easily realized by the ternary OLPL system. The emission color adjustability of binary OLPL needs to be demonstrated. The emission color of binary OLPL systems restricts the color-tuning and emitter dopant selection of the ternary system because the FRET process requires a large overlap between the absorption of exciplexes and the fluorescence of emitter dopants. For example, pure blue emission failed to achieve by the ternary system owing to the green emission of exciplexes. Moreover, since many high-PLQY red and near-infrared emitters possess a small Stokes shift, the yellow to the red binary system will expand the range of emitter dopant selection in the ternary system.
2. The LPL duration is still much shorter than the current inorganic LPL materials. It is

necessary to clarify the detailed emission mechanism and explore the methods to extend the LPL duration.

3. The thick film of this OLPL system has poor flexibility because it consists of only small molecules. Thus, while it provides flexibility in very thin films, they are brittle and have cracks in the bulk state. Therefore, a flexible OLPL system is required for the development of future applications such as fibers, films, and curved products.
4. Because the OLPL system is oxygen-sensitive, improving the stability of the OLPL in the air by applying and further developing encapsulation techniques are necessary.

1.5 Motivation and Outline of This Thesis

The aim of this thesis is to improve the performance of OLPL systems together with tuning the emission color and improving the mechanical properties. Since the researches of room-temperature OLPL systems are still limited and the detailed OLPL mechanism is unknown, molecular design for efficient LPL performance is still difficult. Therefore, I developed new binary OLPL systems with different emission colors and LPL performance, and discovered the excited-states dynamics in OLPL systems. Moreover, I developed a polymer-based OLPL material with excellent flexibility and transparency.

Chapter 2 demonstrates an orange donor/acceptor binary OLPL system by replacing TMB with a low HOMO level donor. **Chapter 3** reports the detailed OLPL emission mechanism. I demonstrate that the energy gap between the lowest singlet excited-state of the exciplex and the donor's lowest triplet excited-state strongly affects OLPL performance, and the absorption of radical cation species generated by the charge separation process also influences the LPL

emission spectra. **Chapter 4** reports the first polymer-based OLPL system with good flexibility and transparency, in which the polymer I used here as an acceptor is a conventional engineering polymer. **Chapter 5** summarizes this thesis and discuss future perspectives.

1.6 References

1 J. Xu and S. Tanabe, *J. Lumin.*, **2019**, *205*, 581.
2 S. Wu, Z. Pan, R. Chen and X. Liu, *Long Afterglow Phosphorescent Materials*, Springer, Cham, ZG, Switzerland, **2017**.
3 T. Matsuzawa, Y. Aoki, N. Takeuchi and Y. Murayama, *J. Electrochem. Soc.*, **1996**, *143*, 2670.
4 T. Maldiney, A. Bessière, J. Seguin, E. Teston, S. K. Sharma, B. Viana, A. J. J. Bos, P. Dorenbos, M. Bessodes, D. Gourier, D. Scherman and C. Richard, *Nat. Mater.*, **2014**, *13*, 418.
5 R. Kabe and C. Adachi, *Nature*, **2017**, *550*, 384.
6 S. Shionoya, W. M. Yen and H. Yamamoto, *Phosphor Handbook*, CRC Press, Boca Raton, FL, USA, **2018**.
7 M. Kasha, *Chem. Rev.*, **1947**, *41*, 401.
8 A. D. Sontakke, A. Ferrier, P. Burner, V. F. Guimarães, M. Salaün, V. Maurel, I. Gautier-Luneau, A. Ibanez and B. Viana, *J. Phys. Chem. Lett.*, **2017**, *8*, 4735.
9 P. F. Smet, D. Poelman and M. P. Hehlen, *Opt. Mater. Express*, **2012**, *2*, 452.
10 E. N. Harvey, *A history of luminescence from the earliest times until 1900*, American Philosophical Society, Philadelphia, **1957**.
11 W. M. Yen and M. J. Weber, *Inorganic Phosphors: Compositions, Preparation and Optical Properties*, CRC Press, **2004**.
12 J. Hölsä, *Electrochem. Soc. Interface*, **2009**, *18*, 42.
13 M. Lastusaari, T. Laamanen, M. Malkamäki, K. O. Eskola, A. Kotlov, S. Carlson, E. Welter, H. F. Brito, M. Bettinelli, H. Jungner and J. Hölsä, *Eur. J. Mineral.*, **2012**, *24*, 885.
14 T. Sidot, *Comptes rendus de l'Académie des sciences*, **1866**, *63*, 188.
15 W. Hoogenstraaten and H. Klasens, *J. Electrochem. Soc.*, **1953**, 100, 366.
16 H. Klasens, *J. Electrochem. Soc.*, **1953**, 100, 72.
17 E. B. Goldstein, *Sensation and Perception*, Cengage Learning, **2009**.
18 D. Poelman, N. Avci and P. F. Smet, *Opt. Express*, **2009**, *17*, 358.
19 Y. Lin, Z. Tang, Z. Zhang, X. Wang and J. Zhang, *J. Mater. Sci. Lett.*, **2001**, *20*, 1505.
20 K. Van den Eeckhout, P. F. Smet and D. Poelman, *Materials*, **2010**, *3*, 2536.
21 P. F. Smet, I. Moreels, Z. Hens and D. Poelman, *Materials*, **2010**, *3*, 2834.
22 P. F. Smet, J. Botterman, K. Van den Eeckhout, K. Korthout and D. Poelman, *Opt. Mater.*, **2014**, *36*, 1913.
23 K. Van den Eeckhout, D. Poelman and P. Smet, *Materials*, **2013**, *6*, 2789.
24 Y. Li, M. Gecevicius and J. Qiu, *Chem. Soc. Rev.*, **2016**, *45*, 2090.
25 Y. Zhuang, Y. Katayama, J. Ueda and S. Tanabe, *Opt. Mater.*, **2014**, *36*, 1907.
26 X. Wang, Z. Zhang, Z. Tang and Y. Lin, *Mater. Chem. Phys.*, **2003**, *80*, 1.
27 S. Yuan, Y. Yang, B. Fang and G. Chen, *Opt. Mater.*, **2007**, *30*, 535.

28 I. Norrbo, J. M. Carvalho, P. Laukkanen, J. Mäkelä, F. Mamedov, M. Peurla, H. Helminen, S. Pihlasalo, H. Härmä, J. Sinkkonen and M. Lastusaari, *Adv. Funct. Mater.*, **2017**, *27*, 1606547.
29 H. Yamamoto and T. Matsuzawa, *J. Lumin.*, **1997**, *72-74*, 287.
30 J. Ueda, *J. Ceram. Soc. Jpn.*, **2015**, *123*, 1059.
31 J. Ueda, K. Kuroishi and S. Tanabe, *Appl. Phys. Lett.*, **2014**, *104*, 101904.
32 H. Luo and P. Dorenbos, *J. Mater. Chem. C*, **2018**, *6*, 4977.
33 T. Lyu and P. Dorenbos, *J. Mater. Chem. C*, **2018**, *6*, 6240.
34 N. Suriyamurthy and B. S. Panigrahi, *J. Lumin.*, **2008**, *128*, 1809.
35 X.-J. Wang, D. Jia and W. M. Yen, *J. Lumin.*, **2003**, *102-103*, 34.
36 Y. Wang and Z. Wang, *J. Rare Earths*, **2006**, *24*, 25.
37 W. Chen, Y. Wang, W. Zeng, S. Han, G. Li, H. Guo, Y. Li and Q. Qiang, *New J. Chem.*, **2016**, *40*, 485.
38 F. Liu, W. Yan, Y.-J. Chuang, Z. Zhen, J. Xie and Z. Pan, *Sci. Rep.*, **2013**, *3*, 1554.
39 Z. Pan, Y.-Y. Lu and F. Liu, *Nat. Mater.*, **2012**, *11*, 58.
40 Y. Liang, F. Liu, Y. Chen, X. Wang, K. Sun and Z. Pan, *Dalton Trans.*, **2017**, *46*, 11149.
41. F. Clabau, X. Rocquefelte, S. Jobic, P. Deniard, M.-H. Whangbo, A. Garcia and T. Le Mercier, *Solid State Sci.*, **2007**, 9, 608.
42 T. Aitasalo, P. Dereń, J. Hölsä, H. Jungner, J. C. Krupa, M. Lastusaari, J. Legendziewicz, J. Niittykoski and W. Stręk, *J. Solid State Chem.*, **2003**, *171*, 114.
43 F. C. Palilla, A. K. Levine and M. R. Tomkus, *J. Electrochem. Soc.*, **1968**, *115*, 642.
44 D. Jia and W. M. Yen, *J. Lumin.*, **2003**, *101*, 115.
45 J. Trojan-Piegza, J. Niittykoski, J. Hölsä and E. Zych, *Chem. Mater.*, **2008**, *20*, 2252.
46 M. P. H. Stumpf and M. A. Porter, *Science*, **2012**, *335*, 665.
47 S. M. Ross, *Introduction to Probability and Statistics for Engineers and Scientists*, Elsevier Science, San Diego, California, USA, **2009**.
48 M. E. J. Newman, *Contemp. Phys.*, **2005**, *46*, 323.
49 ISO, 16069, **2017**.
50 JIS, Z9107, **2008**.
51 R. Chen and S. W. S. McKeever, *Theory of Thermoluminescence and Related Phenomena*, World Scientific, Singapore, **1997**.
52 M. Martini and F. Meinardi, *La Rivista del Nuovo Cimento*, **1997**, *20*, 1.
53 J. T. Randall and M. H. F. Wilkins, *Proc. R. Soc. A-Math. Phy.*, **1945**, *184*, 390.
54 G. F. J. Garlick and A. F. Gibson, *Proc. Phys. Soc.*, **1948**, *60*, 574.
55 C. E. May and J. A. Partridge, **1964**, *40*, 1401.
56 K. Van den Eeckhout, A. J. J. Bos, D. Poelman and P. F. Smet, *Phys. Rev. B*, **2013**, *87*, 045126.
57 J. Chu-Shore, M. B. Westover and M. T. Bianchi, *PLoS One*, **2010**, *5*, e14204.
58 E. V. Anslyn and D. A. Dougherty, *Modern Physical Organic Chemistry*, University Science Books, Sausalito, California, **2006**.
59 A. Köhler, H. Bässler, *Electronic Processes in Organic Semiconductors*, Wiley-VCH, Weinheim, Germany, **2015**.
60 V. Balzani, P. Ceroni and A. Juris, *Photochemistry and Photophysics: Concepts, Research, Applications*, Wiley-VCH, Weinheim, Germany, **2014**.
61 C. Adachi, *Jpn. J. Appl. Phys.*, **2014**, *53*, 060101.
62 H. Uoyama, K. Goushi, K. Shizu, H. Nomura and C. Adachi, *Nature*, **2012**, *492*, 234.

63 K. Goushi, K. Yoshida, K. Sato and C. Adachi, *Nat. Photonics*, **2012**, *6*, 253.
64 S. Hirata, *Adv. Opt. Mater.*, **2017**, *5*, 1700116.
65 Kenry, C. Chen and B. Liu, *Nat. Commun.*, **2019**, *10*, 2111.
66 C. S. Bilen, N. Harrison and D. J. Morantz, *Nature*, **1978,** *271*, 235.
67 D. B. Clapp, *J. Am. Chem. Soc.*, **1939**, *61*, 523.
68 G. Zhang, J. Chen, S. J. Payne, S. E. Kooi, J. N. Demas and C. L. Fraser, *J. Am. Chem. Soc.*, **2007**, *129*, 8942.
69 L. J. C. Love, M. Skrilec and J. G. Habarta, *Anal. Chem.*, **1980**, *52*, 754.
70 N. J. Turro and M. Aikawa, *J. Am. Chem. Soc.*, **1980**, *102*, 4866.
71 S. Scypinski and L. J. C. Love, *Anal. Chem.*, **1984**, *56*, 322.
72 P. Wei, J. Liu, G.-G. Shan, X. Zhang, H. Zhang, J. Qi, W. Zhao, H. H.-Y. Sung, I. D. Williams, J. W. Y. Lam and B. Z. Tang, *Angew. Chem. Int. Ed.*, **2019**, doi:10.1002/anie.201912155.
73 H. Mieno, R. Kabe, N. Notsuka, M. D. Allendorf and C. Adachi, *Adv. Opt. Mater.*, **2016**, *4*, 1015.
74 S. d'Agostino, F. Spinelli, P. Taddei, B. Ventura and F. Grepioni, *Cryst. Growth Des.*, **2019**, *19*, 336.
75 Z. An, C. Zheng, Y. Tao, R. Chen, H. Shi, T. Chen, Z. Wang, H. Li, R. Deng, X. Liu and W. Huang, *Nat. Mater.*, **2015**, *14*, 685.
76 E. Lucenti, A. Forni, C. Botta, L. Carlucci, C. Giannini, D. Marinotto, A. Previtali, S. Righetto and E. Cariati, *J. Phys. Chem. Lett.*, **2017**, *8*, 1894.
77. S. Cai, H. Ma, H. Shi, H. Wang, X. Wang, L. Xiao, W. Ye, K. Huang, X. Cao, N. Gan, C. Ma, M. Gu, L. Song, H. Xu, Y. Tao, C. Zhang, W. Yao, Z. An and W. Huang, *Nat. Commun.*, **2019**, 10, 4247.
78 S. Cai, H. Shi, D. Tian, H. Ma, Z. Cheng, Q. Wu, M. Gu, L. Huang, Z. An, Q. Peng and W. Huang, *Adv. Funct. Mater.*, **2018**, *28*, 1705045.
79 S. Cai, H. Shi, Z. Zhang, X. Wang, H. Ma, N. Gan, Q. Wu, Z. Cheng, K. Ling, M. Gu, C. Ma, L. Gu, Z. An and W. Huang, *Angew. Chem. Int. Ed.*, **2018**, *57*, 4005.
80 T. Ogoshi, H. Tsuchida, T. Kakuta, T.-a. Yamagishi, A. Taema, T. Ono, M. Sugimoto and M. Mizuno, *Adv. Funct. Mater.*, **2018**, *28*, 1707369.
81 K. Seki, Y. Sonoda and R. Katoh, *J. Phys. Chem. C*, **2018**, *122*, 11659.
82 H. Linschitz, M. G. Berry and D. Schweitzer, *J. Am. Chem. Soc.*, **1954**, *76*, 5833.
83 J. Mayer, J. Kuriata and J. Kroh, *J. Radioanal. Nucl. Chem.*, **1986**, *97*, 65.
84 H. Ohkita, W. Sakai, A. Tsuchida and M. Yamamoto, *Macromolecules*, **1997**, *30*, 5376.
85 G. N. Lewis and D. Lipkin, *J. Am. Chem. Soc.*, **1942**, *64*, 2801.
86 G. N. Lewis and J. Bigeleisen, *J. Am. Chem. Soc.*, **1943**, *65*, 2419.
87 G. N. Lewis and J. Bigeleisen, *J. Am. Chem. Soc.*, **1943**, *65*, 2424.
88 J. B. Gallivan and W. H. Hamill, *J. Chem. Phys.*, **1966**, *44*, 2378.
89 J. E. Willard, *Science*, **1973,** *180*, 553.
90 A. C. Albrecht, *Acc. Chem. Res.*, **1970**, *3*, 238.
91 E. Dolan and A. C. Albrecht, **1962**, *37*, 1149.
92 V. G. Nikolskii and N. Y. Buben, *Doklady Akad. Nauk S.S.S.R.*, **1960**, *134*, 134.
93 V. G. Nikolskii, L. Y. Zlatkevich, V. A. Borisov and M. Y. Kaplunov, *J. Polym. Sci. Polym. Phys.*, **1974,** *12*, 1259.
94 H. Ohkita, W. Sakai, A. Tsuchida and M. Yamamoto, *J. Phys. Chem. B*, **1997**, *101*, 10241.
95 Y. Hama, Y. Kimura, M. Tsumura and N. Omi, *Chem. Phys.*, **1980**, *53*, 115.

96 Y. Hama and K. Gouda, *Radiat. Phys. Chem.*, **1983**, *21*, 185.
97 P. Debye and J. O. Edwards, *J. Chem. Phys.*, **1952**, *20*, 236.
98 G. C. Abell and A. Mozumder, *J. Chem. Phys.*, **1972**, *56*, 4079.
99 K. M. Hong and J. Noolandi, *J. Chem. Phys.*, **1978**, *68*, 5163.
100 F. Stolzenburg, B. Ries and H. Bässler, *Ber. Bunsen-Ges. Phys. Chem.*, **1987,** *91*, 853.
101 W. H. Hamill and K. Funabashi, *Phys. Rev. B*, **1977**, *16*, 5523.
102 F. Kieffer, C. Meyer and J. Rigaut, *Chem. Phys. Lett.*, **1971**, *11*, 359.
103 F. Kieffer, C. Lapersonne-Meyer and J. Rigaut, *Int. J. Radiat. Phys. Chem.*, **1974**, *6*, 79.
104 M. Tachiya and A. Mozumder, *Chem. Phys. Lett.*, **1975**, *34*, 77.
105 K. Jinnai, N. Nishimura, R. Kabe and C. Adachi, *Chem. Lett.*, **2019,** *48*, 270.
106 K. Jinnai, R. Kabe and C. Adachi, *Adv. Mater.*, **2018**, *30*, 1800365.
107 K. Goushi and C. Adachi, *Appl. Phys. Lett.*, **2012**, *101*, 023306.
108 H. Nakanotani, T. Higuchi, T. Furukawa, K. Masui, K. Morimoto, M. Numata, H. Tanaka, Y. Sagara, T. Yasuda and C. Adachi, *Nat. Commun.*, **2014**, *5*, 4016.
109 S. H. Ali, *Resources*, **2014**, *3*, 123.
110 M. P. Anesh, S. K. H. Gulrez, A. Anis, H. Shaikh, M. E. Ali Mohsin and S. M. Al-Zahrani, *Adv. Polym. Tech.*, **2014**, *33*, 21436.
111 R. E. Rojas-Hernandez, F. Rubio-Marcos, M. Á. Rodriguez and J. F. Fernandez, *Renewable Sustainable Energy Rev.*, **2018**, *81*, 2759.
112 F. Ye, S. Dong, Z. Tian, S. Yao, Z. Zhou and S. Wang, *Opt. Mater.*, **2013**, *36*, 463.
113 X. Zhang, Z. Zhou, F. Ye, X. Liu and Q. Li, *Mater. Sci. Semicond. Process.*, **2015**, *40*, 130.

Chapter 2

Orange Organic Long-persistent Luminescence from an Electron Donor/Acceptor Binary System

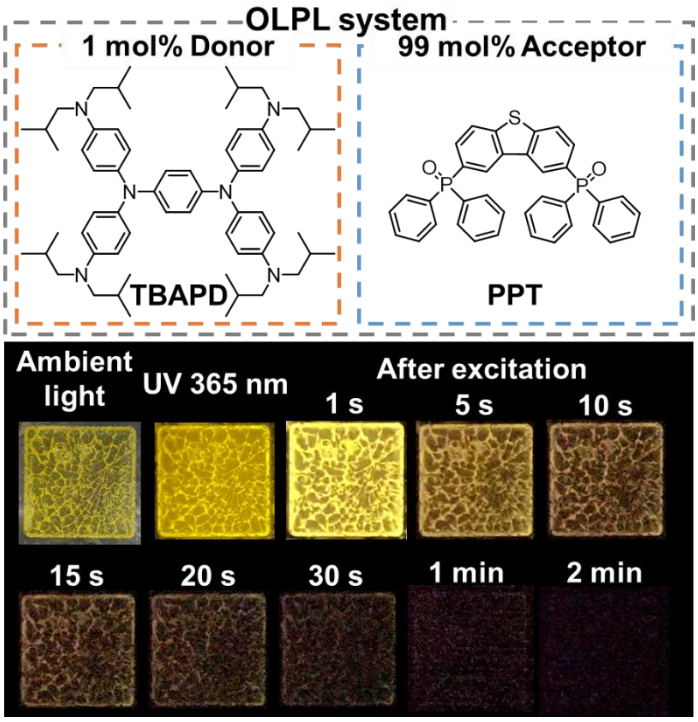

2.1 Introduction

Long-persistent luminescence (LPL) materials, also known as glow-in-the-dark or afterglow materials, are widely used in emergency signs, watch indicators, safety way guidance, and afterglow toys.[1-4] Glow-in-the-dark materials have a long history of usage, and LPL materials have been commonly used since Matsuzawa et al. developed a strontium aluminate-based LPL material in the 1990s.[4] Many commercial high-performance LPL materials are made from metal oxides doped with rare earth elements such as europium and dysprosium.[1] These inorganic LPL materials need high fabrication temperatures of over 1000 ℃ and to be ground into powders and blended with polymers for the majority of their applications.[1,6,7]

In 2017, Kabe et al. reported the first genuine organic LPL (OLPL) system consisting of an electron donor *N,N,N′,N′*-tetramethylbenzidine (TMB) and an electron acceptor *2,8*-bis(diphenylphosphoryl)dibenzo[b,d]thiophene (PPT).[8] This TMB/PPT blend film exhibits LPL for over one hour at room temperature when the concentration of the donor is low (1 mol%). The LPL emission originates from the excited state complex (exciplex) generated by the slow recombination of long-lived intermediate charge-separated (CS) states (Figure 2-1a). Initially, charge transfer (CT) excited states ($D^{\delta+} + A^{\delta-}$) are formed between the donor (D) and acceptor (A) during photo-excitation. Although most of the CT excited states exhibit photoluminescence after turn-off of the photoexcitation, some electrons on acceptors diffuse to surrounding acceptor molecules and form stable charge-separated states ($D^{+} + A^{\cdot}$). Gradual recombination of the electrons on the acceptor and holes on the donor continuously generates CT excited states, so the photoluminescence continues for a very long time. The TMB/PPT film exhibits green LPL emission because the exciplex emission corresponds to a transition from the lowest

unoccupied molecular orbital (LUMO) level of the acceptor to the highest occupied molecular orbital (HOMO) level of the donor. Although the donor-acceptor distance and molecular conformations affect the exciplex emission, the HOMO-LUMO gap play a decisive role in the exciplex emission in the amorphous solid-state. A linear correlation between the exciplex emission peak and the energy gap between the oxidation potential of donors and the reduction potential of acceptors ($E_{A,LUMO} - E_{D,HOMO}$) is reported[9-12] and the HOMO and LUMO levels can be calculated from the oxidation and reduction potentials.[13,14]The LPL emission decay profile follows power-law decay, and the emission intensity at time *t* is given by $I(t) \sim t^{-m}$, with m ≈ 1.[15-19] This power-law emission decay differs from general room-temperature phosphorescence which exhibits exponential emission decay.[20-28]

Our group also reported several electron donor/acceptor binary OLPL systems such as *m*-MTDATA/PPT[29] and polymer-based TMB/PBPO.[7] However, these binary OLPL systems exhibit green emission. Other emission-color systems have not been reported. Later, we also achieved wide-range emission-color tuning from greenish-blue to red and even warm white by energy transfer from the TMB/PPT exciplex to additional emitter dopants.[30] The color-tuning of the binary OLPL system is important because the photo-absorption process is controlled by the donor or acceptor molecules. A large overlap between the exciplex emission and the extra dopant absorption is required for efficient energy transfer.

In this chapter, I report orange LPL emission from a donor/acceptor binary system. To obtain a longer emission wavelength from the exciplex, we adjusted the HOMO level of the donor from that of TMB. Specifically, *N*,*N*,*N'*,*N'*-tetra(*4*-tolyl)-*1*,*4*-phenylenediamine (TTPD) and *N,N,N',N'*-tetrakis[(4-(diisobutylamino)phenyl]-*1*,*4*-phenylenediamine (TBAPD) (Figure

2-1b) are used as donors in this study. The TTPD/PPT film exhibits green LPL emission that continues for about one hour. The TBAPD/PPT film exhibits orange LPL that continues for approximately 5 minutes.

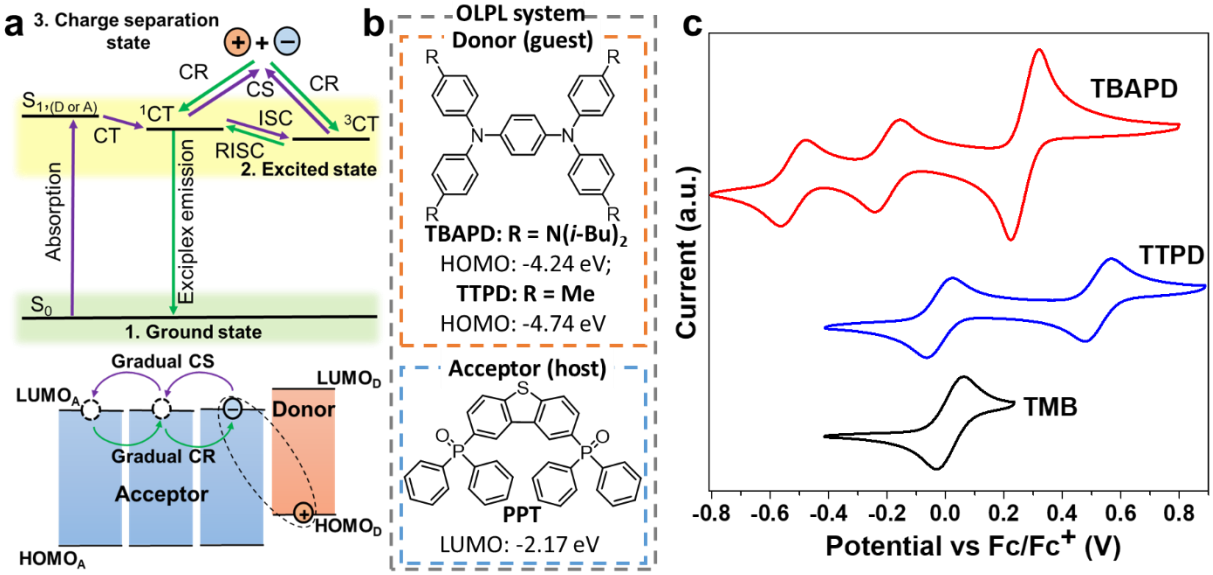

Figure 2-1. (a) Emission mechanism of an OLPL. The dashed cycle represents the charge transfer (CT) exciton of the exciplex. Abbreviations of electron donor (D), acceptor (A), lowest singlet excited state of donor or acceptor ($S_{1,\ (D\ or\ A)}$), CT singlet (^{1}CT) and triplet excited state (^{3}CT), intersystem crossing (ISC), reverse intersystem crossing (RISC), charge separation (CS), and charge recombination (CR) are used. **(b)** Chemical structures of the electron donors (TTPD and TBAPD) and electron acceptor (PPT) and their corresponding HOMO or LUMO levels. (**c**) CV curves of TMB, TTPD, and TBAPD.

2.2 Results and discussion

TTPD was synthesized by Buchwald-Hartwig coupling and PPT was synthesized according to the literature.[31] TBAPD was obtained from TCI chemicals (Tokyo, Japan). All samples were purified by train sublimation. The 0.4 mm-thick TTPD/PPT and TBAPD/PPT films for the optical measurements were prepared by the melt-casting method as reported previously.[30] Thin films for the UV-vis absorption measurements were fabricated by sandwiching the heat-melted materials between two quartz substrates. The concentration of the donor was 1 mol% for all films, according to the previous publication.[8]

To achieve a longer emission wavelength, a shallower HOMO level of the donor is required. Therefore, we introduced electron-donating diisobutylamino substitutions into the *N*,*N*,*N'*,*N'*-tetraphenyl-*1*,*4*-phenylenediamine core, and tetramethyl substitutions are used as the reference. The HOMO levels were calculated to be −4.78 eV (TMB), −4.74 eV (TTPD), and −4.24 eV (TBAPD) from the first oxidation potential of cyclic voltammograms. Although the TBAPD and TTPD exhibit multi oxidation potentials, only the first oxidation potential is important to discuss the LPL emission since the system generates the radical cation of donors and the radical anion of acceptors after the photoexcitation. The LUMO level of PPT is −2.17 eV,[30] and the $E_{\mathrm{A,LUMO}} - E_{\mathrm{D,HOMO}}$ of the donor/acceptor systems were calculated to be 2.61 eV (TMB/PPT), 2.57 eV (TTPD/PPT), and 2.07 eV (TBAPD/PPT). The energy gap of 2.07 eV corresponds to emission at 599 nm, so TBAPD/PPT should exhibit yellow to orange emission.

UV-vis absorption and photoluminescence spectra of TTPD and TBAPD (toluene solutions), and PPT, TTPD/PPT, and TBAPD/PPT films are shown in Figure 2-2. LPL spectra of these two blend films are also shown. The absorption of the two blend films is the sum of the absorption of PPT and the corresponding donor and could not observe clear CT absorption under the present conditions. Thus, the charge-transfer interaction at the ground state is almost negligible. The absorption of the two blend films is the sum of the absorption of PPT and the corresponding donor. Thus, there is no clear charge-transfer interaction at the ground state. In contrast, the TTPD/PPT and TBAPD/PPT films exhibit broad emission peak maxima at 506 nm and 579 nm, respectively. These peak maxima are significantly redshifted compared with the fluorescence and phosphorescence of PPT and the corresponding donor. These emission peaks clearly indicate that the emission of the two blend films originates from the exciplex. The

LPL spectra are slightly redshifted and broader than the corresponding steady-state photoluminescence spectra. This may be because of the reorganization of the emitters at the excited states.

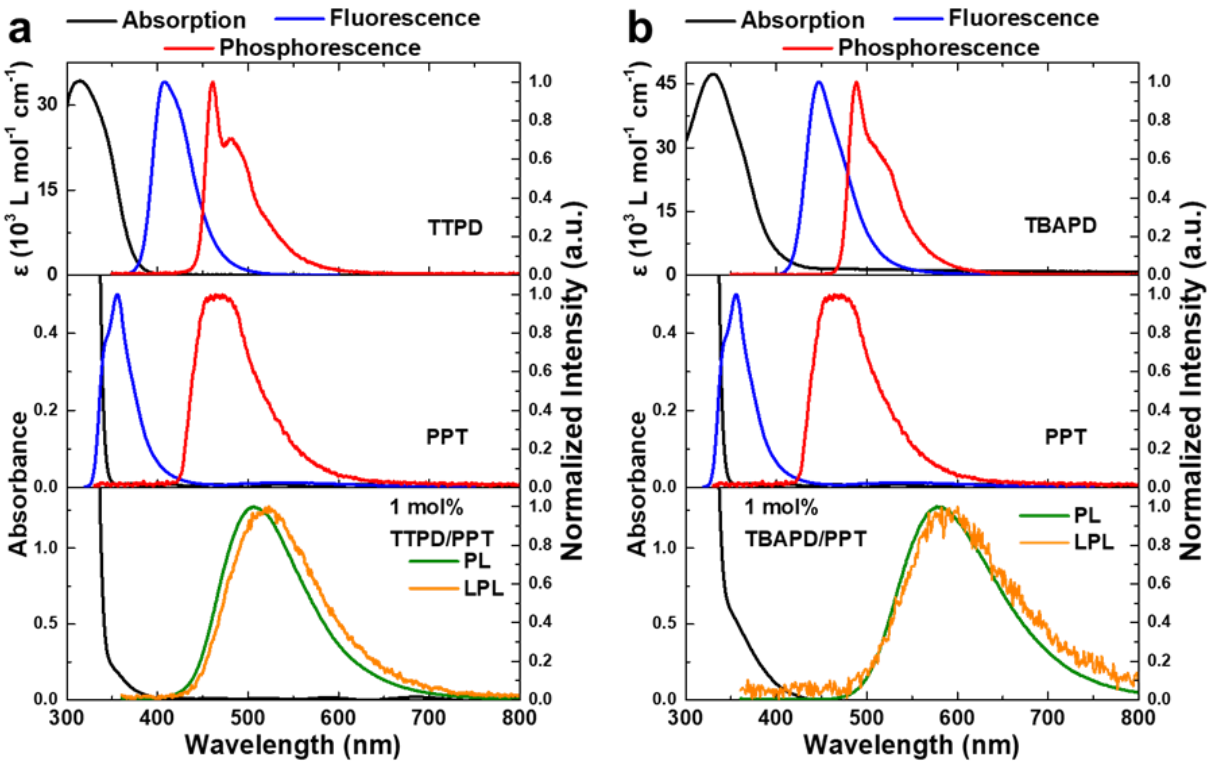

Figure 2-2. (a), (b) UV–vis absorption and photoluminescence spectra of TTPD and TBAPD in toluene (top), PPT film (middle), and 1 mol% TTPD/PPT and TBAPD/PPT films (bottom). The phosphorescence spectra were obtained at 77 K. The photoluminescence (PL) and LPL spectra of 1 mol% TTPD/PPT and TBAPD/PPT films were obtained at 300 K.

The photoluminescence peak maxima of the TTPD/PPT and TBAPD/PPT systems are at 506 nm and 579 nm, corresponding to energy gaps of 2.45 eV and 2.14 eV, respectively. These values show good agreement with the $E_{A,LUMO} - E_{D,HOMO}$ determined from the CV curves. As expected, the TTPD/PPT system exhibits green photoluminescence ($CIE_{x,y}$: 0.26, 0.46) and LPL ($CIE_{x,y}$: 0.31, 0.50), and the TBAPD/PPT system exhibits orange photoluminescence ($CIE_{x,y}$: 0.49, 0.49) and LPL ($CIE_{x,y}$: 0.51, 0.48), as shown in Figure 2-3.

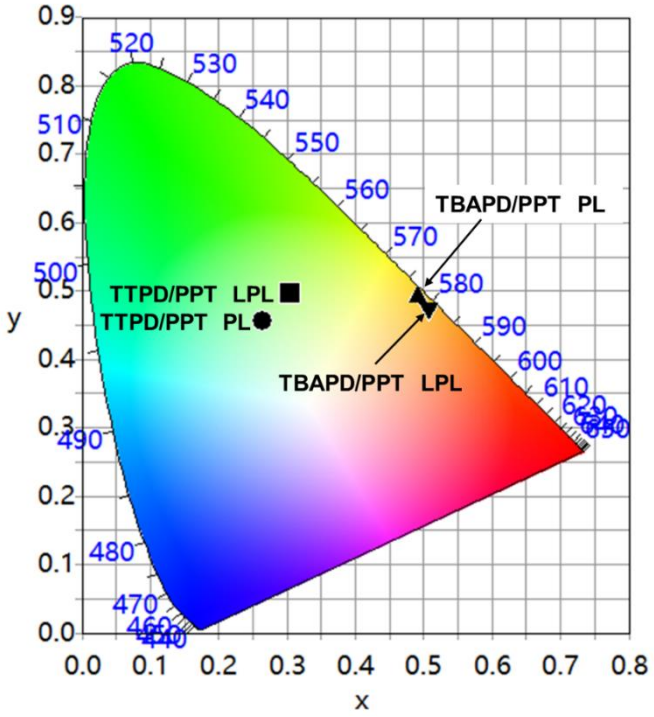

Figure 2-3. CIE 1931 coordinates of photoluminescence (PL) and LPL color of 1 mol% TTPD/PPT and 1mol% TBAPD/PPT film.

The LPL emission decay profiles of 1 mol% TMB/PPT, TTPD/PPT, and TBAPD/PPT blend films under the same excitation conditions are shown in Figure 2-4. After stopping the photo-excitation, all films exhibit LPL emission with a power-law decay profile at room temperature. The 1 mol% TBAPD/PPT film exhibits orange LPL emission, which can be recorded for several minutes using a charge-coupled-device camera. Owing to the very thick film of 0.4 nm, several cracks formed during the rapid cooling process.

Because the photoluminescence quantum yields (Φ_{PL}) measured under nitrogen atmosphere were 16% (TBAPD/PPT), 24% (TMB/PPT) and 41% (TTPD/PPT), the study-state PL intensities under photoexcitation shows the same order. In contrast, the LPL duration of TMB/PPT and TTPD/PPT films are almost identical, although the TTPD/PPT film exhibits a higher Φ_{PL}. Because the final emission comes from the exciplex, the Φ_{PL} is important for LPL emitters. However, emission in the OLPL system occurs through charge separation process

from the CT state to the CS state, charge retention in the CS state, and charge recombination process from the CS state to the CT state. Thus, differences such as charge separation probability from the CT state to the CS state between the TMB/PPT and TTPD/PPT films may lead to the difference between the LPL duration and Φ_{PL}.

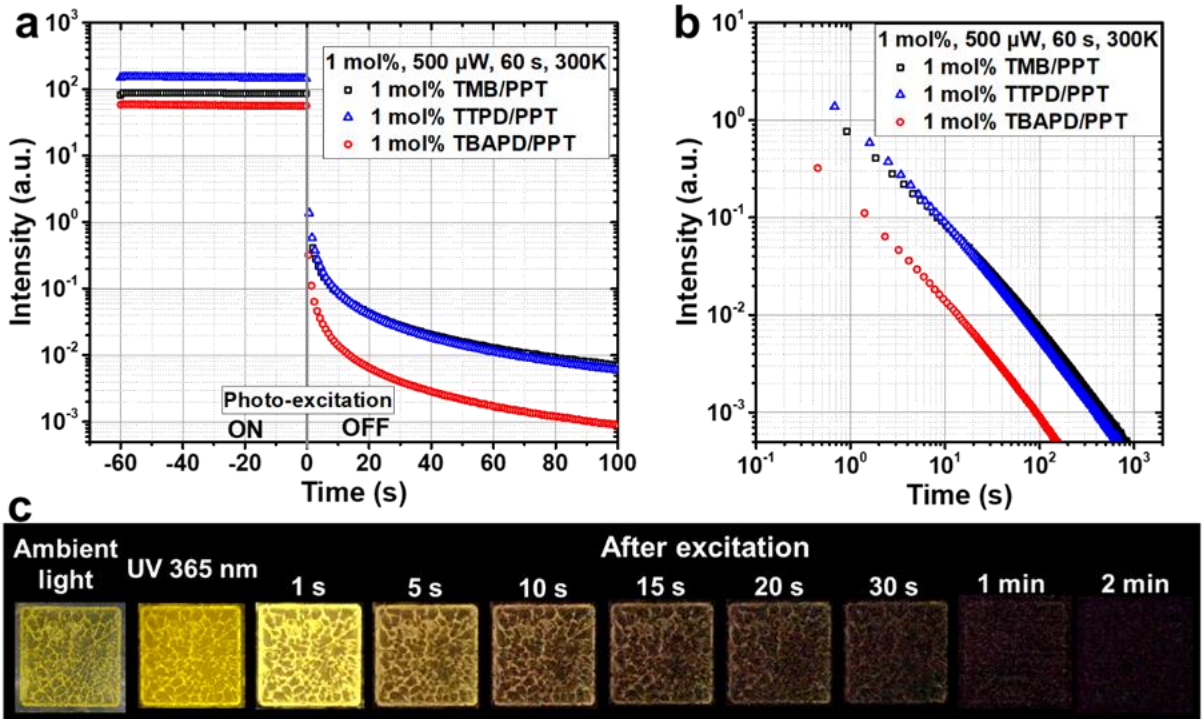

Figure 2-4. (a), (b) Semi-logarithmic plots (a) and logarithmic plots (b) of the emission decay profiles of TMB/PPT, TTPD/PPT, and TBAPD/PPT at 300 K. Samples were excited for 60 s (from −60 to 0 s) by a 340-nm LED source. “PL” means the steady-state photoluminescence, “LPL” means the long-persistent luminescence. **(c)** Photographs of a 1 mol% TBAPD/PPT thick film at room temperature under the ambient light, during excitation by a 365-nm UV lamp, and at various times after turning off the excitation.

2.3 Summary

In conclusion, I demonstrated orange LPL emission from the donor/acceptor binary system, TBAPD/PPT, by tuning the HOMO level of the donor. In contrast, TTPD possesses a similar HOMO level with TMB, so the TTPD/PPT and TMB/PPT blend films both exhibit

green LPL emission. This approach will enable control of the LPL emission color of the donor/acceptor binary system.

2.4 Experimental

Materials: TTPD was synthesized by Buchwald-Hartwig coupling and PPT was synthesized according to the literature. TBAPD was obtained from TCI chemicals (Tokyo, Japan). All samples were purified by train sublimation.

Synthesis of *N,N,N',N'*-tetra-4-tolyl-1,4-phenylenediamine (TTPD): A mixture of *1,4*-diiodobenzine (2.00 g, 6.06 mmol), *4,4'*-ditolyldiphenylamine (2.99 g, 15.16 mmol), $Pd(OAc)_2$ (27.2 mg, 0.12 mmol), $HP(tBu)_3BF_4$ (35.2 mg, 0.12 mmol) and NaO*t*Bu (2.04 g, 21 mmol) was refluxed overnight in 45 mL of dry degassed toluene under argon. After cooling to room temperature, the mixture was poured into water, extracted with CH_2Cl_2, washed with water, and then dried with Na_2SO_4. A pinkish-white product was obtained by column chromatography under dark conditions using $CHCl_3$:hexane = 1:3 as the eluent (2.50 g, 88% yield). A light-yellow product was obtained after purification by train-sublimation. ^{1}H NMR (500 MHz, $CDCl_3$) δ 7.04 (d, *J* = 8.2 Hz, 2H), 6.97 (d, *J* = 8.3 Hz, 2H), 6.91 (s, 1H), 2.29 (s, 3H) ppm; ^{13}C NMR (126 MHz, $CDCl_3$) δ 145.59, 142.70, 131.73, 129.73, 124.58, 123.77, 20.76 ppm. APCI-MS *m*/*z*: 468.93 $[M]^+$.

Characterization: ^{1}H NMR and ^{13}C NMR spectra were recorded with a Bruker AVANCE III 500 MHz spectrometer. Molecular weight was measured in positive-ion atmospheric-pressure chemical ionization mode on a Waters 3100 mass detector (APCI-MS). Film thicknesses were measured in five different positions on each film using a micrometer screw gauge, and reported values are averages of these five measurements. Cyclic voltammetry (CV) curves were recorded using an electrochemical analyzer (Model 608D+DPV, BAS). Measurements were performed in dried and oxygen-free CH_2Cl_2 for the HOMO using 0.1 M tetrabutylammonium hexafluorophosphate ($TBAPF_6$) as a supporting electrolyte. A platinum fiber was used as a working electrode, glassy carbon as a counter electrode, and Ag/Ag^+ as a reference electrode. Redox potentials were referenced against ferrocene/ferrocenium (Fc/Fc^+). The HOMO and LUMO energy levels of TMB, TTPD, and TBAPD were calculated according to the equation: E_{HOMO} (or E_{LUMO}) = − [$E_{onset,ox}$ (or $E_{onset,red}$) + 4.78 V], where $E_{onset,ox}$ and $E_{onset,red}$ are the peaks of the oxidation and reduction potentials, respectively.

Optical measurements: Absorption spectra were recorded on a UV-vis-NIR spectrophotometer (LAMBDA 950, Perkin Elmer). Photoluminescence spectra in air were recorded on a spectrofluorometer (FP-8600, JASCO). Phosphorescence spectra at 77 K were recorded on a multi-channel spectrometer (PMA-12, Hamamatsu Photonics) excited using a 340-nm LED (M340L4, Thorlabs) with a band pass filter (340 ± 5 nm). Absolute photoluminescence quantum yields (Φ_{PL}) were measured using a quantum yield spectrometer (C9920-02, Hamamatsu Photonics) in a glovebox. LPL performance was determined using a purpose-built measurement setup.[19]

2.5 References

1 J. Xu and S. Tanabe, *J. Lumin.* **2019**, *205*, 581.

2 S. Wu, Z. Pan, R. Chen and X. Liu, *Long Afterglow Phosphorescent Materials*, Springer, Cham, ZG, Switzerland, **2017**.

3 Y. Li, M. Gecevicius and J. Qiu, *Chem. Soc. Rev.*, **2016**, 45, 2090.

4 S. Xu, R. Chen, C. Zheng and W. Huang, *Adv. Mater.* **2016**, *28*, 9920.

5 T. Matsuzawa, Y. Aoki, N. Takeuchi and Y. Murayama, *J. Electrochem. Soc.* **1996**, *143*, 2670.

6 M. P. Anesh, S. K. H. Gulrez, A. Anis, H. Shaikh, M. E. Ali Mohsin and S. M. Al-Zahrani, *Adv. Polym. Tech.* **2014**, *33*, 21436.

7 Z. Lin, R. Kabe, N. Nishimura, K. Jinnai and C. Adachi, *Adv. Mater.* **2018**, *30*, 1803713.

8 R. Kabe and C. Adachi, *Nature* **2017**, *550*, 384.

9 A. Gilbert, J. E. Baggott and J. Baggott, Blackwell Scientific Publications, London, **1991**.

10 S. A. Jenekhe and J. A. Osaheni, *Science*, 1994, **265**, 765.

11 D. Kolosov, V. Adamovich, P. Djurovich, M. E. Thompson and C. Adachi, *J. Am. Chem. Soc.*, **2002**, 124, 9945.

12 X. K. Liu, Z. Chen, C. J. Zheng, C. L. Liu, C. S. Lee, F. Li, X. M. Ou and X. H. Zhang, *Adv. Mater.*, **2015**, 27, 2378.

13 J. Pommerehne, H. Vestweber, W. Guss, R. F. Mahrt, H. Bässler, M. Porsch and J. Daub, *Adv. Mater.*, **1995**, 7, 551.

14 Y. Liu, M. S. Liu and A. K.-Y. Jen, *Acta Polym.*, **1999**, 50, 105

15 P. Debye and J. O. Edwards, *J. Chem. Phys.* **1952**, *20*, 236.

16 G. C. Abell and A. Mozumder, *J. Chem. Phys.* ***1972***, *56*, *4079.*

17 M. Tachiya and A. Mozumder, *Chem. Phys. Lett.*, **1975**, 34, 77.

18 Y. Hama, Y. Kimura, M. Tsumura and N. Omi, *Chem. Phys.*, **1980**, 53, 115.

19 H. Ohkita, W. Sakai, A. Tsuchida and M. Yamamoto, *Macromolecules*, **1997**, 30, 5376.

20 S. Hirata, K. Totani, J. Zhang, T. Yamashita, H. Kaji, S. R. Marder, T. Watanabe and C. Adachi, *Adv. Funct. Mater.* **2013**, *23*, 3386.

21 S. Hirata, K. Totani, T. Yamashita, C. Adachi and M. Vacha, *Nat. Mater.* **2014**, *13*, 938.

22 Z. An, C. Zheng, Y. Tao, R. Chen, H. Shi, T. Chen, Z. Wang, H. Li, R. Deng, X. Liu and W. Huang, *Nat. Mater.* **2015**, *14*, 685.

23 W. Zhao, Z. He, J.W. Y. Lam, Q. Peng, H. Ma, Z. Shuai, G. Bai, J. Hao and B. Z. Tang, *Chem* **2016**, *1*, 592.

24 H. Mieno, R. Kabe, N. Notsuka, M. D. Allendorf and C. Adachi, *Adv. Opt. Mater.* **2016**, *4*, 1015.

25 N. Notsuka, R. Kabe, K. Goushi and C. Adachi, *Adv. Funct. Mater.* **2017**, *27*, 1703902.

26 Y. Su, S. Z. F. Phua, Y. Li, X. Zhou, D. Jana, G. Liu, W. Q. Lim, W. K. Ong, C. Yang and Y. Zhao, *Sci. Adv.* **2018**, *4*, eaas9732.

27 D. Li, F. Lu, J. Wang, W. Hu, X.-M. Cao, X. Ma and H. Tian, *J. Am. Chem. Soc.*, **2018**, 140, 1916.

28 L. Gu, H. Shi, L. Bian, M. Gu, K. Ling, X. Wang, H. Ma, S. Cai, W. Ning, L. Fu, H. Wang, S. Wang, Y. Gao, W. Yao, F. Huo, Y. Tao, Z. An, X. Liu and W. Huang, *Nat. Photonics* **2019**, *13*, 406.

29 K. Jinnai, N. Nishimura, R. Kabe and C. Adachi, *Chem. Lett.* **2019**, *48*, 270.

30 K. Jinnai, R. Kabe and C. Adachi, *Adv. Mater.* **2018**, *30*, 1800365.

31 C. Fan, C. Duan, Y. Wei, D. Ding, H. Xu and W. Huang, *Chem. Mater.* **2015**, *27*, 5131.

Chapter 3

Influence of energy gap between charge-transfer and locally excited states on organic long persistence luminescence

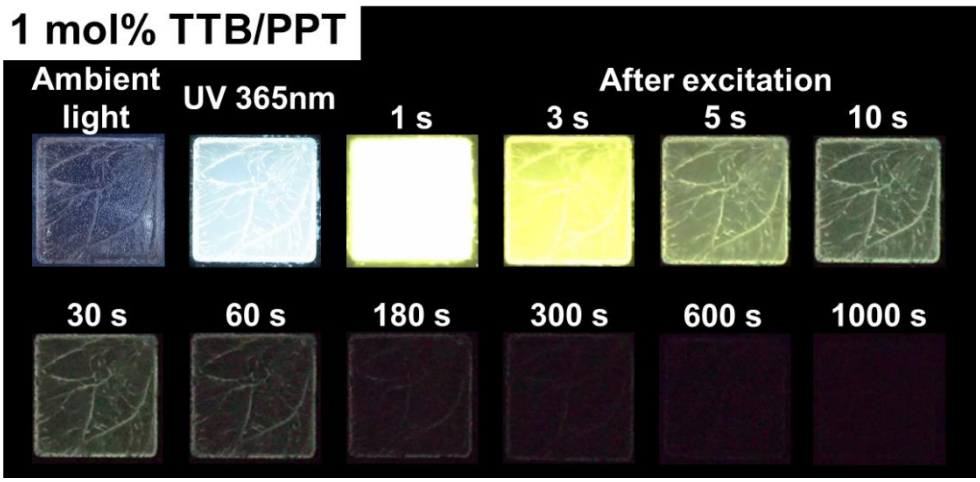

3.1 Introduction

Long-persistent luminescence (LPL), also known as the glow-in-the-dark effect or afterglow, is a phenomenon by which a material emits light for a very long time after the cutoff of photo-excitation.[1,2] The first LPL emitters were based on inorganic crystals, and performance was greatly improved through doping.[1-3] Several charge accumulation mechanisms, such as electron or hole trapping mechanisms, have been proposed to explain inorganic LPL.[1,3] Unlike phosphorescence, which can also be long-lived but is a transition between different spin states (usually from a triplet excited state to the singlet ground state), LPL systems do not follow an exponential decay and usually follow a power-law decay because of the presence of the intermediate states (Figure 3-1).

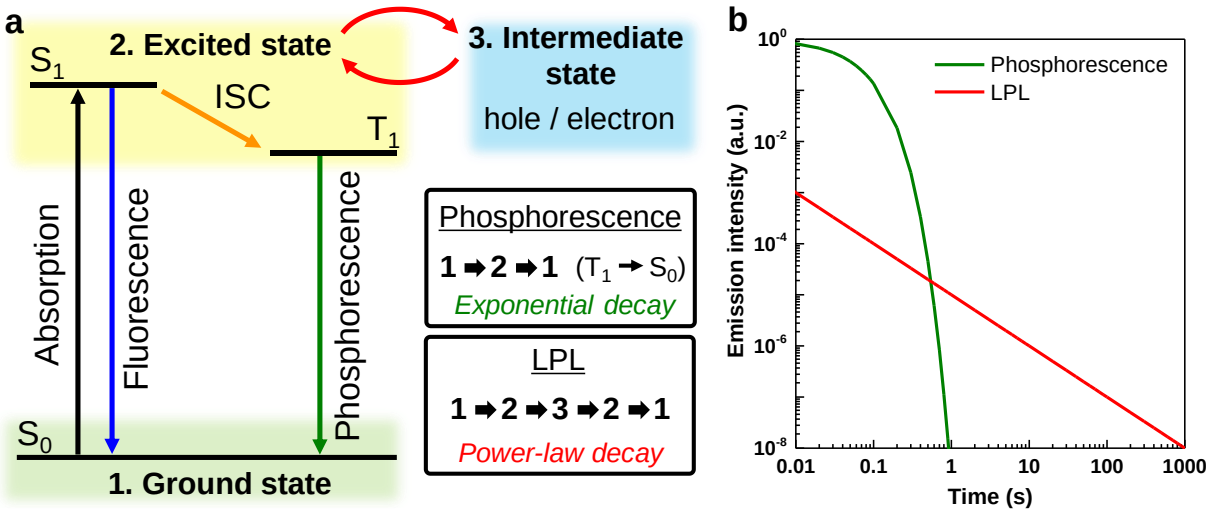

Figure 3-1. Differences between LPL and phosphorescence. **(a)** Schematic diagram of fluorescence, phosphorescence, and LPL. Phosphorescence is a transition from triplet excited state (T_1) to the singlet ground state (S_0). LPL is an emission mechanism in which the energy passes through an intermediate state like a trapped state. There is no restriction regarding the spin state. While LPL is long-lived because of charge separation and subsequent slow recombination (second-order kinetics) of initially generated excitons, phosphorescence is long-lived because of the low probability of the transition (first-order kinetics) occurring in the initially generated excitons. **(b)** The ideal emission decay profiles of phosphorescence and LPL on logarithmic plots. Phosphorescence follows an exponential decay and LPL a power-law decay.

Since the mid-1990s, the blending of inorganic LPL materials with a polymer matrix has been the main route for achieving it in commercial applications such as watch dials, fire safety signs, and glow-in-the-dark toys.[1-3] However, inorganic LPL materials exhibit poor compatibility and transparency in common polymers. Moreover, the most efficient inorganic LPL materials nearly all contain rare earth elements such as Sr, Eu, and Dy.[1,2,4]

Recently, Adachi and coworkers realized the first LPL emission from purely organic-based materials, including organic small molecules and polymers.[5,6] These organic LPL (OLPL) materials can be easily fabricated by mixing an electron donor and an electron acceptor using various methods such as melt-casting, spin coating, or thermal evaporation.[7] Moreover, the emission color of OLPL systems can be controlled by the addition of dopants.[8] However, a large performance gap still exists between the present OLPL system and the commercial high-performance inorganic LPL products (Figure 3-2).

The OLPL emission originates from the charge-transfer (CT) transition of a photo-generated exciplex formed between a donor and an acceptor. Some exciplexes can dissociate to form partially charge-separated (CS) states with very long times. The slow recombination of these separated charge carriers leads to continuous emission for over one hour at room temperature. The LPL process is governed by the recombination of dissociated radical cations and anions with a power-law emission decay,[5,9,10] so that the emission duration of OLPL materials is significantly longer than that of conventional room-temperature phosphorescence, which is ideally a first-order reaction with an exponential emission decay.[1,2,11,12] The power-law kinetic results (power-law kinetic, $I(t) \sim t^{-m}$, $m = 0.1–2$) from charge recombination can be explained by several physical models discussed in previous literatures about LPL from organic

molecules (TMB/poly(alkyl methacrylate)s)[13] and thermoluminescence of the inorganic LiF[14] and the organic molecule polyethylene terephthalate[15]. These models can be separated into the diffusion model[9,10,16,17] and the electron tunneling model[18] of geminate ion recombination. In the diffusion model, we consider the distribution of electrons (radical anions) after the charge separation process. The electron tunneling model is mainly used to explain the isothermal recombination luminescence at low temperatures for irradiated organic compounds.

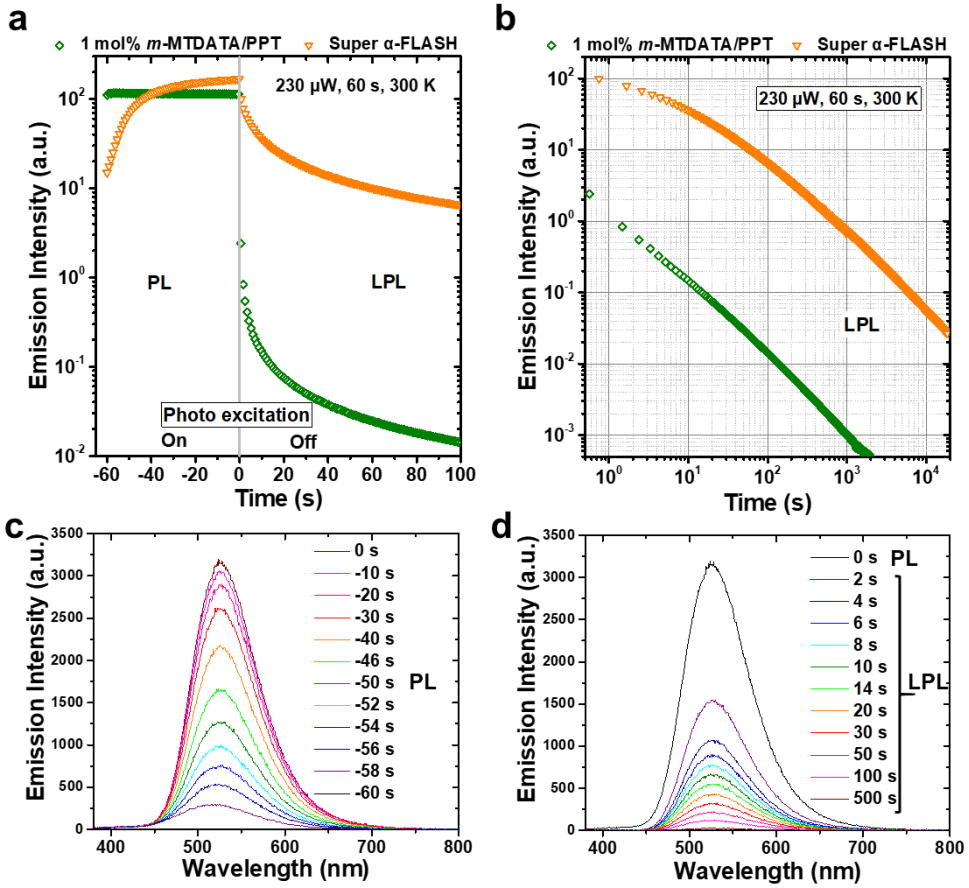

Figure 3-2. Comparison between OLPL and inorganic LPL system. Semi-logarithmic plots **(a)** and logarithmic plots **(b)** of the emission decay profiles of the reported OLPL system (1 mol% *m*-MTDATA/PPT)[7] and a commercial inorganic LPL material (Super α-Flash, LTI corporation, Japan). Emission spectra during photoexcitation **(c)** and after the excitation **(d)** of inorganic LPL material. All samples were 1 cm^2 and were excited for 60 s by a 340-nm LED source with same power 230 μW at 300 K.

Although a molecule's chemical structure greatly influences its optical and mechanical properties such as absorption and emission spectra, flexibility, and bio-compatibility, the

strategy for the design and selection of molecules for the OLPL system still remains unclear. Adachi and coworkers have noted in a previous report that the LPL process, which proceeds through charge dissociation and subsequent recombination, might be affected by the excited-state energy levels of the donor and acceptor and the exciplex formed between them.[6] However, more detailed relationships are still needed to unlock ways to improve the performance of OLPL materials.

In this chapter, I demonstrate that the energy gap between the lowest singlet excited-state of the exciplex (^{1}CT) and the lowest triplet excited-state of the donor (^3LE_D) strongly affects OLPL performance. Changes in the OLPL properties and the emission mechanism are systematically investigated for three donor materials having similar molecular structures but different energy levels. Optimization of excited-state energy levels based on the uncovered relationships between energy levels and performance will aid the development of efficient OLPL systems aiming for future applications.

3.2 Results and discussion

The OLPL systems were fabricated by the melt-casting of a mixture containing 1% of an electron donor and 99% of an electron acceptor.[7] The electron donors, *N*,*N*,*N*′,*N*′-tetramethylbenzidine (TMB), *N*,*N*′-dimethyl-*N*,*N*′-ditolylbenzidine (DMDTB), and *N*,*N*,*N*′,*N*′-tetratolylbenzidine (TTB), and the electron acceptor, 2,8-bis(diphenylphosphoryl)dibenzo[b,d]thiophene (PPT), are shown in Figure 3-3a. The HOMO levels of the donors were determined from the first redox peaks of cyclic voltammograms (Figure 3-3b), and the HOMO levels of DMDTB (−4.88 eV) and TTB (−4.96 eV) were found

to be slightly deeper than that of TMB (−4.78 eV) because of the π-extension provided by the substituent benzene rings.

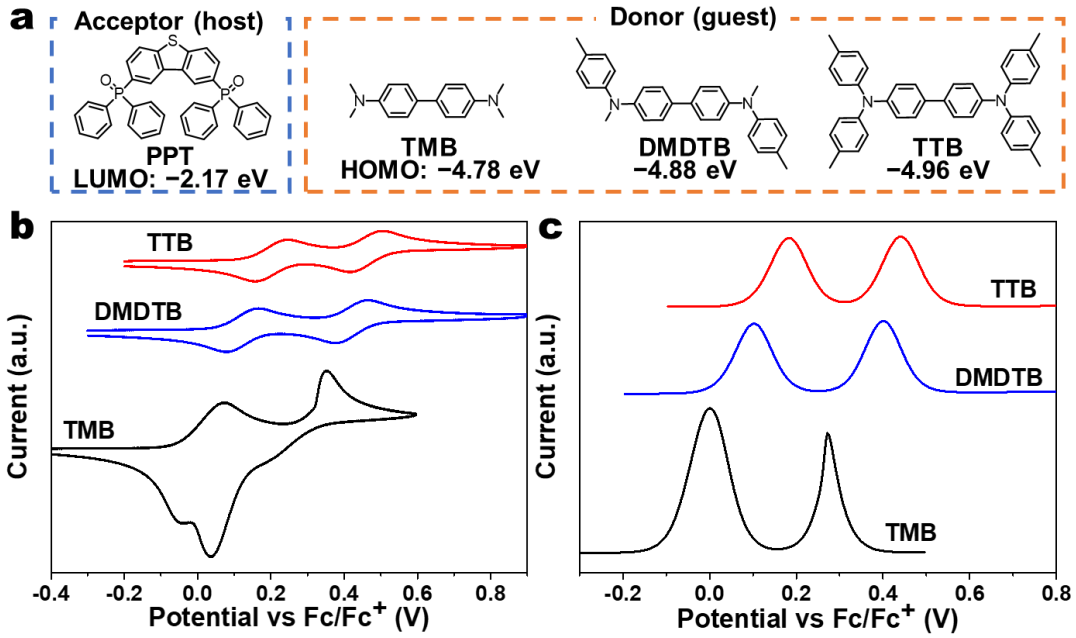

Figure 3-3. (a) Chemical structures and HOMO or LUMO energy levels of the three electron donors (TMB, DMDTB, and TTB) and the electron acceptor (PPT). Cyclic voltammetry (CV) **(b)** and differential pulse voltammetry (DPV) **(c)** curves of TMB, DMDTB, and TTB.

The LPL performance of these donor/acceptor systems greatly depends on the donor. Figure 3-4 shows the steady-state photoluminescence and time-resolved (1–2 s, 4–5 s, 10–30 s, and 100–300 s after stopping excitation) emission spectra of these LPL systems. TMB/PPT and DMDTB/PPT systems showed a slight change of spectral width with the passage of time. On the other hand, the TTB/PPT system exhibits apparent spectral transformation, i.e., two emission peaks, within 10 s after excitation cutoff, indicating the presence of a second emission process. The emission decay profiles of all of the systems are inverse-power functions of time t^{-m} (m = 0.9–1.3) after 10 s (Figure 3-4b, and Table 3-1). This non-exponential decay behavior indicates that the LPL emission originates from intermediate CS states.[19]

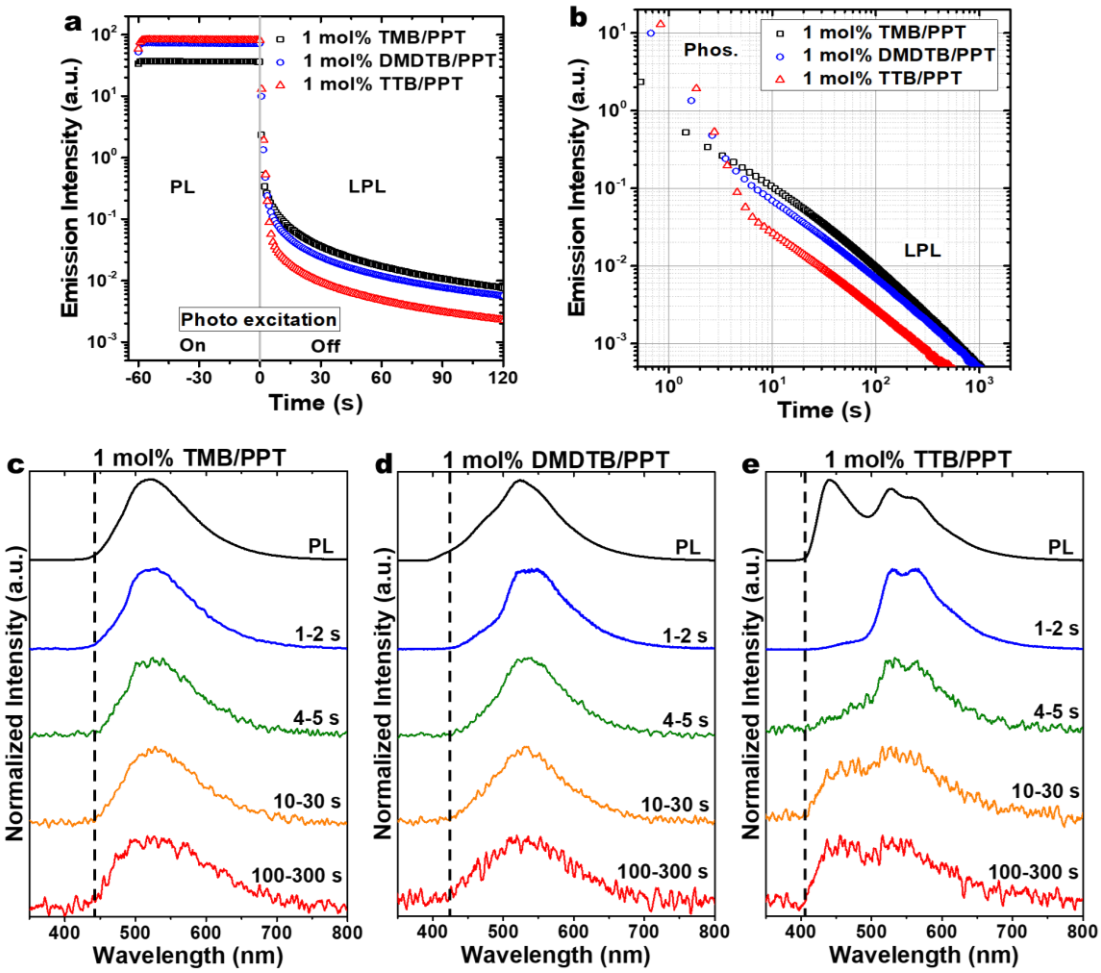

Figure 3-4. Photoluminescence and LPL characteristics of the OLPL systems. **(a), (b).** Semi-logarithmic plots **(a)** and logarithmic plots **(b)** of the emission decay profiles of TMB/PPT, DMTDB/PPT, and TTB/PPT at 300 K. Samples were excited for 60 s (from −60 to 0 s) by a 340-nm LED source. "PL" means the steady-state photoluminescence, "LPL" means the long-persistent luminescence, "Phos." means the phosphorescence. **(c)**–**(e).** The steady-state photoluminescence and time-resolved photoluminescence spectra of 1 mol% TMB/PPT **(c)**, DMDTB/PPT **(d)**, and TTB/PPT **(e)** films at 300 K. The time-resolved spectra were integrated over periods of 1–2, 4–5, 10–30, and 100–300 s after stopping excitation. The dashed lines indicate the onset of the LPL spectra.

Table 3-1. The m values for fits of $I(t) \sim t^{-m}$ to the decay curves of the investigated doped PPT films over different time periods.

Doped films	m (10–30 s)	R^2	m (30–50 s)	R^2	m (50–100 s)	R^2	m (100–300 s)	R^2
TMB/PPT	−0.99	0.9997	−1.08	0.9999	−1.15	0.9999	−1.24	0.9998
DMDTB/PPT	−0.93	0.9998	−1.00	0.9999	−1.05	0.9999	−1.12	0.9996
TTB/PPT	−0.89	0.9997	−0.97	0.9999	−1.04	0.9998	−1.08	0.9993

The m values are from the slopes of double log plots in Figure 3-1c. "R^2" is the coefficient of determination.

To understand the detailed emission mechanisms, we obtained time-resolved emission spectra from the OLPL systems on nanosecond through millisecond timescales by using a streak camera (Figures 3-5 to 3-10). Also, the fluorescence and phosphorescence spectra of the donors were obtained from 1-wt%-donor doped films of the cyclic olefin copolymer ZEONOR, which acts as a nonpolar solid matrix that does not form a CT complex with the donor dopants.[20] The optical properties of the donors doped in ZEONOR films are almost identical to those in toluene solutions, indicating that there are no aggregation or polarization effects (Figure 3-11). Moreover, since the solid-state matrix can prevent the nonradiative deactivation of the dopants, the room-temperature phosphorescence of the donors can be obtained. The phosphorescence decays of the donors (Figure 3-11) are exponential with lifetimes of 1.43 s (TMB), 0.79 s (DMDTB), and 0.72 s (TTB). The fluorescence spectra were obtained in air, which quenches the photo-generated triplet excitons because of the presence of oxygen. Optical properties and the energy levels calculated from the onsets of the emission spectra are summarized in Table 3-2.

Table 3-2. Photophysical properties of the donors, acceptors, and OLPL systems.

Sample	HOMO [eV][a]	LUMO [eV][a]	Φ_{PL}	$\tau_{flu.}$ [ns]	τ_{phos} [s]	^1LE_D or ^1LE_A [eV][b]	^3LE_D or ^3LE_A [eV][b]	Sample	Φ_{PL}	^1CT [eV][c]	$\Delta E(^1CT-^3LE_D)$ [eV]
TMB	−4.78		52%[d]	9.92[d]	1.43[d]	3.56[d]	2.63[d]	**TMB/PPT**	24%	2.79	0.16
DMDTB	−4.88		50%[d]	1.76[d]	0.79[d]	3.43[d]	2.62[d]	**DMDTB/PPT**	27%	2.87	0.25
TTB	−4.96		47%[d]	1.30[d]	0.72[d]	3.25[d]	2.50[d]	**TTB/PPT**	28%	3.04	0.54
PPT		−2.17	1%[e]	1.15[e]	1.01[f]	3.76[e]	2.91[f]				

[a] Calculated from CV or DPV peaks. [b] Calculated from onset of the emission spectra. [c] Calculated from onset of the LPL spectra. [d] In ZEONOR film at 300 K. [e] In neat film at 300 K. [f] In neat film at 77 K.

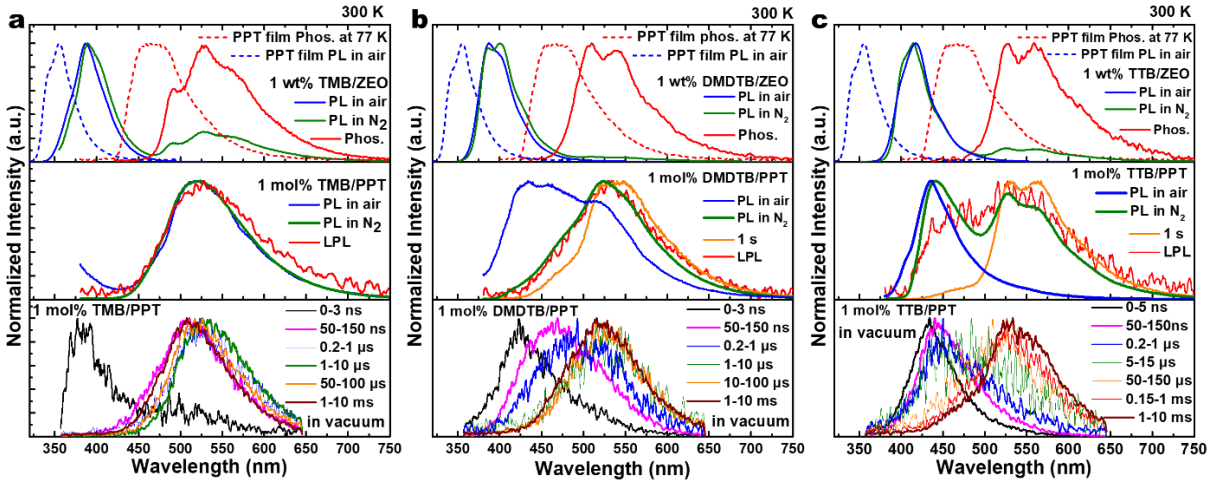

Figure 3-5. Study-state and time-resolved emission spectra of the OLPL systems. **a.** Fluorescence and phosphorescence spectra (top), steady-state photoluminescence (PL) and LPL spectra (middle), and time-resolved emission spectra (bottom) of TMB/PPT. **b**. DMDTB/PPT. **c**. TTB/PPT. Optical properties of TMB, DMDTB, and TTB were obtained in ZEONOR films at 300 K. Fluorescence and phosphorescence spectra of PPT were obtained from a neat thin film at 300 K and 77 K, respectively. Time-resolved emission spectra were obtained from streak images at 300 K.

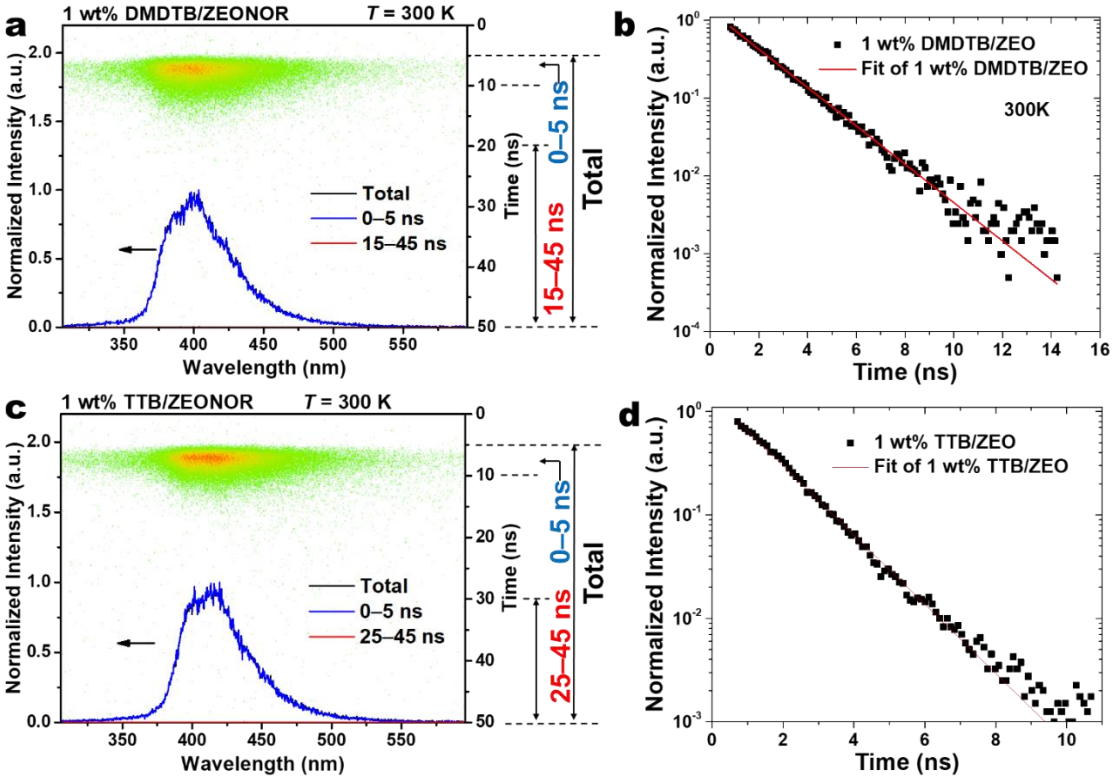

Figure 3-6. The streak images, transient emission spectra **(a)**, **(c)**, and emission decay profiles **(b)**, **(d)** of 1 wt% DMDTB/ZEONOR and TTB/ZEONOR films on a 50 microsecond timescale at 300 K.

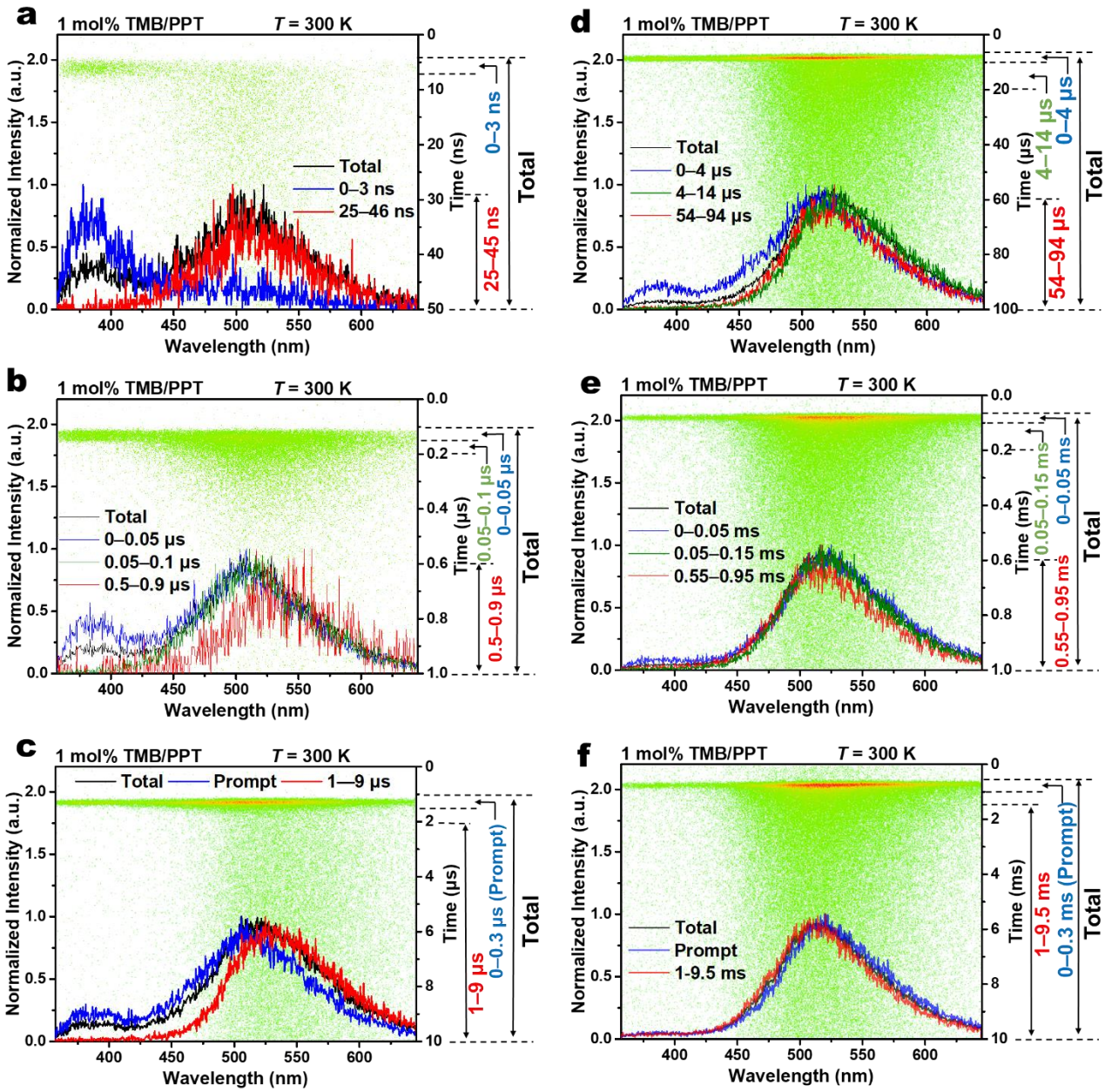

Figure 3-7. Streak images and transient emission spectra of 1 mol% TMB/PPT films on different time scales at 300 K in vacuum. **(a)** 50 ns; **(b)** 1 µs; **(c)** 10 µs; **(d)** 100 µs; **(e)** 1 ms; **(f)** 10 ms.

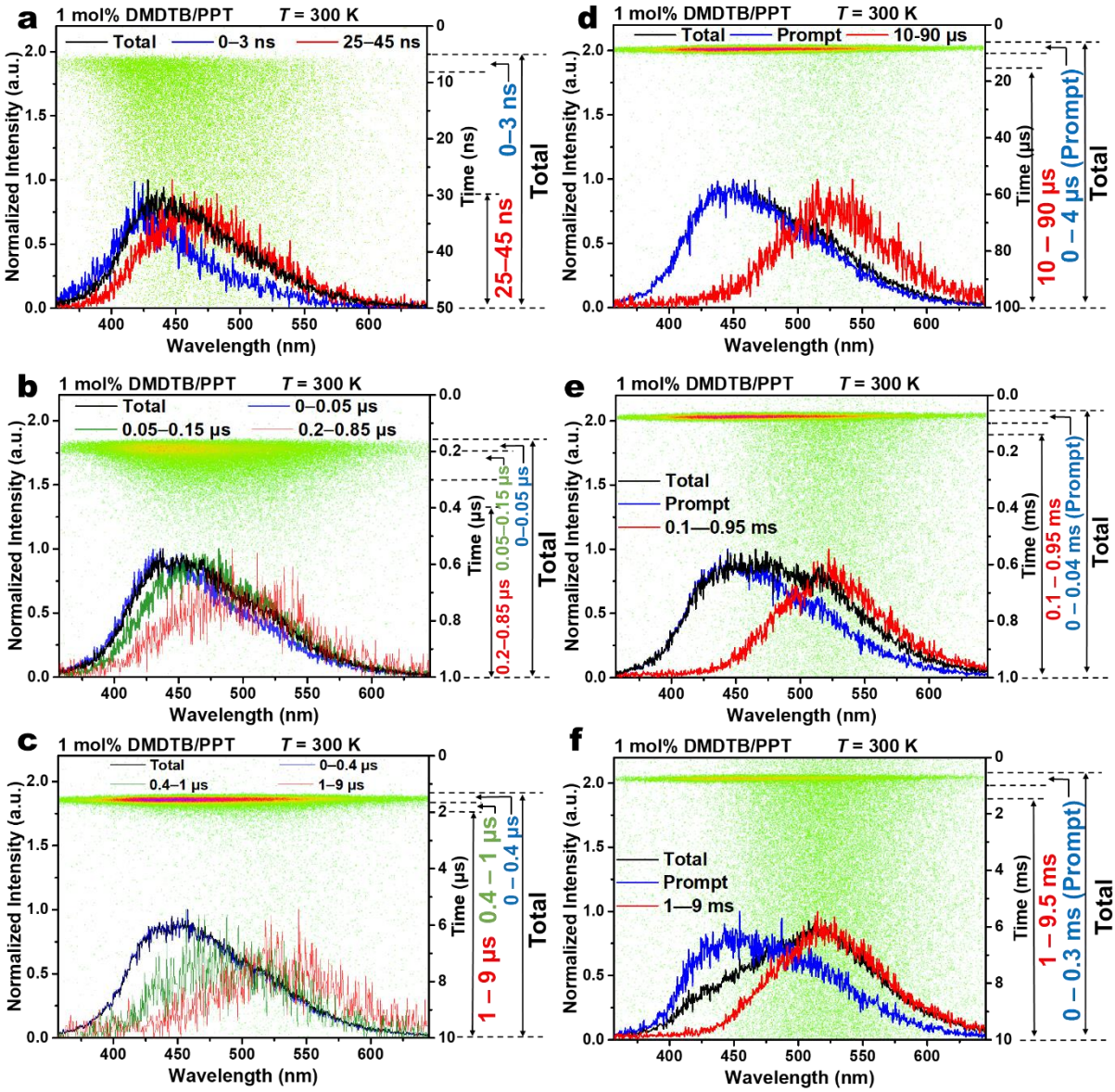

Figure 3-8. Streak images and transient emission spectra of 1 mol% DMDTB/PPT films on different time scales at 300 K in vacuum. **(a)** 50 ns; **(b)** 1 µs; **(c)** 10 µs; **(d)** 100 µs; **(e)** 1 ms; **(f)** 10 ms.

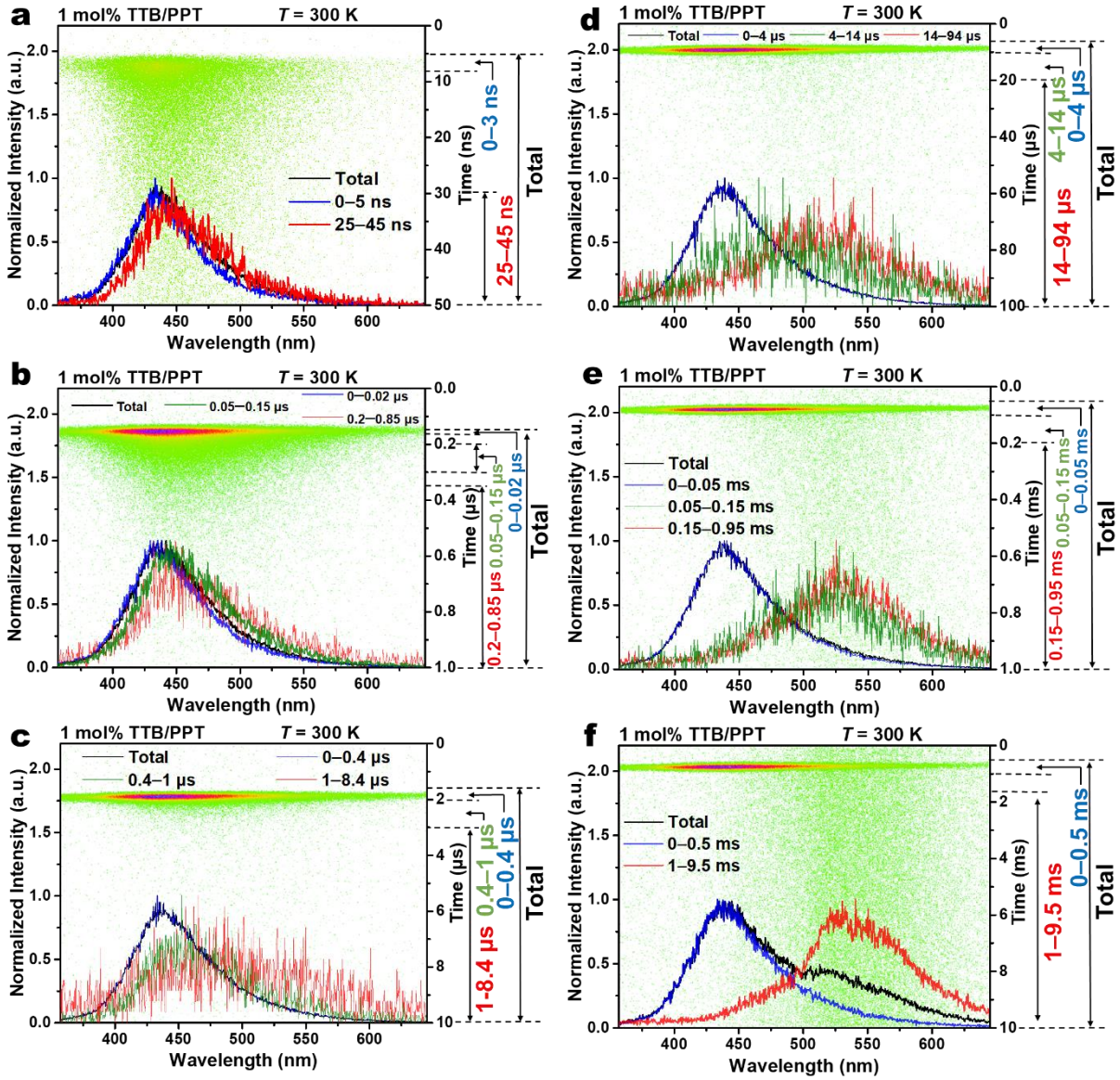

Figure 3-9. Streak images and transient emission spectra of 1 mol% TTB/PPT films on different time scales at 300 K in vacuum. **(a)** 50 ns; **(b)** 1 µs; **(c)** 10 µs; **(d)** 100 µs; **(e)** 1 ms; **(f)** 10 ms.

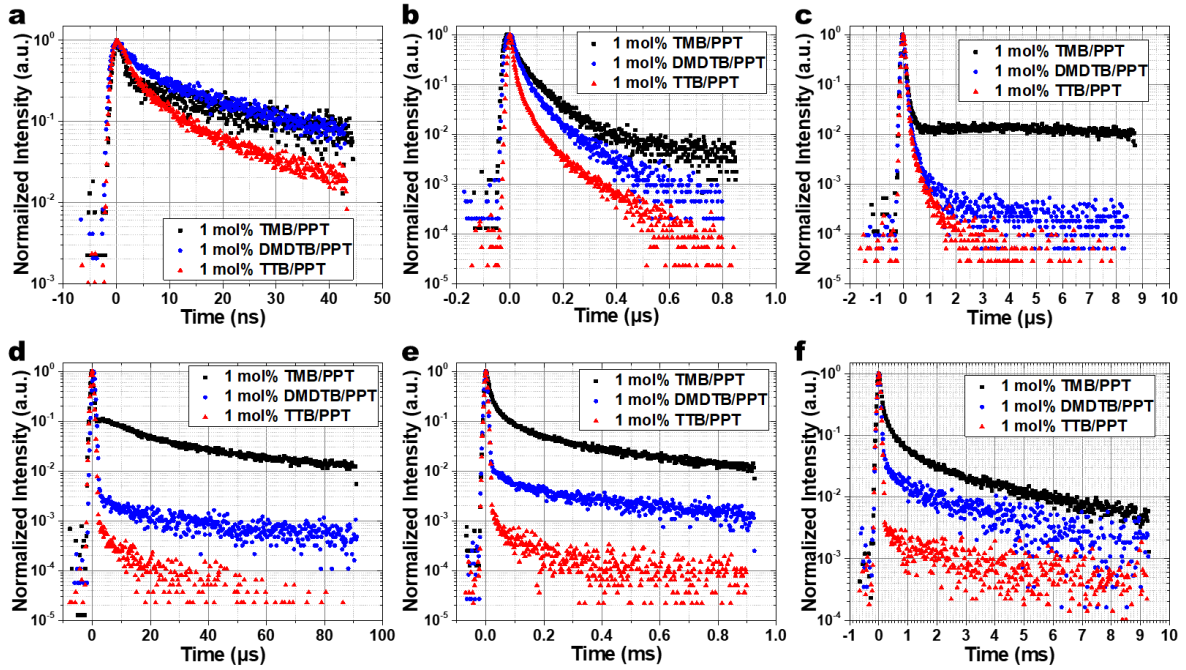

Figure 3-10. Transient emission decay curves (semi-logarithmic plots) of TMB/PPT, DMDTB/PPT, and TTB/PPT on different time scales at 300 K. **(a)** 50 ns; **(b)** 1 μs; **(c)** 10 μs; **(d)** 100 μs; **(e)** 1 ms; **(f)** 10 ms.

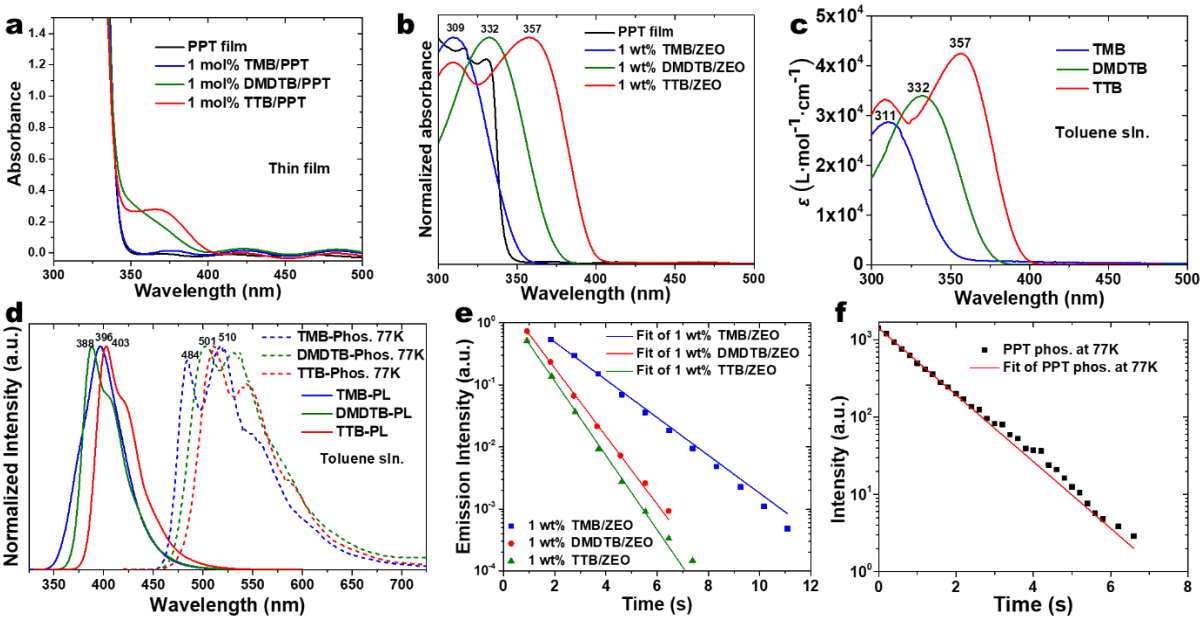

Figure 3-11. (a) UV–vis absorption spectra of PPT, TMB/PPT, DMDTB/PPT, and TTB/PPT. **(b)** UV–vis absorption spectra of PPT, TMB/ZEONOR, DMDTB/ZEONOR, and TTB/ZEONOR. **(c)** UV–vis absorption spectra of TMB, DMDTB, and TTB in the dilute toluene solutions (10^{-5} M). ε is molar extinction coefficient. **(d)** Steady-state photoluminescence spectra at 300 K and phosphorescence at 77 K of TMB, DMDTB, and TTB in toluene solutions (10^{-5} M). **(e)** Phosphorescence decay profiles of TMB/ZEONOR, DMDTB/ZEONOR, and TTB/ZEONOR at 300 K. **(f)** Phosphorescence decay profiles of a PPT thin film at 77 K.

The time-resolved emission spectra of TMB/PPT system indicate the presence of weak fluorescence from TMB for at least 3 ns after excitation cutoff (Figures 3-5a and 3-7). This fluorescence originates from the TMB molecules which do not form CT with PPT. After the initial fluorescence of TMB, an exciplex emission that slightly shifts with time was obtained. The temperature dependencies of the time-resolved emission spectra and the emission decay profiles on a microsecond timescale clearly indicate the presence of thermally activated delayed fluorescence (TADF), which is often obtained from exciplex systems (Figure 3-12).[21,22] The spectral shift of the exciplex emission can be explained by the large dipole moment of PPT. Because the CT excited-states have large dipole moments (Table 3-3), reorganization of the PPT matrix in the excited-state—so-called solid-state solvation—induces the spectral shift during the TADF process.[23-25]

Table 3-3. Dipole moments of PPT, TMB, DMDTB, and TTB in S_0, S_1, T_1, and radical states.

Dipole moment (Debye)	S_0	S_1	T_1	Radical ion
PPT	4.82	3.50	3.45	26.89 [a)]
TMB	0.16	0.0084	0.0018	21.22 [b)]
DMDTB (conformer A) [c)]	0.12	0.93	0.17	9.74 [b)]
DMDTB (conformer F) [c)]	2.57	0.51	1.30	18.08 [b)]
TTB	0.0084	0.036	0.012	13.06 [b)]

[a)] Radical anion; [b)] Radical cation. [c)] Calculations based on conformers at ground state as shown in Figure 3-18. Level of theory: DFT-PBE0, basis set: ma-Def2-TZVP. The excited state of the exciplex always exhibits a large dipole moment.[23]

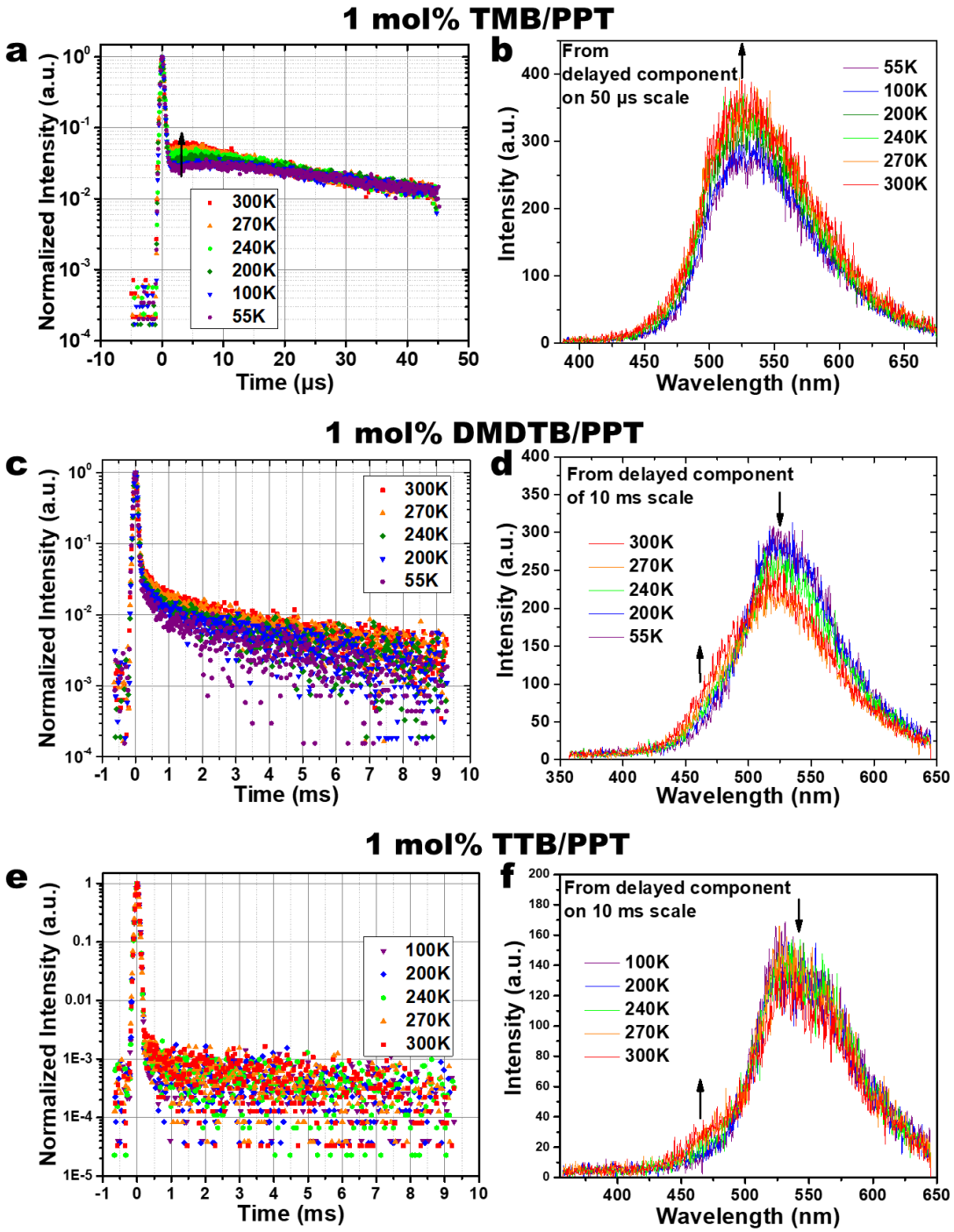

Figure 3-12. Temperature dependence of the transient emission decay curves (semi-logarithmic plots) and emission spectra of TMB/PPT **(a)**, **(b)**, DMDTB/PPT **(c)**, **(d)**, and TTB/PPT **(e)**, **(f)**.

The proposed emission mechanism and energy diagrams obtained from the onsets of the emission spectra are shown in Figure 3-13. Since the lowest triplet excited-state emission of the exciplex (^{3}CT) could not be obtained directly, we assume that ^{3}CT is almost identical to the lowest singlet excited-state of the exciplex (^{1}CT) because excellent separation of the HOMO and the LUMO orbitals on the donor and acceptor, respectively, of the exciplex induces a small energy gap between ^{1}CT and ^{3}CT.[21,22,26,27] Recent studies of TADF molecules indicate that the locally excited (LE) triplet state of donor or acceptor units, which are analogous to the triplet states located on the donor or acceptor molecule in an exciplex, contribute the reverse intersystem crossing (RISC) process, thus this is one important factor we considered when investigating the emission mechanism.[28-31]

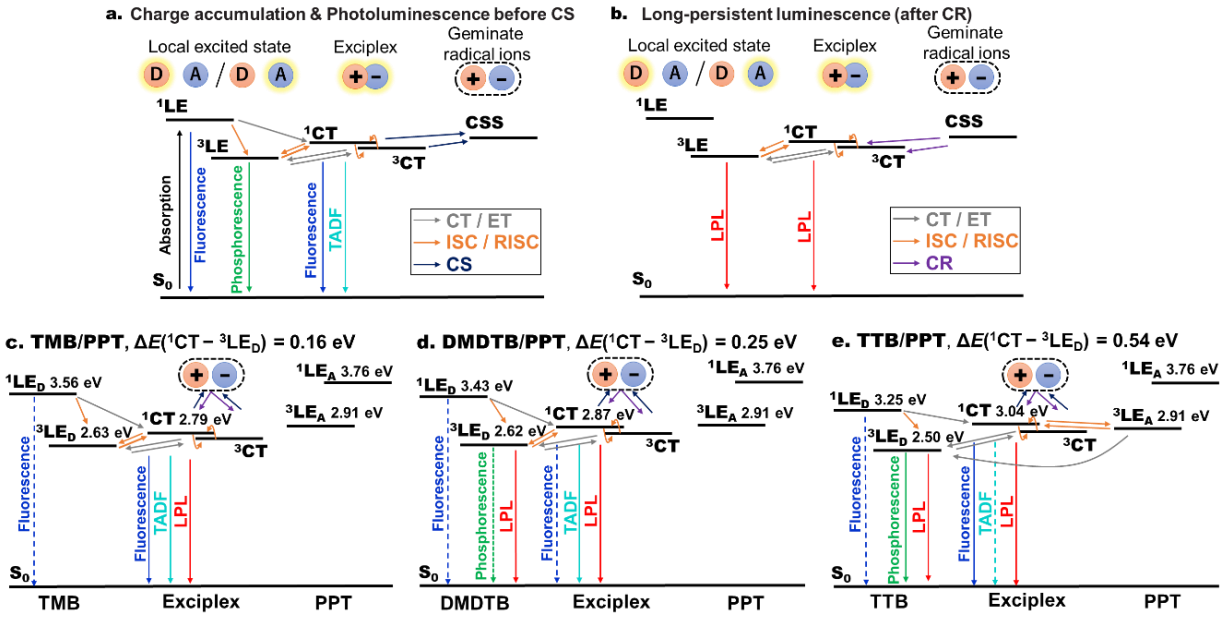

Figure 3-13. Proposed emission mechanism before (**a**) and after (**b**) recombination of charges and LPL path in TMB/PPT (**c**), DMDTB/PPT (**d**), and TTB/PPT (**e**). The energy levels were calculated from the onsets of the corresponding emission spectra. Abbreviations of electron donor (D), acceptor (A), charge transfer (CT), electron transfer (ET), charge separated state (CSS), charge separation (CS), and charge recombination (CR) are used. The dotted lines represent weaker luminescence processes and the solid lines stronger ones.

In the case of TMB, the lowest triplet excited-state of the donor (^3LE_D) is slightly lower than the lowest singlet CT excited-state of the exciplex (^1CT). This relatively small energy gap between ^3LE_D and ^1CT ($\Delta E(^1CT-^3LE_D)$ = 0.16 eV) enhances the TADF activity through the processes of ISC and RISC. Although the emission decay of an ideal TADF material follows a biexponential decay consisting of a fast fluorescence component and a slow TADF component, the emission decay of TMB/PPT is mostly dominated by the power-law decay originating from the charge recombination process and, therefore, does not exhibit biexponential decay. The emission decay profiles and the corresponding time-resolved spectra indicate that the TMB/PPT system exhibits fluorescence from TMB, prompt fluorescence from exciplexes, TADF from exciplexes, and finally LPL emission from exciplexes via charge separation and recombination processes, successively.

The steady-state photoluminescence spectrum of the TTB/PPT system exhibits clear two distinct emission features with the peaks at 440 nm and 530 nm originating from exciplex fluorescence and donor phosphorescence, respectively (Figure 3-4e). Although the emission peak at 440 nm is close to the peaks of PPT phosphorescence and TTB fluorescence, this peak can be attributed to exciplex fluorescence for two reasons. First, PPT phosphorescence is quenched by oxygen, but the TTB/PPT film in air still exhibits a similar peak at 435 nm. Second, the emission decay at 440 nm of TTB/PPT is much longer than that of TTB fluorescence. The sharpness of the exciplex emission can be ascribed to the self-absorption by the radical cation species of TTB (Figure 3-14). The contribution of delayed fluorescence by triplet-triplet annihilation is almost negligible since the donor concentration is only 1% and the phosphorescence time scale is much shorter than that of LPL. The TTB concentration

dependence of the emission spectra and emission decay profiles (Figure 3-15) are also consistent with exciplex emission. The LPL duration becomes shorter at higher concentrations of donor because the accumulated changes can more easily recombine with donor molecules. For higher donor concentrations, the exciplex emission was slightly redshifted and the room temperature phosphorescence from donors became weaker because of aggregation of donor molecules.

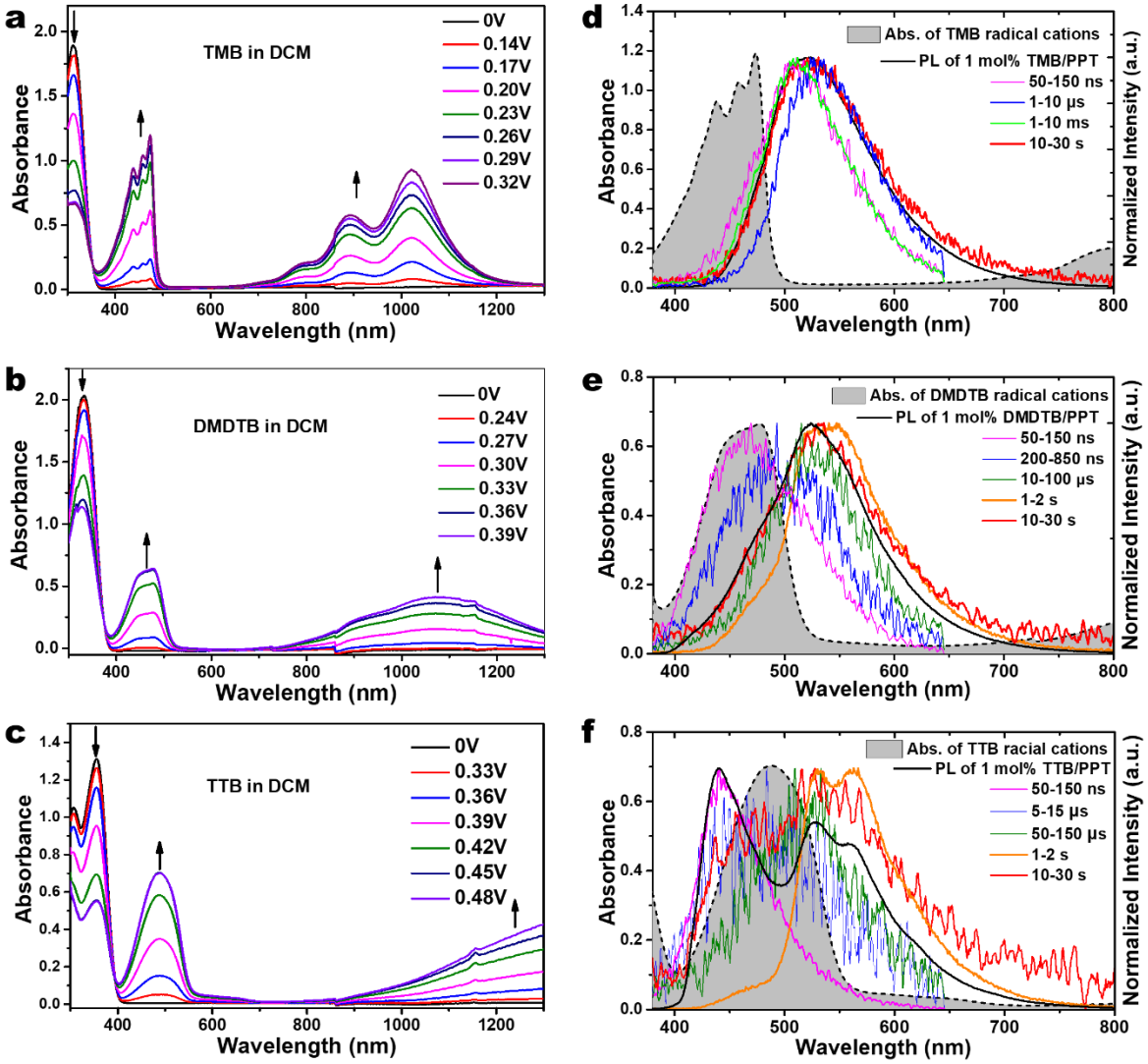

Figure 3-14. (a)–(c) Changes in absorption spectra for TMB, DMDTB and TTB during the first oxidation at various applied potentials in CH_2Cl_2 containing 0.1 M $TBAPF_6$. **(d)–(f)** UV–vis absorption spectra of radical cations of the three donors [obtained from **(a)–(c)**] and the steady-state photoluminescence, LPL, and some transient luminescence spectra of three doped PPT films at 300K.

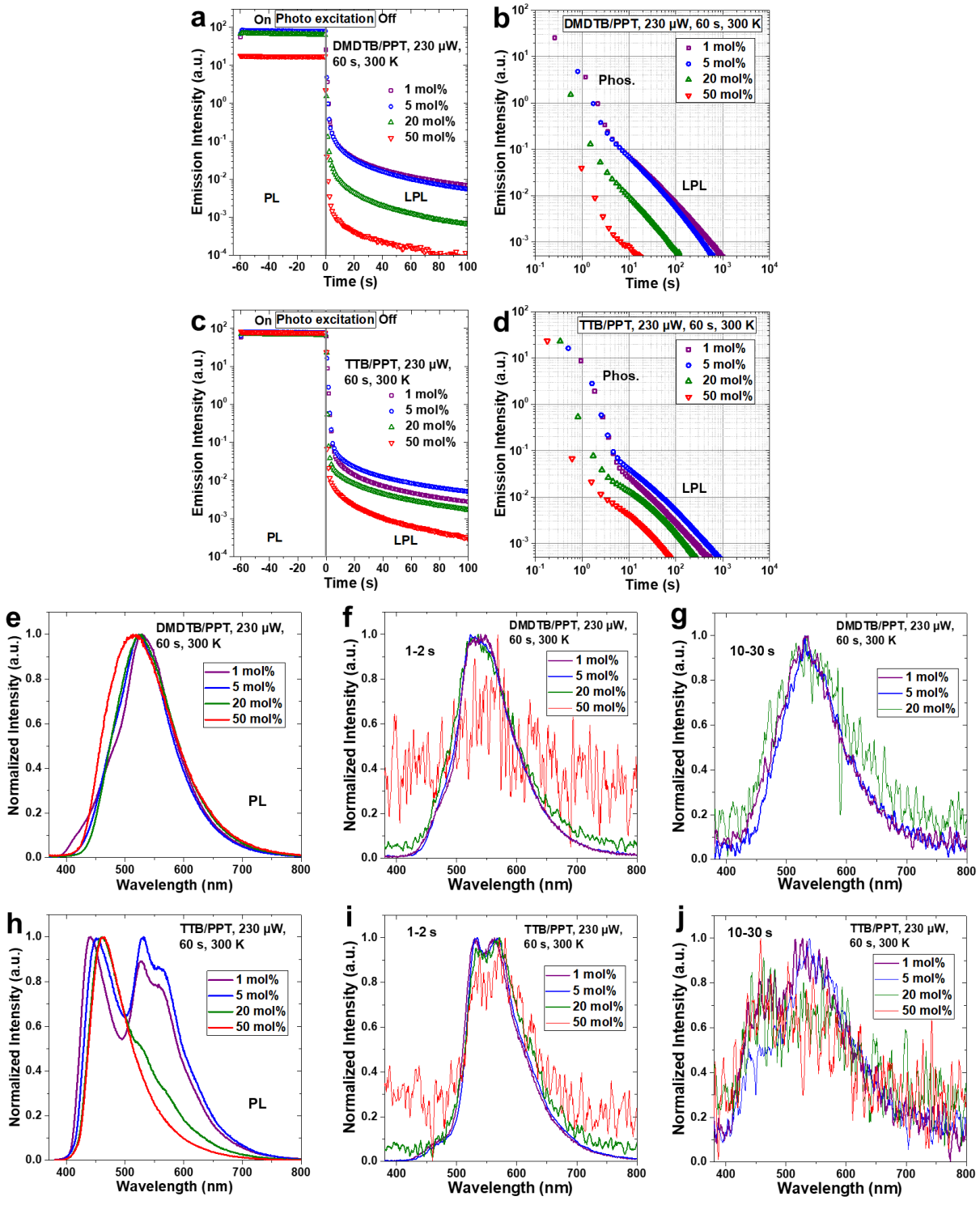

Figure 3-15. Donor concentration dependence. Semi-logarithmic plots **(a), (c**) and logarithmic plots (**b), (d**) of the emission decay profiles, steady-state photoluminescence spectra (**c), (h**) and time-resolved spectra **(f), (g), (i), (j)** of DMTDB/PPT, and TTB/PPT with different donor concentration. Samples were excited for 60 s by a 340-nm LED source with same power 230 μW at 300 K. "PL" means the steady-state photoluminescence, "LPL" means the long-persistent luminescence, "Phos." means the phosphorescence. The time-resolved spectra were integrated over periods of 1–2 and 10–30 s after stopping excitation.

In the case of TTB/PPT system, the TADF process is almost completely quenched because the ^3LE_D of TTB is much lower than the ^1CT. This large energy gap ($\Delta E(^1CT-^3LE_D) = 0.54$ eV) suppresses the RISC process, so that photo-generated excitons are becomes trapped on ^3LE_D, leading to room-temperature phosphorescence from TTB. Since the energy gap between the ^1CT and the lowest triplet excited-state of the acceptor (^3LE_A) is small enough, these energy levels should contribute to the TADF process. However, the generated ^3LE_A excitons can easily decay to the lower ^3LE_D.[32,33] Because the TADF process is suppressed at low temperatures, the emission spectra at 10 K contain stronger phosphorescence components from TTB than the spectrum at room temperature (Figure 3-16). Further, after the decay of phosphorescence from the TTB triplet excited-states, the emission occurs from the excitons generated by the CS state. Because charge recombination generates both singlet (^1CT) and triplet (^3CT) exciplexes, the LPL emission consists of both exciplex fluorescence from ^1CT and donor phosphorescence from ^3LE_D, which is populated by the transfer of excitons from ^3CT to ^3LE_D. Because of the dual emission from ^1CT and ^3LE_D, TTB/PPT system exhibits white emission. The CIE coordinates (CIE_x, CIE_y) of the steady-state photoluminescence and LPL spectra are (0.27, 0.33) and (0.31, 0.37), respectively (Figure 3-17).

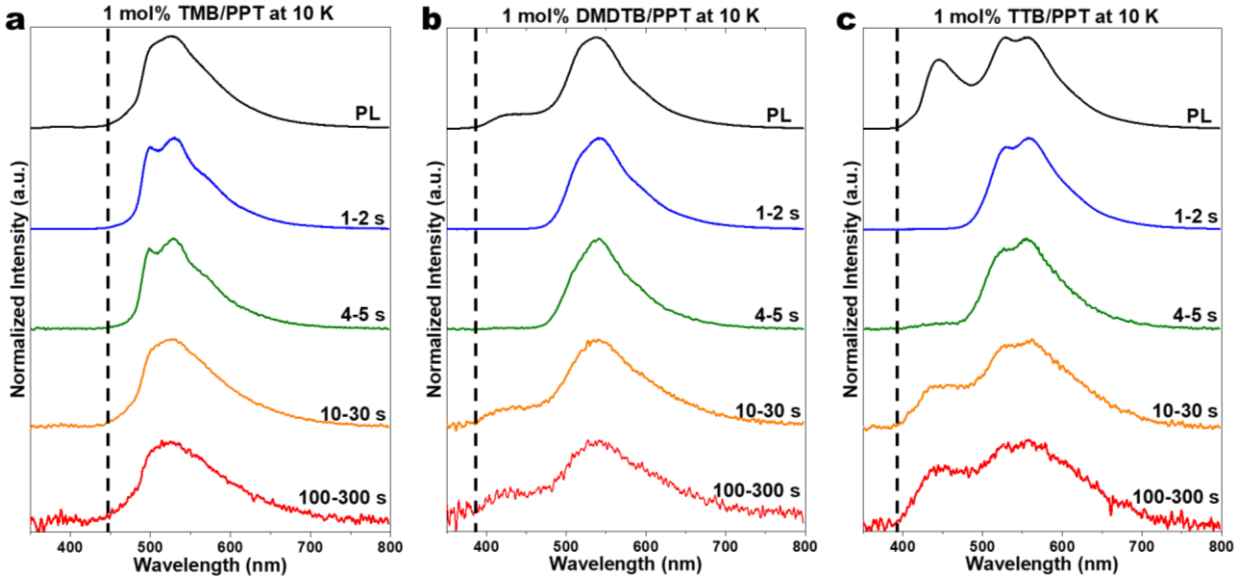

Figure 3-16. The steady-state photoluminescence (PL) and time-resolved photoluminescence spectra of 1 mol% TMB/PPT (**a**), DMDTB/PPT (**b**), and TTB/PPT (**c**) films at 10 K. The time-resolved spectra were integrated during the periods of 1–2, 4–5, 10–30, and 100–300 s after stopping the excitation. The dashed lines indicate the onset of the spectra.

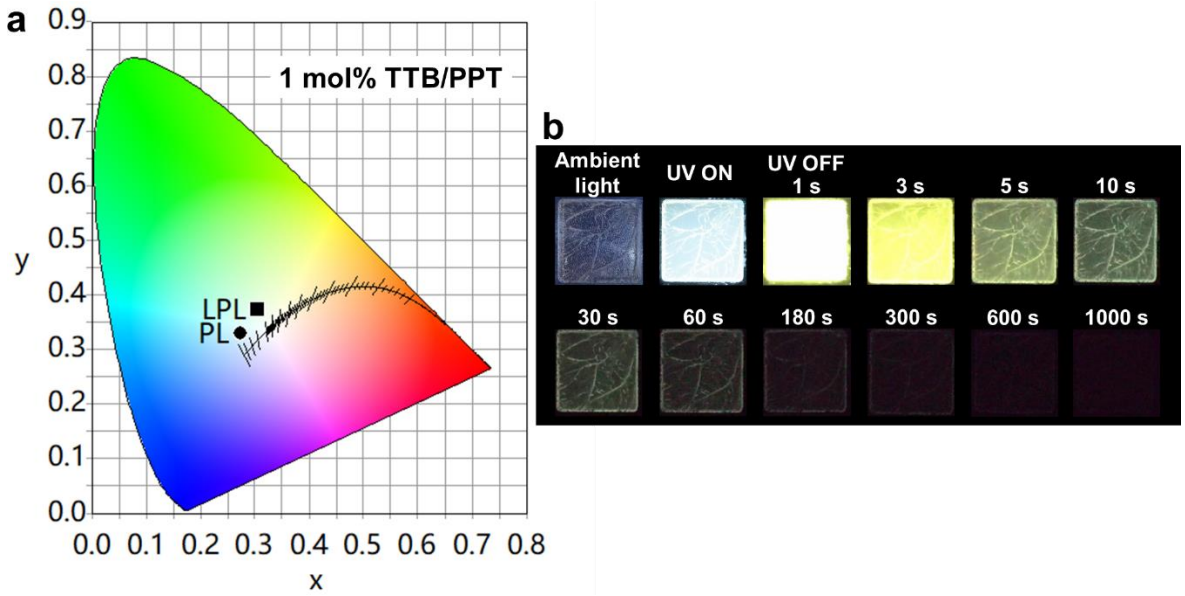

Figure 3-17. (a) CIE 1931 coordinates of photoluminescence (PL) and LPL of 1 mol% TTB/PPT; **(b)** Photograph of 1 mol% TTB/PPT thick film at 300 K under the ambient light, during excitation by a 365 nm UV lamp, and at various times after turning off the excitation.

The energy gap $\Delta E(^1\text{CT}-^3\text{LE}_\text{D})$ = 0.25 eV of DMDTB/PPT system is between those of TMB/PPT and TTB/PPT systems. Therefore, DMDTB/PPT system also exhibits dual emission from both exciplex fluorescence (^{1}CT) and DMDTB phosphorescence ($^3\text{LE}_\text{D}$). The exciplex

emission of DMDTB/PPT shows a large spectral shift during the TADF process. This large emission shift would be derived from the excited-state conformational change between the structural conformers of DMDTB (Figure 3-18).[24] Because of this large spectral shift, the exciplex fluorescence and DMDTB phosphorescence have a large spectral overlap. The lack of spectral shift and TADF emission in the LPL emission spectrum at 10 K confirms the contribution of TADF to the emission of the DMDTB/PPT system at room temperature.

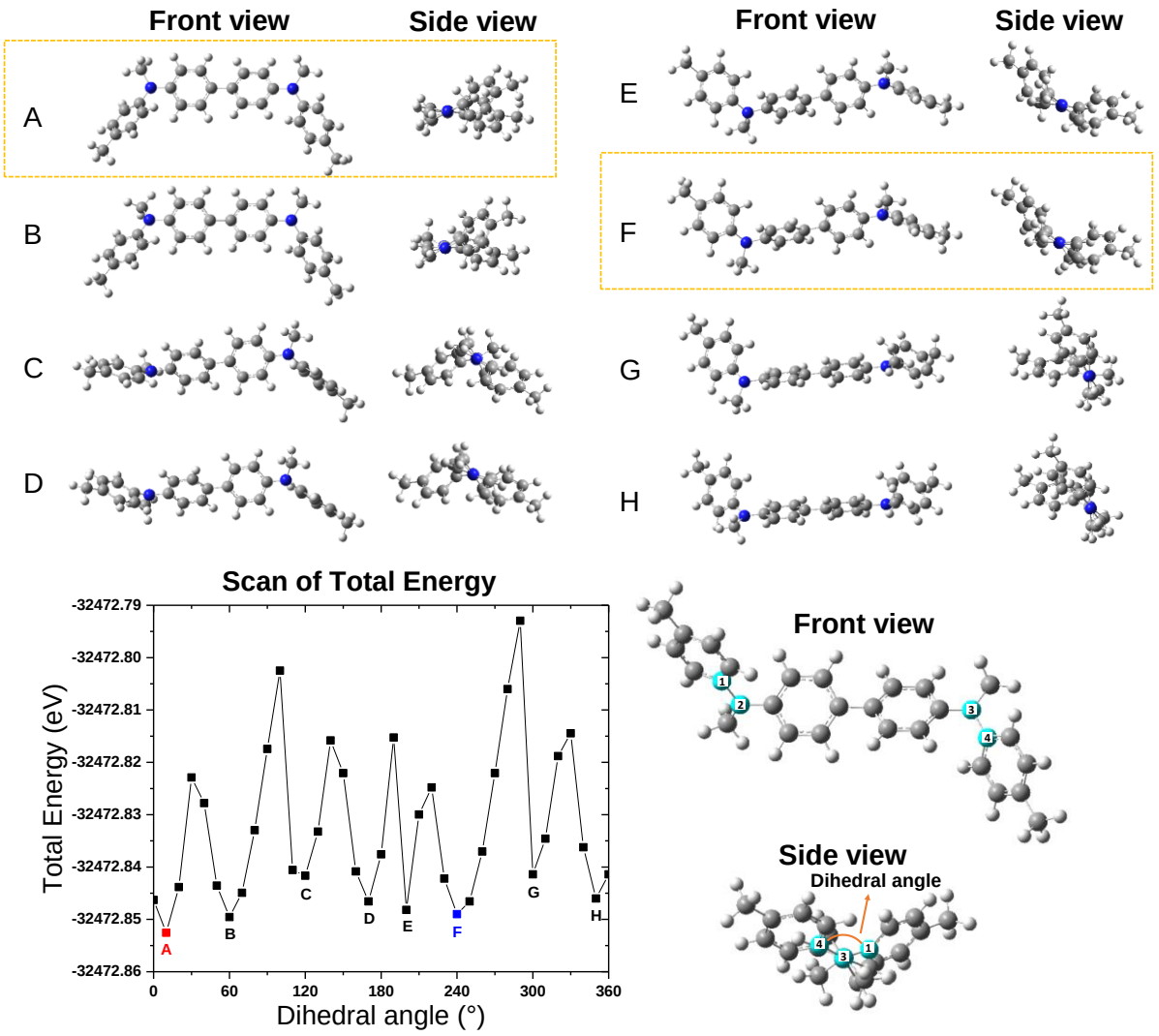

Figure 3-18. The potential energy surface and the conformations of DMDTB at the ground states in vacuum at the B3LPY/6-31G level (refer to the method of Ref. 34). The dipole moments of conformers A and F were calculated using DFT at the PBE1PBE/ma-Def2-TZVP level.

These results clearly indicate the importance of the energy level of ^3LE_D for obtaining efficient LPL emission. Since ^3LE excitons are less likely to undergo the charge transfer step needed for creating separated charges that contribute to LPL, the higher exciton population on ^3LE_D induced by a large energy gap of $\Delta E(^1CT-^3LE_D)$ will reduce the number of excitons that can convert into CS states. Thus, efficient LPL emission requires a small energy gap to ensure a higher number of ^1CT excitons that can contribute to the accumulation of separated charges.

Notably, the presented photoluminescence quantum yields (Φ_{PL}) do not completely reflect the LPL components (Table 3-2). The quantum efficiency of LPL emission is difficult to define because the charge accumulation and release processes are slow and complicated in contrast to those of long-lived phosphorescence. Furthermore, the LPL emission depends on the excitation time as well as the excitation power, while the phosphorescence component is constant (Figure 3-19 and 3-20). Because the LPL system continuously provides the new excited states after turning off the photoexcitation, we cannot calculate the Φ_{PL} from the steady-state photoluminescence spectra (Figure 3-21). This is why Φ_{PL} is not discussed even in inorganic LPL materials.[1,2,3]

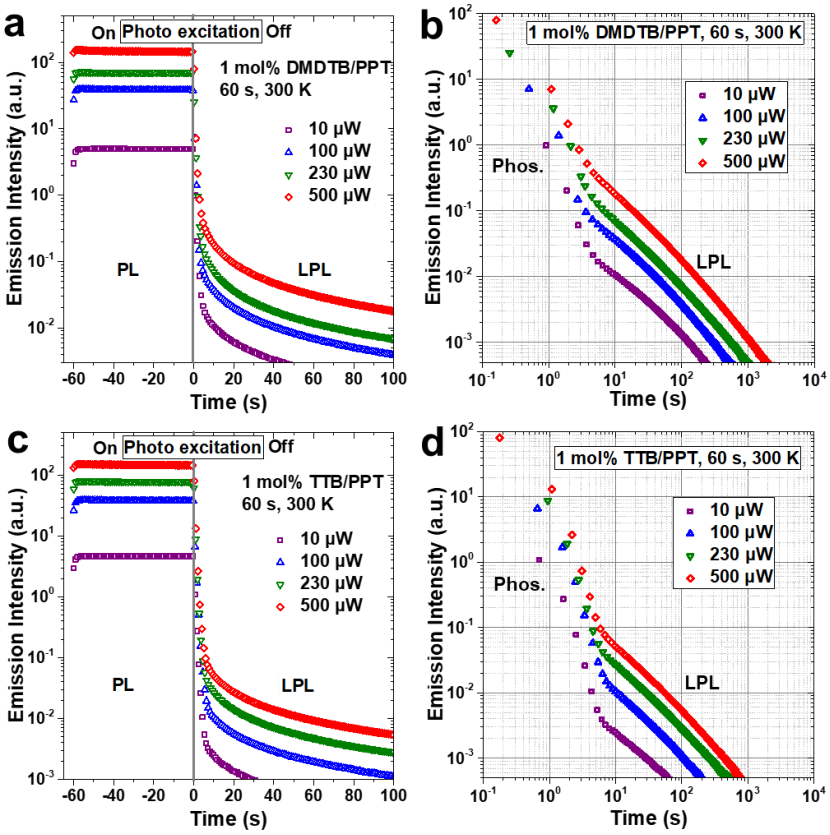

Figure 3-19. Excitation power dependence. Semi-logarithmic plots **(a), (c)** and logarithmic plots **(b), (d)** of the emission decay profiles of 1 mol% DMTDB/PPT and 1 mol% TTB/PPT with different excitation powers. Samples were all excited for 60 s (from −60 to 0 s) by a 340-nm LED source at 300 K. "PL" means the steady-state photoluminescence, "LPL" means the long-persistent luminescence, and "Phos." means the phosphorescence.

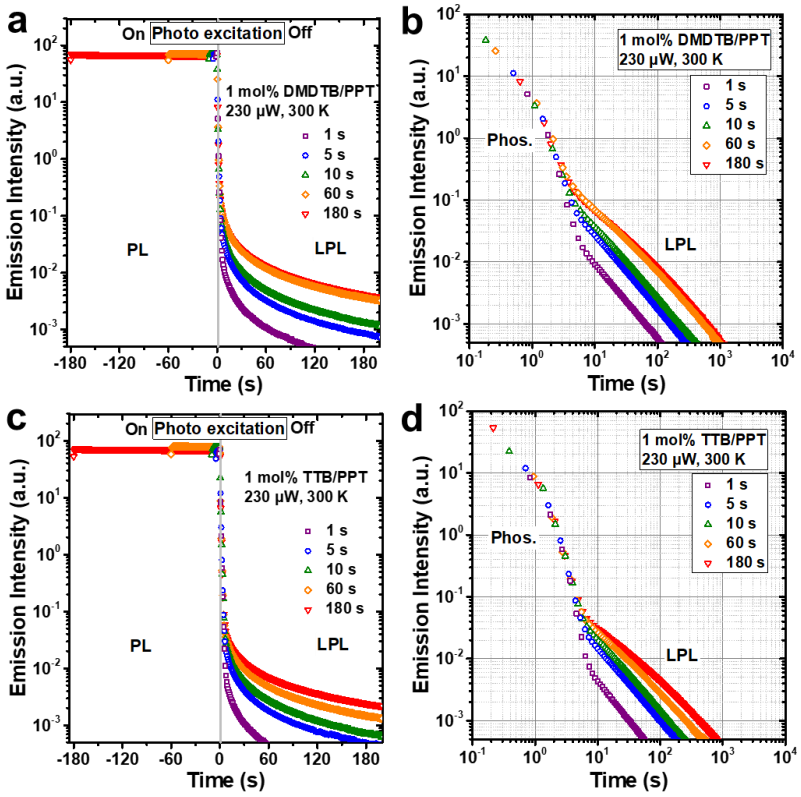

Figure 3-20. Excitation time dependence. Semi-logarithmic plots **(a), (c)** and logarithmic plots **(b), (d)** of the emission decay profiles of 1 mol% DMTDB/PPT and 1 mol% TTB/PPT with different excitation times. Samples were all excited by a 340-nm LED source with a power 230 μW at 300 K. "PL" means the steady-state photoluminescence, "LPL" means the long-persistent luminescence, and "Phos." means the phosphorescence.

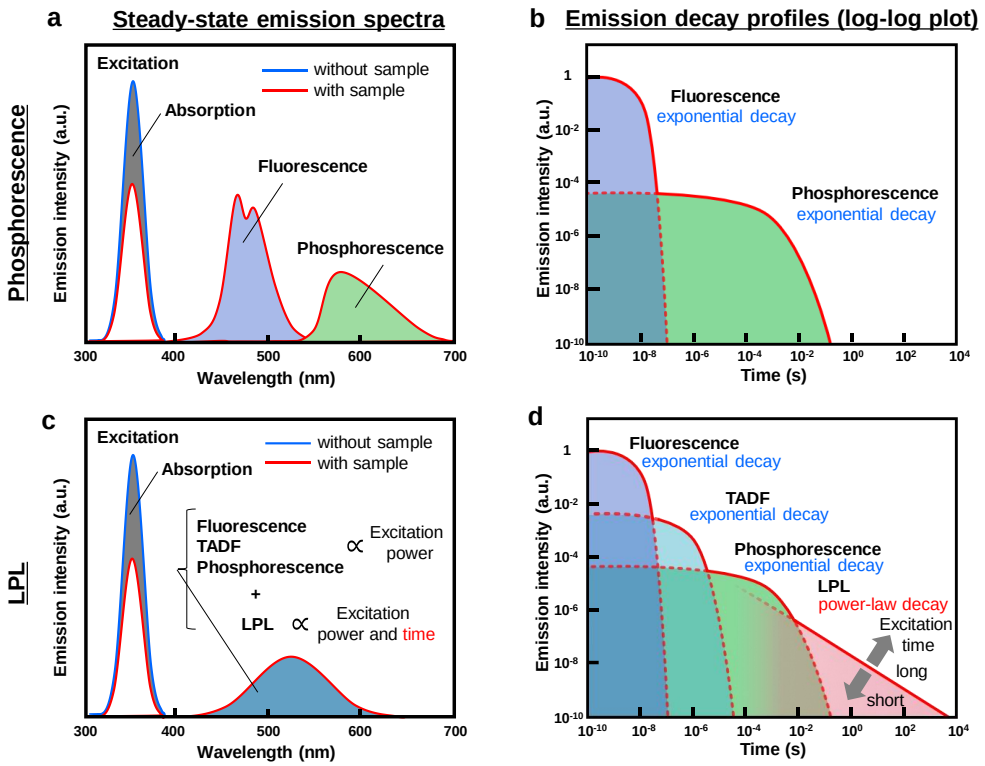

Figure 3-21. Ideal emission spectra and logarithmic plots of the emission decay profiles of phosphorescent materials **(a), (b)** and OLPL materials **(c), (d)**. The phosphorescence quantum yield can be calculated from the areas under the absorption and phosphorescence emission spectra (**a**). If the fluorescence and phosphorescence spectra have a large overlap, phosphorescence quantum yield can be estimated from the emission decay profiles because both fluorescence and phosphorescence follow an exponential decay (**b**). The OLPL system exhibits fluorescence, TADF, phosphorescence, and LPL from similar energy levels (**c**). Although the fluorescence, TADF, and phosphorescence follow an exponential decay, the power-law decay of LPL makes it difficult to estimate the LPL contribution since it depends on the excitation time as well as power (**d**).

3.3 Summary

In summary, I demonstrated that the lowest triplet excited-state of the donor (^3LE_D) influences LPL emission by changing the energy gap of $\Delta E(^1CT–^3LE_D)$. When the energy level of ^3LE_D is significantly lower than that of the ^1CT, the OLPL efficiency was reduced. Because a large energy gap induces a higher ^3LE_D population through ISC and energy transfer from ^3CT to ^3LE_D, the emission from both ^1CT and ^3LE_D contributed to LPL. This dual emission from

both ^{1}CT and ^3LE_D produced white light without the use of additional dopants. Moreover, we found that absorption by radical cation species generated by the charge separation process also affects the LPL emission spectra. Future efficient OLPL systems using both small molecules and polymers will be developed based on these considerations.

3.4 Experimental

3.4.1 Materials and Synthesis

Materials: TMB and TTB were purchased from TCI Chemicals (Tokyo, Japan). DMDTB was synthesized according to Scheme 3-1. PPT was prepared as described in the literature. All materials were purified by recrystallization and sublimation and stored in amber bottles in a glovebox. ZEONOR 1060R was obtained from ZEON Japan (Tokyo, Japan). Other materials were used as received. Inorganic LPL product was obtained from LTI Corporation (Kyoto, Japan).

Synthesis of N,N'-dimethyl-N,N'-ditolylbenzidine (DMDTB): A mixture of *4,4'*-dibromobiphenyl (2.0 g, 6.4 mmol), *N*-methyl-*p*-toluidine (2 mL, 16 mmol), $Pd(OAc)_2$ (28.6 mg, 0.13 mmol), tri-*t*-butylphosphine tetrafluoroborate (42.1 mg, 0.15 mmol) and NaO*t*Bu (2.5 g, 26 mmol) was refluxed overnight in 30 mL dry degassed toluene under argon. After cooling to room temperature, the mixture was poured into water, extracted with CH_2Cl_2, washed with water, and then dried with Na_2SO_4. A pinkish-white product was obtained by column chromatography under dark conditions using $CHCl_3$:hexane = 1:3 as eluent (2.27 g, 90% yield). A white pure product was obtained by purification by train-sublimation. ^{1}H NMR (500 MHz, chloroform-*d*) δ 7.51 – 7.33 (m, 4H), 7.20 – 7.08 (app d, 4H), 7.07 – 7.00 (m, 4H), 7.00 – 6.91

(m, 4H), 3.31 (s, 6H), 2.33 (s, 6H). ^{13}C NMR (126 MHz, $CDCl_3$) δ 147.98, 146.49, 132.47, 132.03, 129.90, 127.01, 122.53, 118.36, 40.36, 20.75. APCI-MS *m/z*: 392.22 $[M]^+$. Element Analysis (calculated & found for $C_{28}H_{28}N_2$): C (85.67%, 85.68%), H (7.19%, 7.21%), N (7.14%, 7.17%).

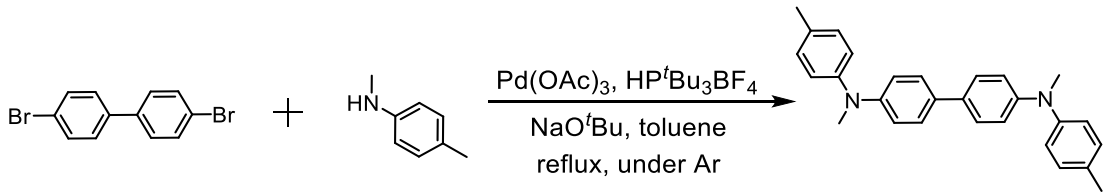

Scheme 3-1. Synthetic route for DMDTB.

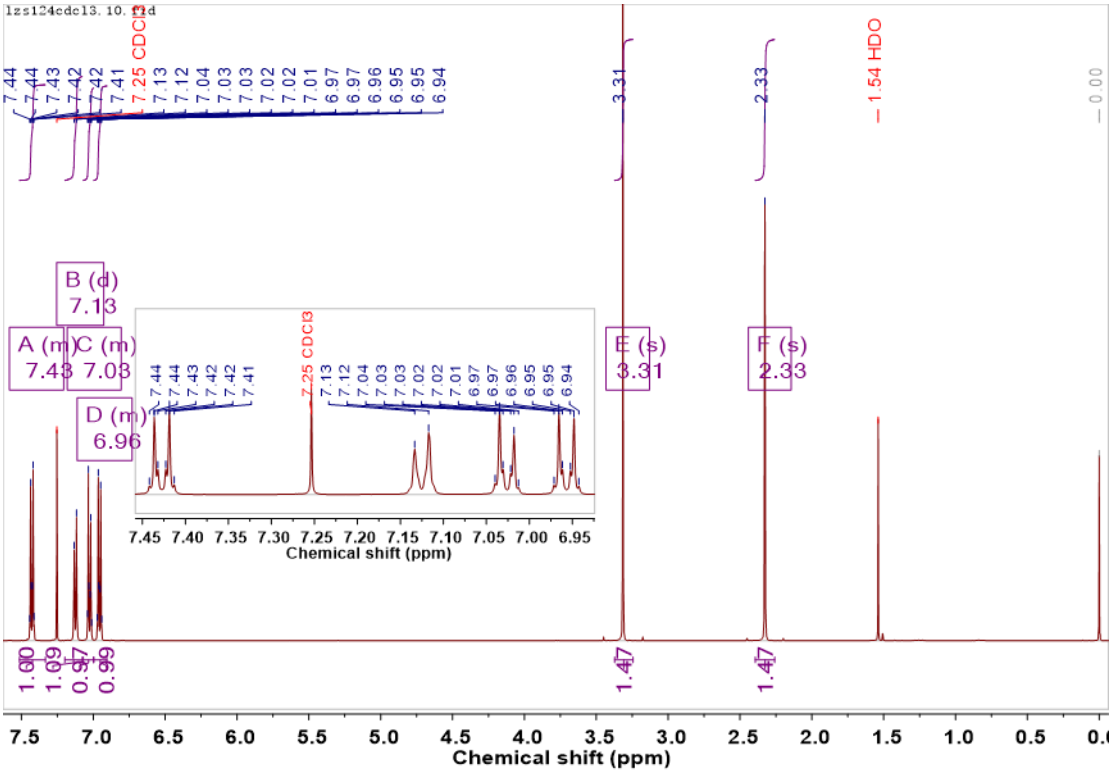

Figure 3-22. ^{1}H NMR spectra of DMDTB.

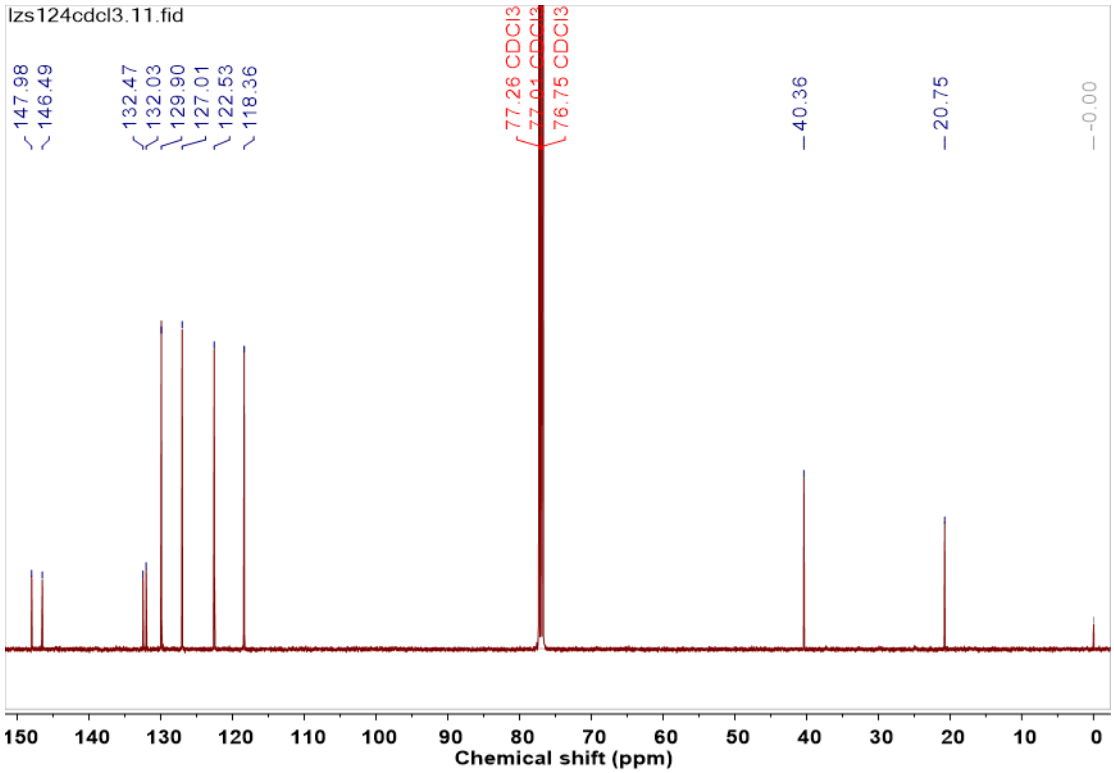

Figure 3-23. ^{13}C NMR spectra of DMDTB.

3.4.2 General Methods

Characterization: ^{1}H NMR and ^{13}C NMR spectra were recorded with a Bruker AVANCE III 500 MHz spectrometer. Molecular weight was measured in positive-ion atmospheric-pressure chemical ionization mode on a Waters 3100 mass detector (APCI-MS). Elemental analysis (C, H, and N) was carried out with a Yanaco MT-5 elemental analyzer. Film thicknesses were measured in five different positions on each film using a micrometer screw gauge and averaged. The cyclic voltammetry (CV) and differential pulse voltammetry (DPV) measurements were carried out using an electrochemical analyzer (Model 608D+DPV, BAS). The measurements were performed in dried and oxygen-free CH_2Cl_2 using 0.1 M tetrabutylammonium hexafluorophosphate ($TBAPF_6$) as a supporting electrolyte. A platinum fiber was used as a working electrode, glassy carbon as a counter electrode, and Ag/Ag^+ as a reference electrode.

Redox potentials were referenced against ferrocene/ferrocenium (Fc/Fc^+). The CV curves were recorded at a scan rate of 100 mVs^{-1}, and the DPV curves were obtained with a pulse width (ΔE_{pulse}) of 0.2 s. The HOMO energy levels of the three donors were calculated according to the equations of $E_{HOMO} = -E_{ox}(vs.\ Fc/Fc^+) - 4.78$ eV and $E_{ox} = E_{peak,ox} + \Delta E_{pulse}/2$, where E_{ox} and $E_{peak,ox}$ are the formal electrode potentials and the DPV peak potentials of the oxidation and reduction, respectively. The LUMO energy levels of PPT was calculated from the CV data of PPT in DMF[8] according to the equations of $E_{LUMO} = -E_{red}(vs.\ Fc/Fc^+) - 4.8$ eV and $E_{red} = (E_{pa,red} + E_{pc,red})/2$, where E_{red}, $E_{pa,red}$ and $E_{pc,red}$ are the formal electrode potentials of the reduction and the potentials of CV peaks on the anodic wave and cathodic wave, respectively.

Optical measurements: The absorption spectra were recorded on a UV-vis-NIR spectrophotometer (LAMBDA 950, Perkin Elmer). The absorption spectra of the radical species were obtained under electrical oxidation in solution containing 0.1 M $TBAPF_6$. The photoluminescence spectra in air were recorded on a spectrofluorometer (FP-8600, JASCO). The phosphorescence spectra at 77 K were recorded on a multi-channel spectrometer (PMA-12, Hamamatsu Photonics) excited using a 340-nm LED (M340L4, Thorlabs) with a band pass filter (340 ±5 nm). The absolute photoluminescence quantum yields (Φ_{PL}) were measured using a quantum yield spectrometer (C9920-02, Hamamatsu Photonics). The streak images, transient photoluminescence spectra, and decay profiles on various timescales were measured in vacuum using a streak camera system (C4334, Hamamatsu Photonics) equipped with a cryostat (GASESCRT-006-2000, Iwatani), and excitation was provided by a nitrogen gas laser (KEN-X, USHO). LPL performance was obtained using a homemade measurement setup with an excitation power of 230 μW and excitation duration of 60 s.[8]

3.4.3 Quantum Chemistry Calculations of the Dipole Moment

All dipole moment values were calculated using the program Gaussian 09. The *cis*- and *trans*-conformations of DMDTB in the ground state were determined using density functional theory (DFT) at the B3LYP/6-31G(d) level. Geometry optimizations of the ground state were performed using DFT at the PBE1PBE/ma-Def2TZVP level. The S_1 and T_1 states as well as the oxidation and reduction states of the investigated three donors and PPT were calculated at the same level.

3.4.4 Film Fabrication

Thick films (0.4 mm) for the optical measurement were fabricated by a melt-casting method.[7] Mixed materials were heated up the melting point of the acceptor (250 ℃) in a nitrogen-filed glovebox. After melting, the substrate was cooled rapidly to room temperature. Thin films for the UV-vis absorption measurements were fabricated by sandwiching the heat-melted materials between two quartz substrates. Film thickness were 18 ± 4 μm (PPT), 25 ± 3 μm (TMB/PPT), 7 ± 4 μm (DMDTB/PPT) and 16 ± 8 μm (TTB/PPT). The ZEONOR doped films were fabricated by solution processing.[6] Materials were dissolved in xylene by ultrasonication and drop-cast on the substrate at 80 ℃ and then annealed for 1 h at 170 ℃ in a nitrogen-filed glovebox.

3.5 References

1 S. Wu, Z. Pan, R. Chen and X. Liu, *Long Afterglow Phosphorescent Materials*, Springer, Cham, ZG, Switzerland, **2017**.

2 S. Xu, R. Chen, C. Zheng and W. Huang, *Adv. Mater.* **2016**, *28*, 9920.

3 T. Matsuzawa, Y. Aoki, N. Takeuchi and Y. Murayama, *J. Electrochem. Soc.* **1996**, *143*, 2670.

4 S. H. Ali, *Resources* **2014**, *3*, 123.

5 R. Kabe and C. Adachi, *Nature* **2017**, *550*, 384.

6 Z. Lin, R. Kabe, N. Nishimura, K. Jinnai and C. Adachi, *Adv. Mater.* **2018**, *30*, 1870341.

7 K. Jinnai, N. Nishimura, R. Kabe and C. Adachi, *Chem. Lett.* **2019**, *48*, 270.

8 K. Jinnai, R. Kabe and C. Adachi, *Adv. Mater.* **2018**, *30*, 1800365.

9 G. C. Abell and A. Mozumder, *J. Chem. Phys.* **1972**, *56*, 4079.

10 K. M. Hong and J. Noolandi, *J. Chem. Phys.* **1978**, *68*, 5163.

11 S. Hirata, *J. Mater. Chem. C* **2018**, *6*, 11785.

12 R. Gao, X. Mei, D. Yan, R. Liang and M. Wei, *Nat. Commun.* **2018**, *9*, 2798.

13 H. Ohkita, W. Sakai, A. Tsuchida and M. Yamamoto, *Macromolecules* **1997**, *30*, 5376.

14 C. A. Boyd, *J. Chem. Phys.* **1949**, *17*, 1221.

15 Y. Hama, Y. Kimura, M. Tsumura and N. Omi, *Chem. Phys.* **1980**, *53*, 115.

16 P. Debye and J. O. Edwards, *J. Chem. Phys.* **1952**, *20*, 236.

17 F. Stolzenburg, B. Ries and H. Bässler, *Ber. Bunsenges. Phys. Chem.* **1987**, *91*, 853.

18 M. Tachiya and A. Mozumder, *Chem. Phys. Lett.* **1975**, *34*, 77.

19 A. Köhler and H. Bässler, *Electronic Processes in Organic Semiconductors*, Wiley-VCH, Weinheim, Germany, **2015**.

20 M. Yamazaki, *J. Mol. Catal. A: Chem.* **2004**, *213*, 81.

21 K. Goushi, K. Yoshida, K. Sato and C. Adachi, *Nat. Photonics* **2012**, *6*, 253.

22 M. Sarma and K.-T. Wong, *ACS Appl. Mater. Interfaces* **2018**, *10*, 19279.

23 S. E. Mylon, S. N. Smirnov and C. L. Braun, *J. Phys. Chem. A* **1998**, *102*, 6558.

24 C. Deng, L. Zhang, D. Wang, T. Tsuboi and Q. Zhang, *Adv. Opt. Mater.* **2019**, *0*, 1801644.

25 G. Méhes, K. Goushi, W. J. Potscavage and C. Adachi, *Org. Electron.* **2014**, *15*, 2027.

26 Y.-S. Park, S. Lee, K.-H. Kim, S.-Y. Kim, J.-H. Lee and J.-J. Kim, *Adv. Funct. Mater.* **2013**, *23*, 4914.

27 V. Jankus, C.-J. Chiang, F. Dias and A. P. Monkman, *Adv. Mater.* **2013**, *25*, 1455.

28 M. K. Etherington, J. Gibson, H. F. Higginbotham, T. J. Penfold and A. P. Monkman, *Nat. Commun.* **2016**, *7*, 13680.

29 H. Noda, H. Nakanotani and C. Adachi, *Sci. Adv.* **2018**, *4*, eaao6910.

30 M. Mamada, G. Tian, H. Nakanotani, J. Su and C. Adachi, *Angew. Chem. Int. Ed.* **2018**, *130*, 12560.

31 X. Cai, W. Qiu, M. Li, B. Li, Z. Wang, X. Wu, D. Chen, X. Jiang, Y. Cao and S.-J. Su, *Adv. Opt. Mater.* **2019**, *7*, 1801554.

32 R. Gao and D. Yan, *Chem. Sci.* **2017**, *8*, 590.

33 B. Zhou and D. Yan, *Adv. Funct. Mater.* **2019**, *29*, 1807599.

34 K. Wang, C.-J. Zheng, W. Liu, K. Liang, Y.-Z. Shi, S.-L. Tao, C.-S. Lee, X.-M. Ou and X.-H. Zhang, *Adv. Mater.* **2017**, *29*, 1701476.

Chapter 4

Polymer-Based Organic Long Persistent Luminescence Materials

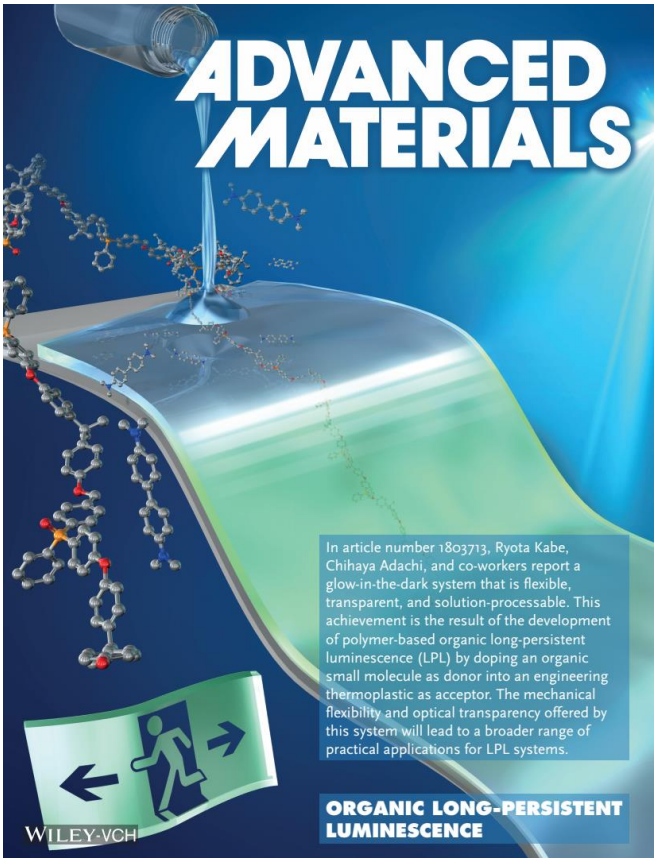

4.1 Introduction

Long persistent luminescence (LPL), also called long afterglow, is the phenomenon when, after being excited, a material in the dark emits light for several seconds, minutes, hours, or even days.[1,2] Since the discovery of the green inorganic LPL material $SrAl_2O_4:Eu^{2+}$, Dy^{3+} by Matsuzawa et al. in 1996, the research and use of inorganic LPL has rapidly grown.[3] Inorganic LPL materials have a wide range of applications including in luminous (also called glow-in-the-dark or noctilucent) ceramics, glass, paint, ink, plastic, fibers, etc.[1] Inorganic LPL materials needs to be ground into a powder and blended with a polymer in the majority of applications,[4] but the poor compatibility of the inorganic powders with common polymers results in poor dispersibility.[4,5] Moreover, the particle size and uniformity of the inorganic powder affect the mechanical properties and transparency of the polymer,[4,5] especially in polymer fibers and films with micrometer-scale diameters or thicknesses.[6,7] At present, these problems can only be partially solved by the surface treatment of the particles[7] and preparation of nanometer-scale inorganic LPL powders.[5] However, these approaches increase the complexity of the fabrication process and still cannot be used to achieve a transparent LPL system.[5]

Since organic emitters potentially combine flexibility and transparency, many types of long-lived phosphorescent emitters have been investigated to date.[8-15] However, because the definition of phosphorescence is a radiative transition between different spin states (usually from a triplet excited state to a singlet ground state), ideal phosphorescence shows an exponential emission decay, and the longest phosphorescent lifetime is still only a few tens of seconds.[8,16-18] Thus, LPL emitters required non-exponential emission decay to achieve a sufficiently long emission duration. In 2017, Adachi an coworkers discovered the first genuine

organic LPL (OLPL) system: a blend of the electron acceptor 2,8-bis(diphenylphosphoryl)dibenzo[b,d]thiophene (PPT) and 1 mol% of the strong electron donor *N,N,N',N'*-tetramethylbenzidine (TMB, Figure 4-1a), which can generate a very stable radical cation.[19] This OLPL system, which is based on emission from exciplexes upon the recombination of long-lived charge-separated states and exhibits a decay profile following the Debye–Edwards law (t^{-m}, with m=1),[20] can be excited with weak power sources and can glow persistently for more than one hour at room temperature.[19] However, this OLPL system has poor flexibility because it consists of only small molecules, which are flexible in very thin films but are brittle and can crack in the bulk state. Therefore, a flexible OLPL system is required for the development of future applications such as fibers, films, and curved products.

In this chapter, I demonstrate the first polymer-based OLPL system: a blend of TMB as an electron donor and a poly(arylene ether phosphine oxide), namely PBPO, as an electron acceptor that can suppress non-radiative deactivation by forming a rigid amorphous environment (Figure 4-1). After low-power excitation at room temperature, this system emits phosphorescence for the first ten seconds followed by LPL lasting more than 7 min, which is significantly longer than conventional room-temperature phosphorescence from polymer systems.[1,15,21-24] Unlike polymer-based OLPL systems utilizing two-photon ionization of organic guest molecules,[25,26] this system does not require strong excitation powers and low temperatures. Moreover, this polymer-based OLPL material can provide the mechanical flexibility needed for the fabrication of various plastic products, fibers, and films (Figure 4-1c). Because PBPO is an engineering plastic, this OLPL system has high performance in terms of

mechanical properties, thermal stability, metal adhesion, flame resistance and oxygen-plasma resistance.[27-30]

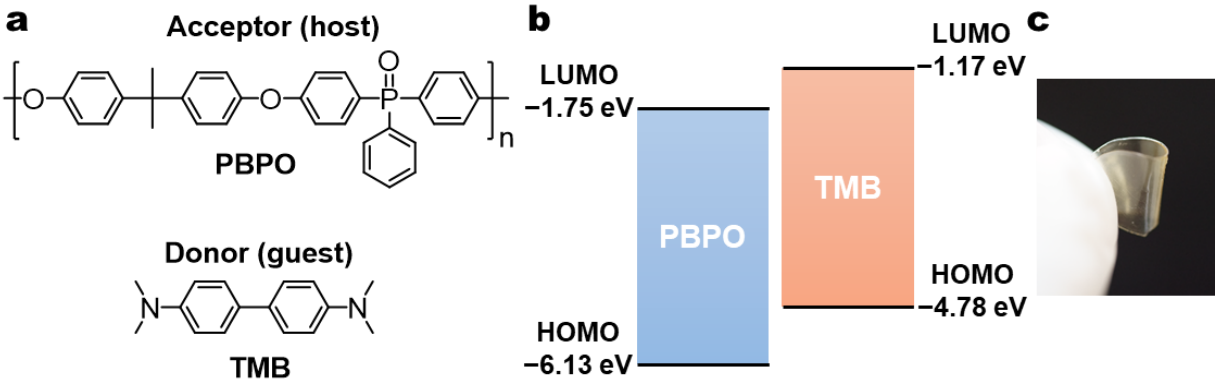

Figure 4-1. (a) Chemical structures. **(b)** The HOMO and LUMO energies of PBPO and TMB. **(c)** Photographs of a bent 1 wt% TMB/PBPO thick film under the ambient light

4.2 Results and Discussion

The electron-accepting polymer PBPO can be easily obtained by polymerization of bisphenol A and bis(4-fluorophenyl)-phenylphosphine oxide (Scheme 4-1) and is very soluble in many polar organic solvents, *e.g.*, chloroform, tetrahydrofuran, *N*,*N*-dimethylformamide, and *N*,*N*-dimethylacetamide (DMAc). The PBPO has good thermal stability (Figure 4-2) and can form amorphous film (Figure 4-3). We prepared thin and thick films of PBPO and 1 wt% TMB/PBPO by drop-casting from DMAc solutions. As a reference polymer, the cyclic olefin copolymer ZEONOR[31] was used in this study because it can provide a nonpolar and rigid amorphous environment without forming a charge-transfer state with TMB. The highest occupied molecular orbital (HOMO) and the lowest unoccupied molecular orbital (LUMO) of PBPO and TMB were estimated from cyclic voltammetry (Figure 4-4) or, in the case of the LUMO of TMB, the absorption spectrum (Figure 4-1b).

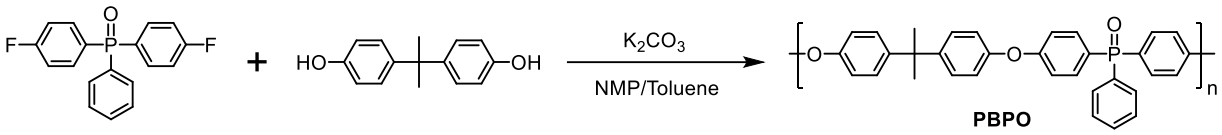

Scheme 4-1. Synthetic route of PBPO.

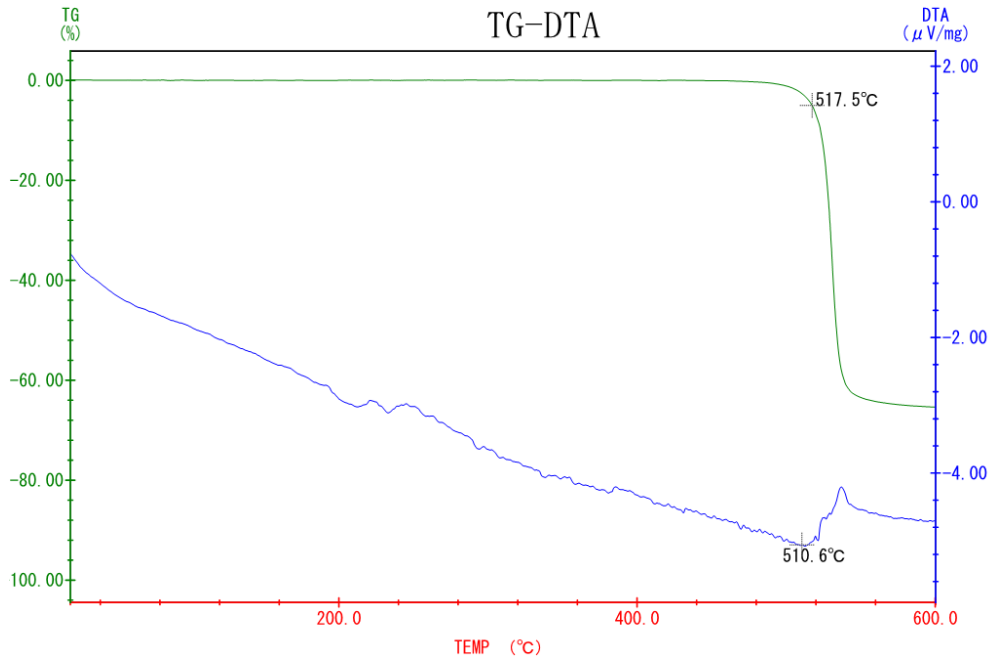

Figure 4-2. The TGA trace of PBPO.

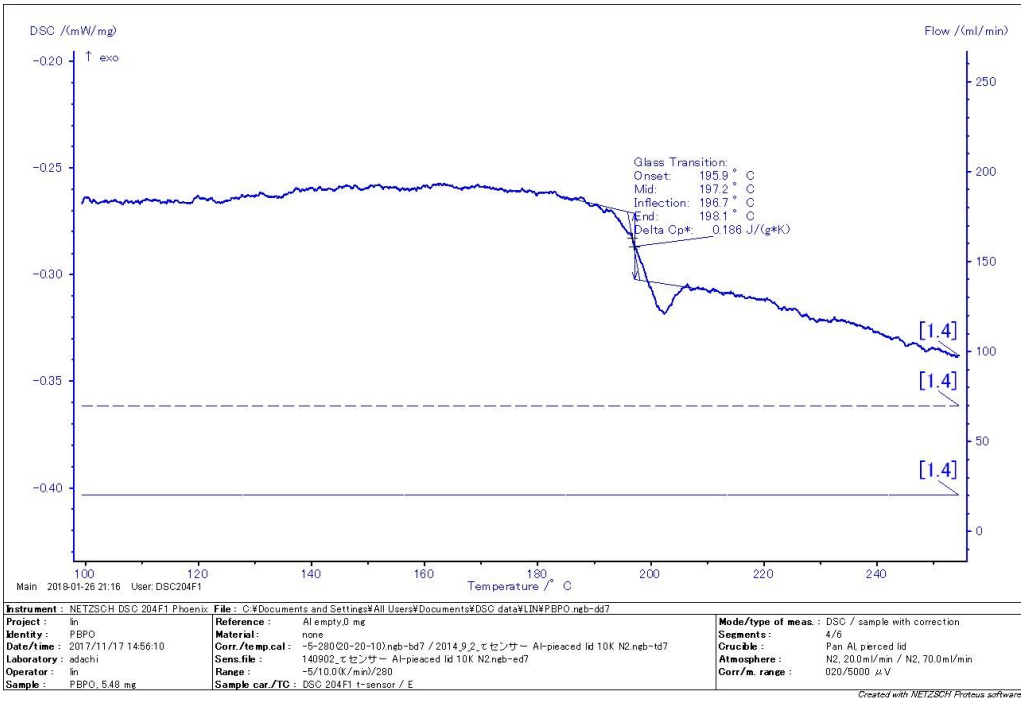

Figure 4-3. The DSC trace of PBPO.

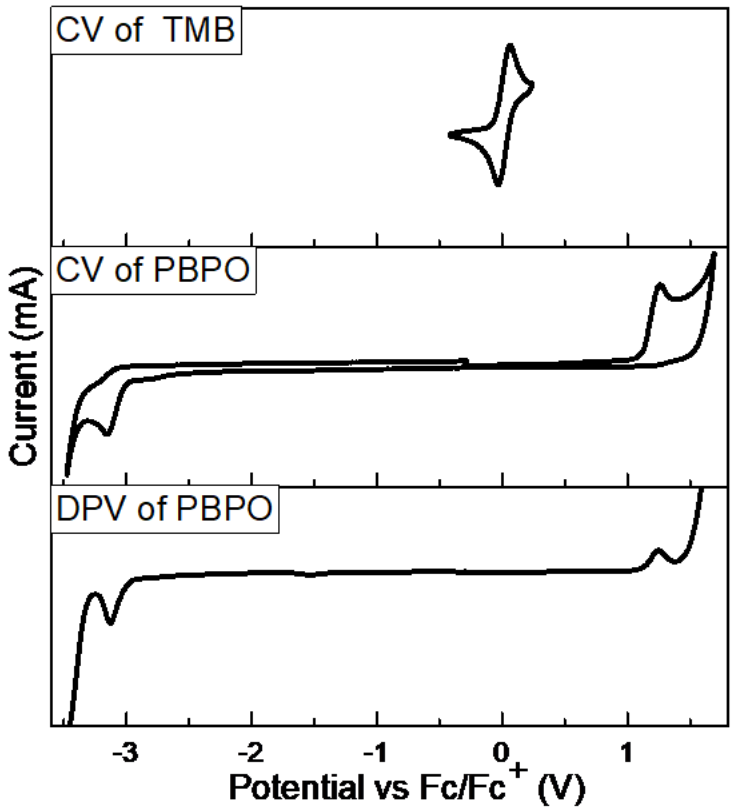

Figure 4-4. The CV curves of TMB and PBPO and the DPV curves of PBPO.

Figure 4-5a shows the ultraviolet-visible (UV-vis) absorption and photoluminescence spectra of PBPO, 1 wt% TMB/PBPO, and 1 wt% TMB/ZEONOR films. The PBPO and 1 wt% TMB/PBPO films have weak apparent absorbance in the visible light region mainly because of Rayleigh scattering by molecules with high polarizability,[32] so their thin films are colorless and transparent while their thick films appear yellowish brown (Figure 4-6). The neat PBPO film exhibited fluorescence at room temperature with an emission peak located at 358 nm and phosphorescence at low temperatures with the main peak and shoulder peaks located at 448 nm, 410 nm, and 480 nm, respectively. The 1 wt% TMB/ZEONOR film at room temperature in N_2 exhibits two distinct emission features with peaks at 387 nm and 526 nm originating from fluorescence and phosphorescence of TMB, respectively. The presence of room-temperature phosphorescence is the result of the rigid environment of the ZEONOR film suppressing the

non-radiative decay of TMB. Quenching of triplets by oxygen causes the phosphorescence to disappear when the photoluminescence is measured in air. Because of this oxygen quenching, the steady-state emission quantum yields (PLQYs) in air of 1wt% TMB/ZEONOR and TMB/PBPO film are 33% ± 2% and 3% ± 1%, respectively. The emission decay lifetimes of the fluorescence (387 nm) and phosphorescence (526 nm) of TMB in ZEONOR were 9.92 ns and 1.09 s, respectively. Here, the lowest singlet excited state and the lowest triplet excited state of donor ($S_{1,D}$ and $T_{1,D}$) and acceptor ($S_{1,A}$ and $T_{1,A}$) were estimated from the emission edge of fluorescence and phosphorescence spectra of 1 wt% TMB/ZEONOR and PBPO film, respectively (Figure 4-5).

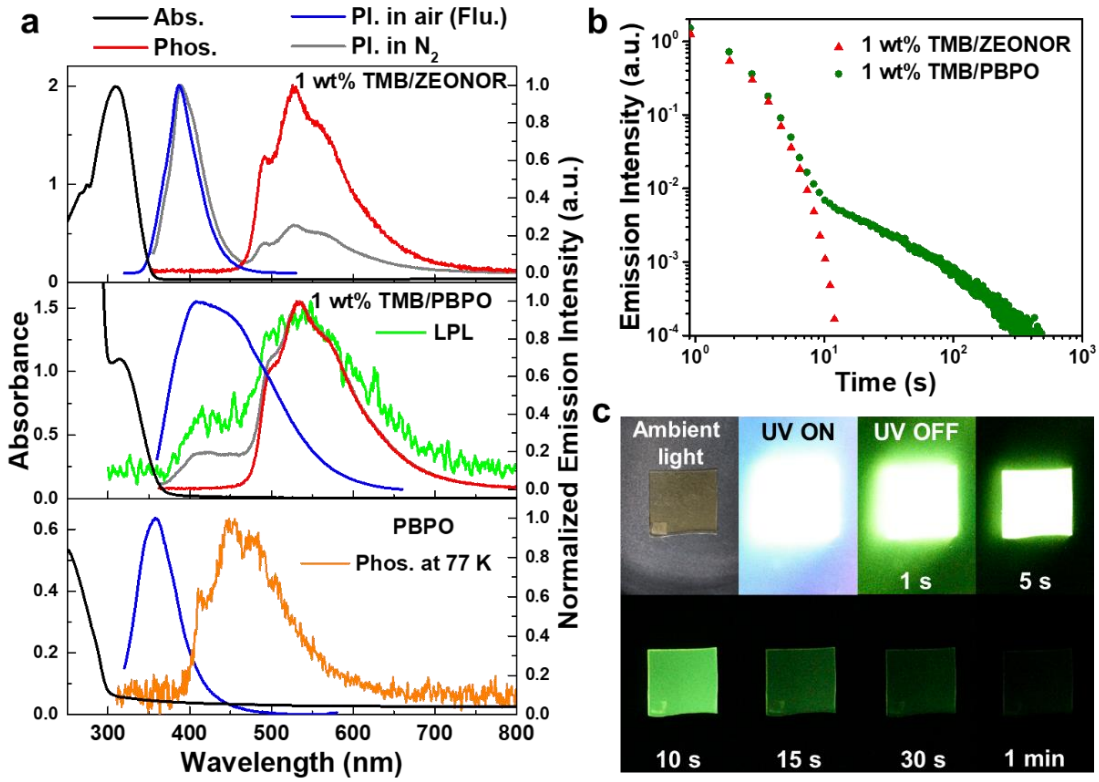

Figure 4-5. (a) UV/Vis absorption, phosphorescence (PBPO: 77 K in vacuum; others: 298 K in N_2), and photoluminescence spectra (298 K in air or N_2) of PBPO, 1% weight percentage (1 wt%) TMB/PBPO, and 1 wt% TMB/ZEONOR films. The absorption spectra of PBPO and 1 wt% TMB/PBPO are from thin films and all other spectra are from thick films. **(b)** Log–log plots of the emission decay profiles of a 1 wt% TMB/PBPO thick film and a 1 wt% TMB/ZEONOR thick film at 298 K. **(c)** Photographs of a 1 wt% TMB/PBPO thick film at 298 K under the ambient light, during excitation by a 365-nm UV lamp, and at various times after turning off the excitation.

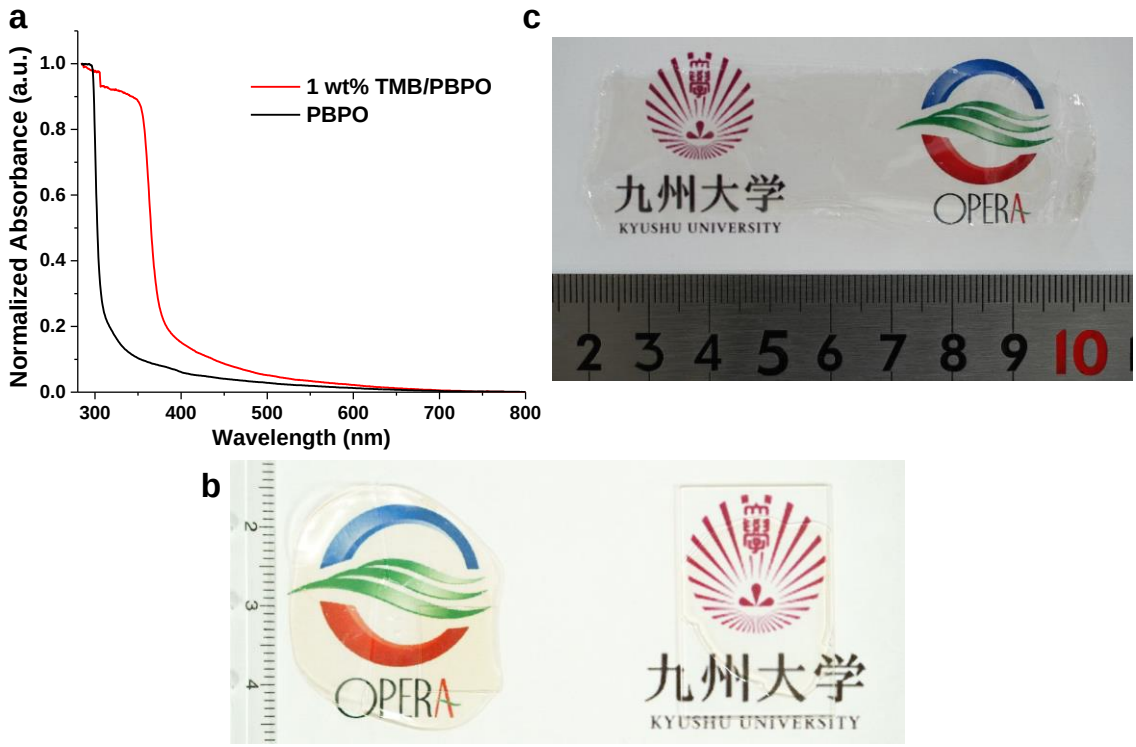

Figure 4-6. (a) The UV/Vis absorption spectra of PBPO and 1 wt% TMB/PBPO thick films; **(b)** the photograph of the 1 wt% TMB/PBPO thick and thin films (left and right, respectively); **(c)** the photograph of the 1 wt% TMB/PBPO large-size thin film.

The 1 wt% TMB/PBPO film in N_2 also exhibits emission peaks from phosphorescence and fluorescence, but the phosphorescence peak is more intense than the fluorescence peak. The fluorescence spectrum obtained in air is much broader than that of the TMB/ZEONOR film because of a contribution to emission from exciplexes formed between TMB and PBPO. Since there are two fluorescence processes, that from TMB itself and that from exciplexes, the emission decay profiles measured at 370 nm and 500 nm were different (Figure 4-7), and the photoluminescence spectrum integrated over 85–185 ns is shifted from that integrated over 0–5 ns (Figure 4-8). The absorption peak at 315 nm and the fluorescence peak at 408 nm of the 1 wt% TMB/PBPO film were slightly red-shifted relative to those of the TMB/ZEONOR film (309 nm and 387 nm, respectively) because of the larger polarity of PBPO.

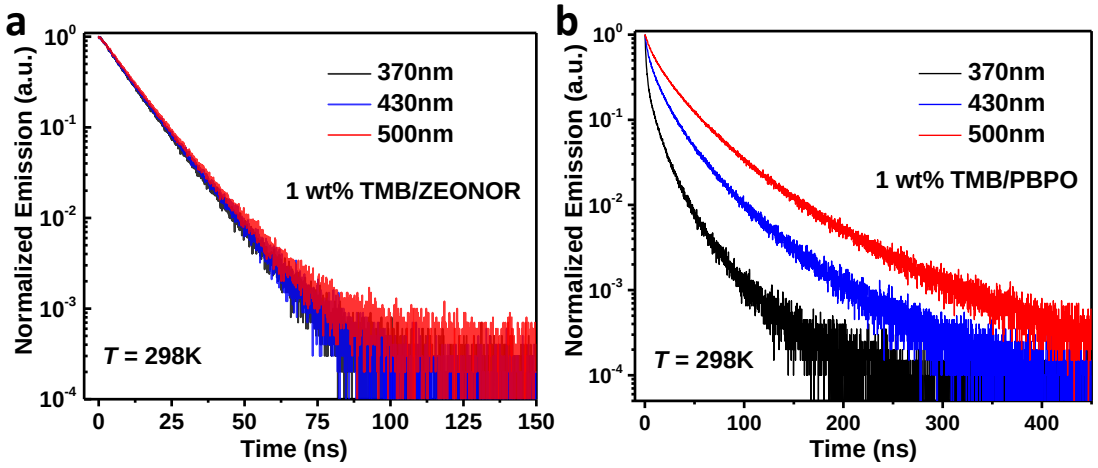

Figure 4-7. (a) and **(b)** Transient photoluminescence decay curves of the 1 wt% TMB/ZEONOR and 1 wt% TMB/PBPO film at the different emission wavelengths at 298 K in air.

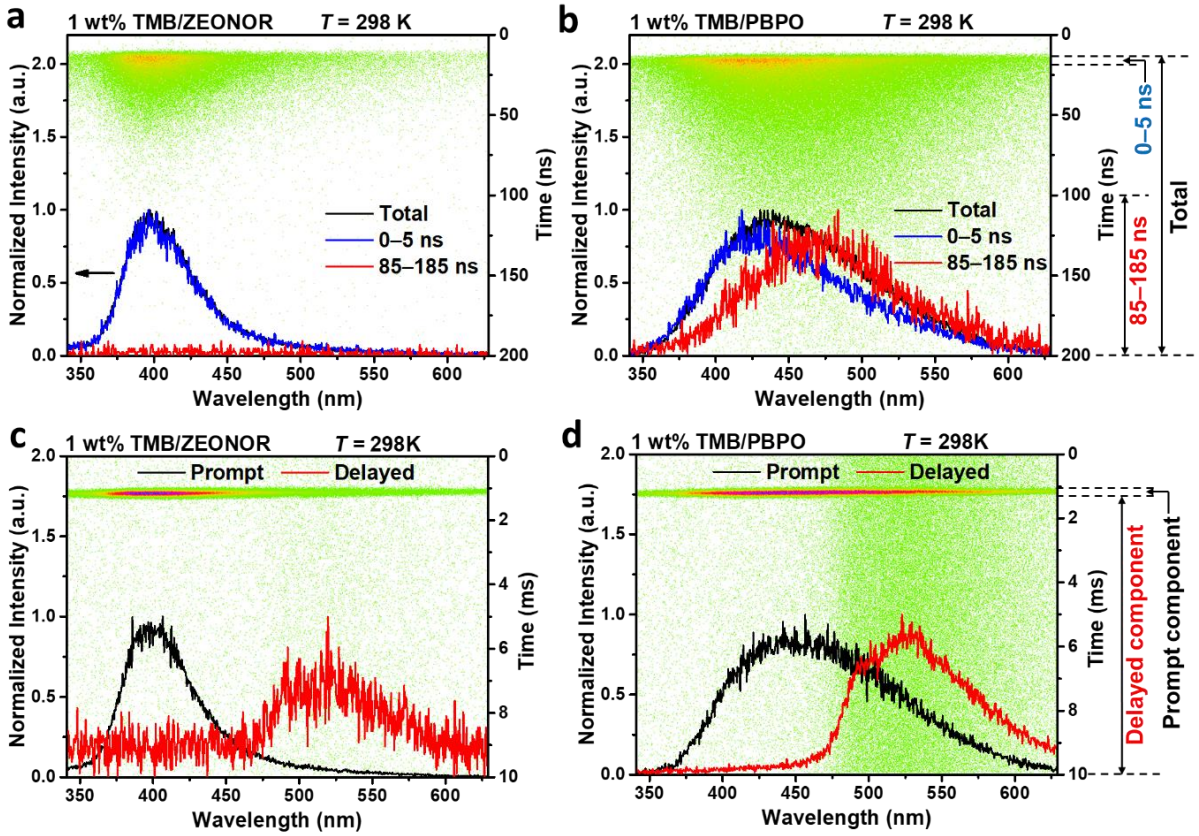

Figure 4-8. (a), (b), (c), (d) Streak images and photoluminescence spectra of 1 wt% TMB/ZEONOR and 1 wt% TMB/PBPO films at 298 K in vacuum. The photoluminescence spectra were resolved into total spectra and prompt and delayed components, in which the spectra of (b) were also resolved into the components in 0–5 ns and 85–185 ns after the maximum of photoluminescence intensity.

Although both the TMB/PBPO and TMB/ZEONOR films exhibit exponential decay from the phosphorescence of TMB up to 10 s after turning off the excitation, only the TMB/PBPO film exhibits LPL emission with a non-exponential decay, which can be clearly distinguished 10 s after turning off the excitation (Figures 4-5b and 4-9). However, the LPL emission spectrum is similar to the phosphorescence of TMB and not the fluorescence of the exciplex between TMB and PBPO (Figure 4-5a). Therefore, this LPL mainly originates from the triplet state of TMB, which is different than the exciplex emission observed in the TMB/PPT system.[19] This LPL emission continues for more than 7 minutes at room temperature (Figure 4-5c). Moreover, the thin TMB/PBPO film exhibits good transparency and mechanical flexibility because of the engineering plastic PBPO, and the emission process is not affected by bending.

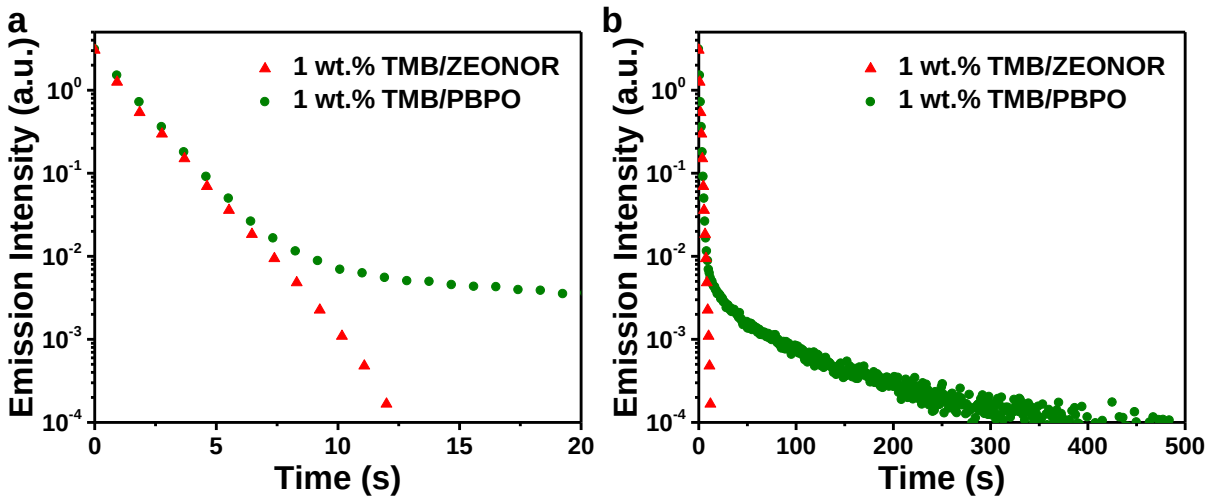

Figure 4-9. Semi-log plots of the emission decay profiles of the 1 wt% TMB/PBPO thick film and the 1 wt% TMB/ZEONOR thick film at 298 K **(a)** from 0 to 20 s; **(b)** from 0 to 500 s.

Based on these results, the proposed emission mechanism is shown in Figure 4-10, in which the LPL process is represented by green arrows. When the TMB/PBPO film is photo-excited under inert atmosphere or vacuum conditions, singlet excited states are excited in TMB ($S_{1,D}$). Since the charge transfer (CT) interaction between TMB and PBPO is not efficient, the

generated excitons are not fully converted into exciplex singlet excited states ($S_{1,E}$). Therefore, the remaining singlet excitons ($S_{1,D}$) exhibit fluorescence and also room-temperature phosphorescence through intersystem crossing (ISC) from $S_{1,D}$ to the triplet excited state ($T_{1,D}$). The generated exciplex singlet states can reversibly convert between the triplet ($T_{1,E}$) and singlet states via ISC and reverse ISC (RISC) because of the small energy gap between $S_{1,E}$ and $T_{1,E}$ at room temperature.[33] However, the triplet exciplex ($T_{1,E}$) does not produce delayed emission because the energy level of $T_{1,D}$ is lower than that of $T_{1,E}$. Here, the exact $T_{1,E}$ value is difficult to estimate because the broad emission mixes with the phosphorescence of TMB, but it should be slightly less than $S_{1,E}$, which appears to be at a higher energy than $T_{1,D}$ based on comparison of the exciplex fluorescence and TMB phosphorescence spectra. In this combination of donor and acceptor, $T_{1,E}$ is higher than $T_{1,D}$ and $T_{1,A}$, which can happen since the energy levels of the exciplex are related to the HOMO of donor and LUMO of acceptor.[34] Therefore, the triplet exciplex ($T_{1,E}$) quickly transfers to TMB ($T_{1,D}$) through a CT process[35] and emits light through phosphorescence from TMB. This is why the steady-state phosphorescence component is a much larger fraction of the overall emission spectrum for the TMB/PBPO film than the TMB/ZEONOR film (Figure 4-5a gray lines).

Because most of the exciplex excitons transfer to $T_{1,D}$ or undergo fluorescence before charge separation (CS), the steady-state emission of the TMB/PBPO film is a mixture of TMB fluorescence and phosphorescence and exciplex fluorescence (Figure 4-5a gray line). All of these emission processes follow an exponential decay. By contrast, some exciplex excitons separate into radical ion pairs through the process of charge separation (CS). The generated radical cation is localized on TMB, and the radical anion diffuses through the PBPO host and

is stored for long periods. After charge recombination (CR) of radical ion pairs, both singlet ($S_{1,E}$) and triplet ($T_{1,E}$) exciplexes are generated, resulting in LPL emission consisting of exciplex fluorescence and, since triplet exciplexes transfer to TMB before radiative decay, TMB phosphorescence. Because this CR process is the rate-determining step, the LPL emission does not follow an exponential decay.

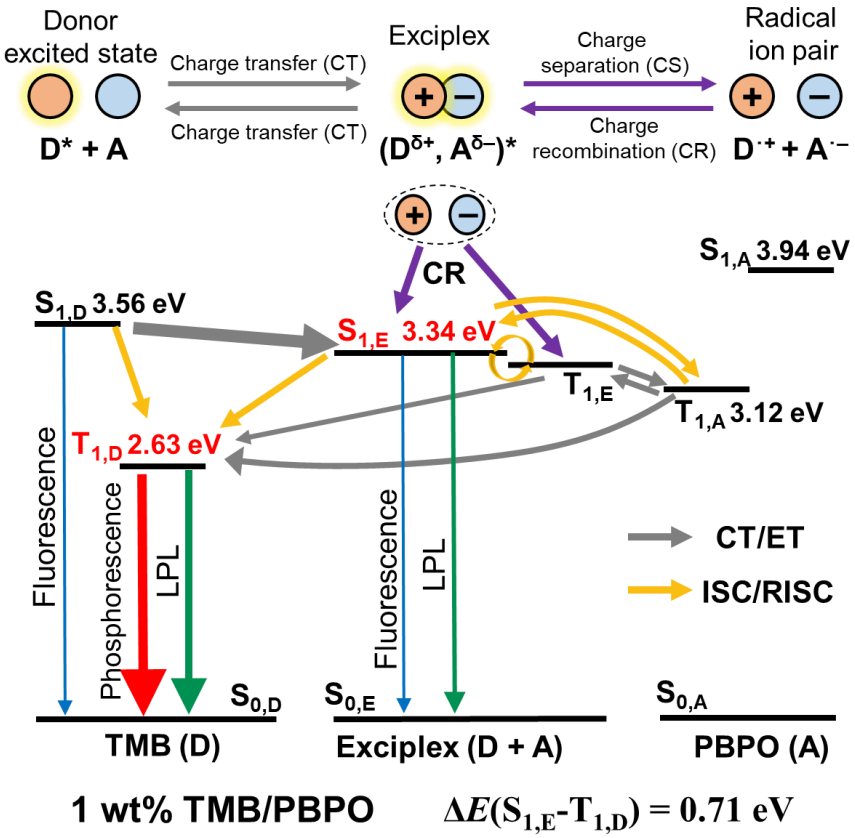

Figure 4-10. Proposed emission mechanism of LPL in a 1 wt% TMB/PBPO film. Here, $S_{1,D}$ and $T_{1,D}$ indicate the singlet and triplet states of TMB, $S_{1,E}$ and $T_{1,E}$ indicate the singlet and triplet states of an exciplex formed between TMB and PBPO, and $S_{1,A}$ and $T_{1,A}$ indicate the singlet and triplet states of PBPO, which were calculated from fluorescence and phosphorescence spectra of 1 wt% TMB/ZEONOR and PBPO films, respectively.

4.3 Summary

In summary, I achieved the first polymer-based OLPL system by blending, using solution processes, a simple organic molecule as the donor with an engineering plastic as acceptor. Unlike small-molecule OLPL systems,[19] this polymer system exhibits good mechanical flexibility and can be bent without making cracks. Incomplete charge transfer and charge separation result in the transient decay of the present polymer-based OLPL system consisting of three parts: first, TMB and exciplex fluorescence; second, TMB phosphorescence; and, finally, LPL consisting of TMB phosphorescence and exciplex fluorescence. The LPL emission of 1 wt% TMB/PBPO in an inert atmosphere at room temperature continues for more than 7 minutes after cutting off the excitation, which is significantly longer than traditional room-temperature phosphorescence.[2] However, because of incomplete charge transfer and charge separation between the small-molecule donor and polymer acceptor, the emission duration of this blend is far less than that of our previous small-molecule OLPL system. Since the photoluminescence efficiency from triplet excited states is usually not efficient for conventional organic molecules, future optimization using donor and acceptor units with lowest triplet states that are higher than $T_{1,E}$ will help improve LPL emission efficiency since exciplex triplet energy can be harvested as emission from singlets through TADF. Energy transfer from the exciplex to an additional emitter provides another path to drastically improve the emission duration along with color purity.[36] Such techniques combined with encapsulation will realize flexible and transparent OLPL under everyday conditions.

4.4 Experimental

4.4.1 Materials and Synthesis

Materials: TMB was purchased from TCI Chemicals (Tokyo, Japan), purified by recrystallization and sublimation, and stored in a brown bottle in a glovebox. ZEONOR 1060R was obtained from ZEON Japan. The starting materials bisphenol A and bis-(4-fluorophenyl) phenylphosphine oxide were purchased from TCI Chemicals (Tokyo, Japan) and Sigma-Aldrich (St. Louis, USA) and were used as received. Potassium carbonate (anhydrous), N-methyl-2-pyrrolidone (NMP), dry toluene, dimethylacetamide (DMAc) and xylene were purchased from Wako Pure Chemical Industries (Osaka, Japan).

Synthesis of PBPO: PBPO was synthesized according to literature [28] and was further purified twice by dissolution/precipitation method (the rude product was dissolved in NMP, filtrated, and precipitated in a large amount of methanol) and once by Soxhlet extraction (methanol, 1d). Yield: 55%. ^{1}H NMR (500 MHz, Chloroform-d) δ: 7.66 (m, 2H), 7.58 (ddd, 4H), 7.51 (t, 1H), 7.44 (tt, 2H), 7.22 (d, 4H), 7.01 (d, 4H), 6.95 (d, 4H), 1.67 (s, 6H) ppm. ^{31}P NMR (203 MHz, Chloroform-d) δ: 28.96 (s) ppm. T_g: 197.2 ^{o}C. $T_{d,5\%}$: 517.5 ^{o}C. Mw: 35600 Da; PDI: 2.80.

4.4.2 General Methods

Measurements and Characterization: ^{1}H NMR and ^{31}P NMR spectra were recorded with a Bruker AVANCE III 500 MHz spectrometer. Molecular weights of the polymers were measured by gel permeation chromatography (GPC) on Shimadzu LC and Shodex column GPC KF-403 HQ with polystyrene as the standard and DMAc as the eluent. Thermal gravimetric analysis (TGA) and differential scanning calorimetry (DSC) were performed with a SHIMADZU DTG-60AH and NETZSCH DSC 204 instrument, respectively, under nitrogen at

a heating rate of 10 ℃/min. Film thicknesses were measured in three different positions on each film using a micrometer screw gauge and averaged.

Optical Measurements: Ultraviolet-visible (UV/Vis) absorption and fluorescence spectra were recorded on a Perkin-Elmer Lambda 950 KPA spectrophotometer and a Jobin Yvon FluoroMax-3 fluorospectrophotometer. Phosphorescent spectra of PBPO were recorded on a JASCO FP-6500 fluorescence spectrophotometer at 77 K. The photoluminescence under nitrogen (Pl. in N_2), the phosphorescence of the 1 wt% TMB/ZEONOR film and the 1wt% TMB/PBPO film, and the LPL (decay profile and spectra) of the 1wt% TMB/PBPO film were obtained at room temperature using the measurement system we reported with an excitation power of 500 μW and excitation duration of 60 s.[3] The absolute photoluminescence quantum yields (PLQY) were measured using the Hamamatsu Photonics Quantaurus-QY in air at room temperature. The transient photoluminescence decay curves of films were recorded in air using a Quantaurus-Tau fluorescence lifetime measurement system (C11367-03, Hamamatsu Photonics) and 340-nm excitation. The streak images and photoluminescence spectra of films on various timescales were measured in vacuum using a streak camera system (Hamamatsu Photonics, C4334) equipped with a cryostat (Iwatani, GASESCRT-006-2000, Japan), and excitation was provided by a nitrogen gas laser (Lasertechnik Berlin, MNL200) with an excitation wavelength of 337 nm. The photograph and video were recorded on a Sony α7sII digital camera with the sample excited using a 365-nm UV lamp. The emission decay lifetimes (τ) of fluorescence and phosphorescence of TMB in ZEONOR were obtained by fitting the transient photoluminescence decay curve (Figure 4-3) and the emission decay profile of phosphorescence (Figure 4-5b or 4-6) with an exponential decay function of

$$I(t) = I(0)e^{-\frac{t}{\tau}} \quad (4\text{-}1)$$

where $I(t)$ and $I(0)$ represent the luminescence intensity at decay time $t = t$ and 0, for exponential decay profiles.

Electrochemistry Characterization: Cyclic voltammetry (CV) and differential pulse voltammetry (DPV) curves were recorded at room temperature on a CHI600 voltammetric analyzer with a conventional three electrode configuration consisting of a platinum-disk working electrode, a platinum-wire auxiliary electrode, and an Ag-wire pseudo-reference electrode. Ferrocene was used as the reference and tetrabutylammonium hexafluorophosphate ($TBAPF_6$) was used as the supporting electrolyte. Nitrogen-purged DCM was used as the solvent for the oxidation scan of PBPO and TMB, THF for the reduction scan of PBPO. The CV curves were recorded at a scan rate of 100 mV/s, and the DPV curve of PBPO was obtained with a pulse width (ΔE_{pulse}) of 0.2 s. The HOMO and LUMO energy levels of PBPO were calculated according to the equation E_{HOMO} (or E_{LUMO}) = −[$E^{\circ\prime}_{ox}$ (or $E^{\circ\prime}_{red}$) + 4.78 eV] and $E^{\circ\prime}_{ox}$ (or $E^{\circ\prime}_{red}$) = $E_{peak,ox}$ (or $E_{peak,red}$) + ΔE_{pulse} / 2, where $E^{\circ\prime}_{ox}$, $E^{\circ\prime}_{red}$ and $E_{peak,ox}$, $E_{peak,red}$ are the formal electrode potentials and the DPV peak potentials of the oxidation and reduction, respectively. The HOMO of TMB was calculated according to the same equation, where $E^{\circ\prime}_{ox}$ = $E_{onset,ox}$ and the $E_{onset,ox}$ was the onset of the oxidation potential in CV. The LUMO of TMB was calculated from the E_{HOMO} of TMB and the onset of UV/Vis absorption spectrum of TMB in toluene from the previous report.[19]

4.4.3 Film Fabrication

Fabrication of 1 wt% TMB/PBPO film: First, 100 mg of PBPO was dissolved in 1 mL of DMAc and degassed by Ar bubbling for 3 min. Then, 1 mg of TMB was dissolved in this

solution under dark conditions. In a nitrogen-filled glovebox, this solution was drop-cast on the substrate at 110 ℃ and then annealed for 1 h at 170 ℃ and then 1 h at 190 ℃. The film was further dried at 100 ℃ in a vacuum oven for 24 h. A thin film (16 ± 5 μm) fabricated on the quartz substrate was used for the UV-vis absorption measurement (Figure 4-5a). A thick film (124 ± 20 μm) fabricated on a PTFE substrate was peeled off, cut into a 1 cm^2 piece (140 ± 4 μm) for the emission measurements (Figure 4-5) and the other part (124 ± 15 μm) for the UV-vis absorption measurement of the thick film (Figure 4-6a) and the flexible display (Figure 4-1c). A large size thin film (35 ± 20 μm) fabricated on the silicon wafer substrate was used for showing the flexibility.

Fabrication of PBPO film: The procedure was the same as for the TMB/PBPO films except that only PBPO (100 mg) was dissolved in DMAc (1 mL). The thickness of the thin and thick films was 22 ± 4 μm and 125 ± 6 μm, respectively.

Fabrication of 1 wt% TMB/ZEONOR film: The preparation method was the same as 1wt% TMB/PBPO film except that PBPO was replaced with ZEONOR which was dissolved in the solvent by ultrasonication, xylene was used as the solvent, and the quartz substrate was 80 ℃ when drop-casting was performed. Only a thick film, with a thickness of 105 ± 9 μm, was fabricated.

4.5 References

1 S. Wu, Z. Pan, R. Chen and X. Liu, *Long Afterglow Phosphorescent Materials*, Springer, Cham, ZG, Switzerland, **2017**.

2 S. Xu, R. Chen, C. Zheng and W. Huang, *Adv. Mater.* **2016**, *28*, 9920.

3 T. Matsuzawa, Y. Aoki, N. Takeuchi and Y. Murayama, *J. Electrochem. Soc.* **1996**, *143*, 2670.

4 M. P. Anesh, S. K. H. Gulrez, A. Anis, H. Shaikh, M. E. Ali Mohsin and S. M. Al-Zahrani, *Adv. Polym. Technol.* **2014**, *33*, 21436.

5 R. E. Rojas-Hernandez, F. Rubio-Marcos, M. Á. Rodriguez and J. F. Fernandez, *Renew. Sust. Energ. Rev.* **2018**, *81*, 2759.

6 F. Ye, S. Dong, Z. Tian, S. Yao, Z. Zhou and S. Wang, *Opt. Mater.* **2013**, *36*, 463;

7 X. Zhang, Z. Zhou, F. Ye, X. Liu and Q. Li, *Mater. Sci. Semicond. Process.* **2015**, *40*, 130.

8 S. Hirata, *Adv. Opt. Mater.* **2017**, *5*, 1700116.

9 Z. An, C. Zheng, Y. Tao, R. Chen, H. Shi, T. Chen, Z. Wang, H. Li, R. Deng, X. Liu and W. Huang, *Nat. Mater.* **2015**, *14*, 685.

10 W. Zhao, Z. He, J. W. Y. Lam, Q. Peng, H. Ma, Z. Shuai, G. Bai, J. Hao and B. Z. Tang, *Chem* **2016**, *1*, 592.

11 Y. Xie, Y. Ge, Q. Peng, C. Li, Q. Li and Z. Li, *Adv. Mater.* **2017**, *29*, 1606829.

12 J. Yang, X. Zhen, B. Wang, X. Gao, Z. Ren, J. Wang, Y. Xie, J. Li, Q. Peng, K. Pu and Z. Li, *Nat. Commun.* **2018**, *9*, 840.

13 L. Gu, H. Shi, M. Gu, K. Ling, H. Ma, S. Cai, L. Song, C. Ma, H. Li, G. Xing, X. Hang, J. Li, Y. Gao, W. Yao, Z. Shuai, Z. An, X. Liu and W. Huang, *Angew. Chem. Int. Ed.* **2018**, *57*, 8425.

14 Y. Su, S. Z. F. Phua, Y. Li, X. Zhou, D. Jana, G. Liu, W. Q. Lim, W. K. Ong, C. Yang and Y. Zhao, *Sci. Adv.* **2018**, *4*, eaas9732.

15 T. Ogoshi, H. Tsuchida, T. Kakuta, T. Yamagishi, A. Taema, T. Ono, M. Sugimoto and M. Mizuno, *Adv. Funct. Mater.* **2018**, *28*, 1707369.

16 J. L. Kropp and W. R. Dawson, *J. Phys. Chem.* **1967**, *71*, 4499.

17 H. Mieno, R. Kabe, N. Notsuka, M. D. Allendorf and C. Adachi, *Adv. Opt. Mater.* **2016**, *4*, 1015.

18 S. Hirata and M. Vacha, *Adv. Opt. Mater.* **2017**, *5*, 1600996.

19 R. Kabe and C. Adachi, *Nature* **2017**, *550*, 384.

20 P. Debye and J. O. Edwards, *J. Chem. Phys.* **1952**, *20*, 236.

21 G. Zhang, J. Chen, S. J. Payne, S. E. Kooi, J. N. Demas and C. L. Fraser, *J. Am. Chem. Soc.* **2007**, *129*, 8942.

22 H. A. Al-Attar and A. P. Monkman, *Adv. Funct. Mater.* **2012**, *22*, 3824.

23 C. A. DeRosa, J. Samonina-Kosicka, Z. Fan, H. C. Hendargo, D. H. Weitzel, G. M. Palmer and C. L. Fraser, *Macromolecules* **2015**, *48*, 2967.

24 X. Chen, C. Xu, T. Wang, C. Zhou, J. Du, Z. Wang, H. Xu, T. Xie, G. Bi, J. Jiang, X. Zhang, J. N. Demas, C. O. Trindle, Y. Luo and G. Zhang, *Angew. Chem. Int. Ed.* **2016**, *55*, 9872.

25 H. Ohkita, W. Sakai, A. Tsuchida and M. Yamamoto, *Macromolecules* **1997**, *30*, 5376.

26 H. Ohkita, W. Sakai, A. Tsuchida and M. Yamamoto, *J. Phys. Chem. B* **1997**, *101*, 10241.

27 D. J. Riley, A. Gungor, S. A. Srinivasan, M. Sankarapandian, C. Tchatchoua, M. W. Muggli, T. C. Ward and J. E. McGrath, *Polym. Eng. Sci.* **1997**, *37*, 1501.

28 H. Satpathi, D. Pospiech, S. Banerjee and B. Voit, *Polym. Degrad. Stab.* **2014**, *107*, 53.

29 K. U. Jeong, I. Y. Park, I. C. Kim and T. H. Yoon, *J. Appl. Polym. Sci.* **2001**, *80*, 1198.

30 C. D. Smith, H. Grubbs, H. F. Webster, A. Gungör, J. P. Wightman and J. E. McGrath, *High Perform. Polym.* **1991**, *3*, 211.
31 M. Yamazaki, *J. Mol. Catal. A: Chem.* **2004**, *213*, 81.
32 Y. Takezawa, N. Taketani, S. Tanno and S. Ohara, *J. Appl. Polym. Sci.* **1992**, *46*, 1835.
33 K. Goushi, K. Yoshida, K. Sato and C. Adachi, *Nat. Photon.* **2012**, *6*, 253.
34 X. K. Liu, Z. Chen, C. J. Zheng, C. L. Liu, C. S. Lee, F. Li, X. M. Ou and X. H. Zhang, *Adv. Mater.* **2015**, *27*, 2378.
35 E. V. Anslyn and D. A. Dougherty, *Modern Physical Organic Chemistry*, University Science Books, Sausalito, California **2006**.
36 K. Jinnai, R. Kabe and C. Adachi, *Adv. Mater.* **2018**, *30*, 1800365.

Chapter 5

Conclusions and Perspective

5.1 Conclusions

Realizing LPL from organic systems as well as inorganic LPL materials at room temperature is an important issue to solve the materials, sustainability. In 2017, Kabe and Adachi realized the first OLPL material using the organic donor/acceptor binary system (TMB/PPT), which also has the power-law emission kinetics like inorganic materials and far beyond the emission duration of all existing organic room-temperature phosphorescence systems.[1] However, such a small molecule system has poor mechanical properties and LPL performance that does not meet the requirements of commercial LPL materials, even though it possesses high transparency that is difficult to achieve with inorganic materials. In this thesis, for the development of multicolor, long duration, and flexible OLPL system, the color-tuning and the excited-state dynamics of LPL and were studied. Moreover, the first flexible and transparent polymer-based OLPL system was realized.

In **Chapter 1**, the definition and historical backgrounds of LPL are described. The differences between LPL and phosphorescence are clarified. The advantages and issues of OLPL materials are illustrated.

In **Chapter 2**, an orange donor/acceptor binary OLPL system was demonstrated by replacing TMB with a low HOMO level donor. I found a donor TTPD, which is easier to chemically modify than TMB, exhibits a similar HOMO level to TMB. Then, the lower HOMO donor TBAPD was synthesized by electron-donating substitutions into TTPD. The emission spectra of a TBAPD/PPT film shifted to the orange range and its LPL continued for approximately 5 minutes. This work proved LPL spectra can still

be tuned by adjusting the HOMO level of donors.

In **Chapter 3**, the influence of charge-transfer and local excited states' energy gap, $\Delta E(^1CT-^3LE_D)$, in exciplex system on OLPL was demonstrated by comparing the transient PL spectra in different time-ranges and LPL performance of three donors possessing similar molecular structures but different HOMO and triplet energy levels. The OLPL efficiency was reduced along with decreasing the energy level of ^3LE_D which is lower than that of the ^1CT, because a large $\Delta E(^1CT-^3LE_D)$ encourages a larger population of triplet Frenkel excitons. These excitons on ^3LE_D are difficult not only to re-convert into charge-transfer excitons but also to divide into separated radical ion pairs. They released the exciting energy by the phosphorescence of donors, which induces the dual emission from both ^1CT and ^3LE_D. Especially, the TTB/PPT system showed a white light without the use of additional dopants. Moreover, the LPL emission spectra were also affected by the absorption of the donor radical cations generated by the charge separation process. This work provided a foundation for designing efficient OLPL systems using both small molecules and polymers.

In **Chapter 4**, the first polymer-based OLPL system was achieved by blending the low-concentration TMB into an acceptor polymer, PBPO. Hinging on the high mechanical performance of PBPO, this polymer-based OLPL system exhibits excellent flexibility and the thick film can be bent without making cracks. However, because of the large $\Delta E(^1CT-^3LE_D)$, conspicuous phosphorescence of TMB was observed for the first ten seconds after excitation. The subsequent LPL also contained the phosphoresce component. The outstanding flexibility and high transparency of this polymer-based

OLPL film clearly demonstrated the superiority of polymer-based OLPL systems to polymer composites compounded with inorganic LPL powders.

5.2 Perspective

The mechanism and material development of OLPL have many issues that need to be further studied and solved. Based on the results of this thesis, some fundamental problems were also discovered.

1. The power-law kinetic model of binary OLPL systems uses random walks of electrons/holes or traps distribution like inorganic LPL needs to be clarified. If the OLPL follows the trap model, what is the origin of the traps in the binary system?
2. What is the limit of OLPL performance and what is the origin of the limit?
3. Although the existence of CS states and the importance of CT states to form CS states were proved, the detailed conversion process between CT and CS states, which is the key to LPL, is still unclear. How to reveal this process through experiments is not well established for both OLPLs and organic photovoltaics.
4. I found a closed correlation between the absorption spectra of radical cations and the emission spectra of LPL. However, direct evidence of the negative influence of radical ion absorptions on LPL needs to be provided. The absorptions of radical cations are often similar to that of the triplet excited states. How to eliminate this overlapping?

5. I have demonstrated the influence of the transition from ^{3}LE to CT states and the absorption of radical ions for LPL emission. Is there any other process to retard the CS process or quench the emission after the CR process?
6. Photoaging of polymers originates from the production of free radicals after photoexcitation, leading to the breaking of chemical bonds in the polymer backbone.[2] Therefore, in order to resist aging, radical scavengers are often added to polymers. However, the current OLPL system requires long-lived radical anions and cations. Thus, we need further confirmation whether these free radicals will cause the aging of the polymers.
7. Because of the long-lived active radicals in LPL systems, LPL is easily quenched by oxygen. Therefore, it is important to study the technique of isolating oxygen or the preparation of LPL systems which is insensitive to oxygen.
8. The realization of near-infrared OLPL systems is of great significance for bio-imaging. Although the existing NIR inorganic LPL systems have an outstanding afterglow performance (see Table 1-1), the congenital problem of inorganic materials restricts their *in vivo* application. Inorganic nanoparticles cannot be metabolized by organisms and cannot be excluded from the body.

5.3 References

1 R. Kabe and C. Adachi, *Nature*, **2017**, *550*, 384.

2 J. W. Nicholson, *The Chemistry of Polymers*, Royal Society of Chemistry, Cambridge, UK, **2006**.

Acknowledgements

First and foremost, I would like to take the opportunity to express my heartfelt gratitude and respect to my supervisor, Professor Chihaya Adachi. He gave me the unique opportunity to come to Japan and initiated me into this very fascinating and challenging field of organic electronics and photonics. Without this opportunity, his constant support, encouragement, and motivation, this thesis would be impossible to become a reality.

I am interested in the molecular design of organic semiconductor materials since my college days. But, for some reason, I failed to do this research when I was studying for my master's degree. I always wanted to make up for this regret. Thus, after I graduated with a master's degree and received the MEXT scholarship, I first contacted Professor Adachi who made a major breakthrough in the field of organic electronics at that time. I still remember that the first time I contacted him via email was on a Saturday, and he replied to me on Sunday to agree with me to join his group. I was very excited, so I did not contact other professors but directly came to Kyushu University. In my first year as a Ph.D., owing to my poor foundation in organic photophysics, I encountered many difficulties and was often frustrated. But at each R-MTG, Professor Adachi did not criticize me but always encouraged me to overcome difficulties.

I also deeply grateful to the other members of my committee, Professor Hiroyuki Furuta and Professor Ken Onda for serving on my dissertation committee and their kindly, helpful suggestions and comments on my presentation and thesis.

Furthermore, my sincere thanks go to Associate Professor Ryota Kabe, who advised me in the three years of my doctoral study period, patiently taught me many essential techniques and methods related to my work, carefully revised my three papers and this thesis, and provided a lot of help in academic study and daily life. The most important thing is that if he did not let me do this research about OLPL, there would not be this thesis. Moreover, to submit the paper to Nature Communications (chapter 3), we paid 8 months, during which Associate Professor Kabe spent a lot of time to revise my manuscript and provided a lot of valuable comments. He also did the ESR experiment by himself for answering a comment at the last review, because I

needed to complete another paper on time and really no time to do that. In addition, he gave me substantial suggestions for the refinement of my presentation during the preparation of the oral defense. Professor Adachi and he always encourage me to do valuable research. Improvement of my research taste is my most important harvest in Adachi lab.

I would like to thank Associate Professor Hajime Nakanotani for his careful review of the PPT file of my oral defense and their valuable comments. I wish to acknowledge Associate Professor Yoichi Tsuchiya for his help in GPC and CV (Chapter 4). I want to deeply thank Dr. Kai Wang in Soochow University, who did the quantum chemistry calculation about molecular confirmations and discuss detailed mechanism with me (Chapter 3). I often talk with him about research, life and future development, and I learned a lot from him. It was really a very pleasant experience. I would like to express my special thanks to Dr. William J. Potscavage, Jr., who kindly revised my two papers and gave many valuable comments (Chapter 3&4). I also would like Mr. Kazuya Jinnai and Mr. Naohiro Nishimura. They taught me preparation and measurement methods about OLPL materials when I changed my research direction into OLPL in my second year here. Without their help, the work in Chapter 4 cannot be completed quickly. If Mr. Naohiro Nishimura did not find the impurity effect, I would waster more time and even delayed longer to graduate.

I also would like to express my special gratitude to Assistant Professor Masashi Mamada. He gave me much help in organic synthesis, usage of equipment, and so on. At first year, I often asked him question, he always answer me patiently and gave me many comments kindly. I would like to thank Assistant Professor Kenichi Goushi for his kind help and valuable comments in some photophysical experiments. I also sincerely thank Visiting Professor Jean Charles Ribierre who advised me in the first half year of my doctoral study period.

I am heartily thankful to Professor Chuanjiang Qin; Associate Professor Yan Geng; Dr. Linsong Cui, Chin-Yiu Chan, Hao Ye, Wei Liu, Guojian Tian, Yiu Wing Wong and Yi-Ting Lee. They gave me a lot of advice in research and a lot of help in experiments and daily life in my doctoral study period. For example, Professor Qin taught me the usage of liquid nitrogen tank, Associate Professor Geng taught me grow single crystal, Dr. Linsong Cui taught me the use of evaporation and sublimation equipment, Dr. Chan taught me use the MS and knowledge of CV, Dr. Wei Liu gave me advise in the design of OLED device and mechanism knowledge

of exciplex in my first year, Dr. Guojian Tian taught me the use of CV, Dr. Yiu Wing Wong and Dr. Yi-Ting Lee gave me much help in synthesis. Dr. Hao Ye is my best friend here and gave me too much help in many aspects. I am really lucky and glad to meet him.

Besides them, thanks are due to former and recent Adachi lab members, Associate Professor Toshinori Matsushima, Sandanayaka S. D. Atula; Dr. Fatima Bencheikh, Daehyeon Kim, Matthew Leyden, Morgan Auffray, Umamahesh Balijapalli, Ryutaro Komatsu, Hiroyuki Mieno, Hiroki Noda, Daichi Okada; Mr. Ko Inada, Jonguk Kim, MD Ashadul Islam, Masayuki Yokoyama, Naoto Noutsuka, Masaki Tanaka, Yu Esaki, Ryo Nagata, Ganbaatar Tumen-Ulzii, Buddhika Sanjeewa Bandara Karunathilaka, Tai Cheng, Momoka Miyajima, Yuu Shihara, Muhammad Hasnan Sazzad, Shibin Ruan, Toshiya Fukunaga, Satoshi Maedera, Yuki Kashima, Nguyen Thanh Ba, Seiya Yoshida, Ieuji Ryota, Koudai Ikesue, Kenta Yamaguchi, Ryota Nakamura, Tang Xun, Ryo Akamatsu, Yuhi Ueda, Yuya Oyama, Shinichi Tan, Satoru Watanabe, Chathuranganie Senevirathne, Jaehyun Bae, Tomohiro Ishii, Alasvand Yazdani Sahar, Xuelong Wu, Zhao Feng, and all other students.

And I also want to thank all the staffs of Adachi lab for kindly support on my life, study and experiments. Especially to Ms. Keiko Kusuhara and Nozomi Nakamura for their kind support in materials and help in DSC, TGA. I am thankful to Ms. Rei Sasagawa, Hiroko Kuratomi, Mayumi Kudo, Sachiko Higashikawa, Nao Onishi, Hiromi Aizaki for their kind support and a lot of help from my enrollment to graduation.

Next, I am deeply grateful to Professor Qisheng Zhang in Zhejiang University. I also often ask him question, he always kindly answer me. He really wisdom and love scientific research. I have benefited from every discussion with him.

I learned a lot from them in these years. I hope we have more cooperation in the future.

I acknowledges the Ministry of Education, Culture, Sports, Science and Technology (MEXT) Top Global University Project and the China Scholarship Council (CSC) gave me this opportunity to study in Japan and scholarship. I also acknowledges Japan Science and Technology Agency (JST), ERATO, Adachi Molecular Exciton Engineering Project for financially support that made it possible to complete this study.

Finally, I am deeply indebted to my parents for their unwavering love, everlasting encouragement and support. In the meanwhile, I owe special thanks to my girlfriend, I express

my heartfelt gratitude her love, understanding and moral support. It is their emotional support, love, and encouragement that have inspired me to complete this thesis. I dedicate this thesis to them, and hope that all efforts in my whole life will stand testimony to the fact that all their hard work and sacrifice over the years have not been in vain.

January, 2020

Zesen Lin

Appendix

List of Abbreviations

Materials

N,*N*′-dimethyl-*N*,*N*′-ditolylbenzidine (**DMDTB**)

4,4′,4″-tris[phenyl(*m*-tolyl)amino]-triphenylamine (***m*-MTDATA**)

Poly(alkyl methacrylate)s (**PnBMA**)

Poly(bisphenol-A ether phenyl phosphine oxide) (**PBPO**)

Poly(alkyl methacrylate)s (**PEMA**)

Poly(alkyl methacrylate)s (**PMMA**)

2,8-bis(diphenylphosphoryl)dibenzo[b,d]thiophene (**PPT**)

Polystyrene (**PSt**)

N,N,N',N'-tetrakis[(4-(diisobutylamino)phenyl]-1,4-phenylenediamine (**TBAPD**)

N,*N*,*N*′,*N*′-tetramethylbenzidine (**TMB**)

N,N,N′,N′-tetratolylbenzidine (**TTB**)

N,*N*,*N*′,*N*′-tetra(4-tolyl)-1,4-phenylenediamine (**TTPD**)

Keywords

Conduction band (**CB**)

International Commission on Illumination, "Commission internationale de l'éclairage" (**CIE**)

Charge recombination (**CR**)

Charge separation (**CS**)

Cyclic voltammetry (**CV**)

Differential pulse voltammetry (**DPV**)

Förster energy transfer (**FRET**)

Highest Occupied Molecular Orbital (**HOMO**)

Intersystem crossing (**ISC**)

Isothermal luminescence (**ITL**)

Long-persistent luminescence (**LPL**)

Lowest Unoccupied Molecular Orbital (**LUMO**)

Near infra-red (**NIR**)

Organic light-emitting diodes (**OLEDs**)

Organic long persistent luminescence (**OLPL**)

Organic photovoltaics (**OPVs**)

Reverse intersystem crossing (**RISC**)

Room-temperature phosphorescence (**RTP**)

Thermally activated delayed fluorescence (**TADF**)

Thermoluminescence (**TL**)

Thermally stimulated luminescence (**TSL**)

Ultraviolet (**UV**)

Ultraviolet-visible (**UV-vis**)

Valence band (**VB**)

Symbols

Electron acceptor, or simply acceptor (**A**)

Lowest CT singlet excited state (^{1}**CT**)

Lowest CT triplet excited state (^{3}**CT**)

Electron donor, or simply donor (**D**)

LUMO level of the acceptor ($\boldsymbol{E_{A,LUMO}}$)

HOMO level of the donor ($\boldsymbol{E_{D,HOMO}}$)

Luminescence intensity at time *t* ($\boldsymbol{I(t)}$)

Intensity of delayed fluorescence at time *t* ($\boldsymbol{I_{DF}(t)}$)

Intensity of fluorescence ($\boldsymbol{I_F}$)

Intensity of phosphorescence ($\boldsymbol{I_P}$)

Lowest triplet excited-state of the donor (^{3}**LE$_{D}$**)

Number of spectral lines ($\boldsymbol{N}$)

Charge recombination rate at time *t* (***R* (*t*)**)

Total electron spin quantum number (***S***)

Ground singlet state ($\mathbf{S_0}$)

The first excited singlet state ($\mathbf{S_1}$)

Singlet excited states of donor ($\mathbf{S_{1,D}}$)

Singlet excited states of acceptor ($\mathbf{S_{1,A}}$)

The n^{th} excited singlet state ($\mathbf{S_n}$)

Concentration of T_1 excitons at time 0 ($\mathbf{[T_0]}$)

The first excited triplet state ($\mathbf{T_1}$)

Triplet excited state of donor ($\mathbf{T_{1,D}}$)

Triplet excited state of acceptor ($\mathbf{T_{1,A}}$)

Glass-transition temperature ($\boldsymbol{T_g}$)

The n^{th} excited triplet state ($\mathbf{T_n}$)

Concentration of T_1 excitons at time *t* ($\mathbf{[T_t]}$)

Energy gap between S_1 and T_1 ($\boldsymbol{\Delta E_{ST}}$)

Photoluminescence quantum yields ($\boldsymbol{\Phi_{PL}}$)

Units

arbitrary unit (**a.u.**)

counts per second (**CPS**)

degree Celsius (**℃**)

Electronvolt (**eV**)

Hour (**h**)

Kelvin (**K**)

Liter (**L**)

Micrometer (**μm**)

Microsecond (**μs**)

millicandela (**mcd**)

Millimeter (**mm**)

Millisecond (**ms**)

Minute (**min**)

Molar (**mol**)

Molar per liter (**M**)

Nanometer (**nm**)

Nanosecond (**ns**)

Second (**s** or **sec**)

List of Publications and Conferences

Original papers

1) **Z. Lin**, R. Kabe, and C. Adachi, "Orange Organic Long-persistent Luminescence from an Electron Donor/Acceptor Binary System" *Chem. Lett.*, **in press**, 10.1246/cl.190823. (**Chapter 2**)

2) **Z. Lin**, R. Kabe, K. Wang, and C. Adachi, "Influence of energy gap between charge-transfer and locally excited states on organic long persistence luminescence" *Nat. Commun.*, **in press**, 10.1038/s41467-019-14035-y. (**Chapter 3**)

3) **Z. Lin**, R. Kabe, N. Naohito, K. Jinnai, and C. Adachi, "Organic Long-Persistent Luminescence from a Flexible and Transparent Doped Polymer" *Adv. Mater*., **2018**, 30, 1870341. (**Chapter 4**)

Conferences

1) **Z. Lin**, R. Kabe, and C. Adachi, *The 10th Asian Conference on Organic Electronics (A-COE2018)*, Hong Kong, China, Dec. 5-8, 2018 (Poster).